MONASH University

Modelling the mechanical behaviour of capsule based self-healing composites

Mohonee Vijendra Kumar

A thesis submitted for the degree of Masters by Research at
Monash University in 2017
School of Engineering

Copyright notice

Abstract

Self-healing composites are an important class of materials which seek to restore their initial properties after sustaining damage. They have a huge potential for applications in various industries such as electronics, aerospace, sporting good, etc. Therefore, the interactions between the components of capsule based self-healing composites, release patterns of the healing agents and fracture mechanism of self-healing composites all need to be understood experimentally and theoretically. There is also a necessity for a proper computational model of the capsule based self-healing composite that can simulate the fracture and the healing agent release as well as subsequent healing-fracture-healing cycles. To this end, this study was conducted to establish a basis for the computational modelling of capsule based self-healing composite materials. The first objective of this study was to develop a micro-scale model of a randomly distributed capsule based self-healing composite which can accurately simulate the mechanical response of the material under desired stress conditions. The second objective was to derive the composite material properties from the model when there were variations in capsule distribution and the mechanical properties of the matrix, capsule and capsule filler. The first objective was achieved by creating a Representative Volume Element (RVE) of the composite using a computer aided design feature found in commercial finite element software, ANSYS. The second objective was achieved by reviewing the properties of the material component of the RVE from the literature as well as from results of experiments done by various researchers. The model was solved numerically using ANSYS to obtain the stress distribution within the RVE. The stress distribution was analysed to derive insight concerning how the local stress variations underpin the stress transfers between the matrix and the capsules. This thesis will present an investigation of the effect of several parameters on the mechanical properties of a capsule based self-healing composite material subjected to small static strains. The research will be carried out using computational modelling on ANSYS 17.0 (ANSYS Inc., Canonsburg, Pennsylvania, U.S.A.). The purpose of the research is to establish a basic finite element model for rapid analysis of capsule-based composites which can be further enhanced in future research to include the ability to model composite fracture, self-healing process and subsequent post-healing behaviour.

Declaration

This thesis contains no material which has been accepted for the award of any other degree or diploma at any university or equivalent institution and that, to the best of my knowledge and belief, this thesis contains no material previously published or written by another person, except where due reference is made in the text of the thesis.

Signature: [redacted]

Print Name: **Mohonee Vijendra Kumar**

Date: **06/11/2017**

Acknowledgements

I would like to express my gratitude towards my supervisors, Dr Pooria Pasbakhsh, Dr Goh Kheng Lim and Prof Soh Ai Kah for their guidance. The tuition fee waiver provided by Monash University is gratefully acknowledged.

I would also like to thank Prof Leon Mishnaevsky Jr for his valuable insights, my colleague, Ms Hia Iee Lee for her help and Mr Ahmad Faridzul Hilmi Shamsuddin for his technical advice during this research project.

Table of contents

Copyright notice 2

Abstract 3

Declaration 4

Acknowledgements 5

1. Introduction 9

1.1 Modelling of capsule reinforced composites 9

1.2 Modelling of self-healing composites 9

1.3 Problem Statement 11

1.4 Objectives 11

1.5 Aim 11

1.6 Hypothesis 12

1.7 Outline of thesis 12

2. Literature review 13

2.1 Self-healing mechanisms in nature 13

2.2 Classification of healing mechanisms in synthetic materials 13

2.3 Self-healing of polymer nano-composites 14

2.4 Healing of fiber-reinforced polymers 16

2.5 Non-autonomic healing of thermoplastic materials 16

2.6 Intrinsic self-healing materials 17

2.7 Healing efficiency of self-healing composites 18

2.8 Fracture study of polymer composites 20

2.9 Computational modelling of materials 21

2.10 Finite element analysis of particle reinforced composites 21

2.11 Finite element analysis of metals comprised of 2 distinct phases 23

2.12 Influence of interface cohesive strength between reinforcement and matrix on the mechanical properties of the overall material 27

2.13 3D Progressive damage modelling of composite materials 27

2.14 Fracture modelling using Finite Element Method 30

2.15 Computational modelling of high speed deformation of materials 31

2.16 Multi-scale modelling of composite materials 33

2.17 Modelling the flow of resin in self-healing composites 33
3. Methodology 35
3.1 Description of models 39
3.1.1 Capsule dispersion model 42
3.1.2 Capsule agglomeration model 43
3.1.3 Single agglomeration + dispersion model 44
3.1.4 Multiple agglomerations + dispersion model 45
3.2 Material properties 47
3.3 Material strength limits 47
3.4 Boundary conditions 48
3.5 Meshing 48
3.6 Instruction manual 50
4. Results & discussion 61
4.1 Linear analysis 61
4.1.1 Solid PUF capsules (0.1% strain) 64
4.1.2 Solid epoxy filled capsules (0.1% strain) 65
4.1.3 Solid PUF capsules (0.4% strain) 66
4.1.4 Epoxy filled capsules (0.4% strain) 67
4.1.5 Solid PUF capsules (0.7% strain) 68
4.1.6 Epoxy filled capsules (0.7% strain) 69
4.1.7 Hollow capsules (0.1% strain) 73
4.1.8 Hollow capsules (0.4% strain) 74
4.1.9 Hollow capsules (0.7% strain) 75
4.2 Non-linear analysis (damage model) 77
4.2.1 Epoxy filled capsules, pure agglomeration: 1% strain to 2% strain 78
4.2.2 Epoxy filled capsules, single agglomeration + dispersion: 1% strain to 2% strain 79
4.2.3 Epoxy filled capsules, multiple agglomerations + dispersion: 1% strain to 2% strain 80
4.2.4 Epoxy filled capsules, pure dispersion: 1% strain to 2% strain 81
4.2.5 Solid PUF particles, pure agglomeration: 1% strain to 2% strain 82
4.2.6 Solid PUF particles, single agglomeration + dispersion: 1% strain to 2% strain 83
4.2.7 Solid PUF particles, multiple agglomerations + dispersion: 1% strain to 2% strain 84
4.2.8 Solid PUF particles, pure dispersion: 1% strain to 2% strain 85

4.2.9 Hollow capsules, pure agglomeration: 1% strain to 2% strain 86
4.2.10 Hollow capsules, single agglomeration + dispersion: 1% strain to 2% strain 89
4.2.11 Hollow capsules, multiple agglomerations + dispersion: 1% strain to 2% strain 91
4.2.12 Hollow capsules, pure dispersion: 1% strain to 2% strain 93
5. Conclusion 96
6. Future works 98
References 99

1. Introduction

1.1 Modelling of capsule reinforced composites

Capsule reinforced composites are made by adding judicious amounts of reinforcing capsules to a matrix. Polymers are widely used as the matrix phase in capsule reinforced composites. This addition will enhance the composite properties in various ways depending on the properties of the matrix, the type, shape, orientation, distribution, aspect ratio and volume fraction of reinforcing phase and manufacturing process (Brown, White, & Sottos, 2004; Singh, Shedbale, & Mishra, 2016; Wang, Ji, Shao, & Miao, 2011). The capsules act as reinforcement for the matrix and as storage for healing agents.

The experimental testing of composites to determine their properties is a very costly and time-consuming process. The composite must be synthesized, and the testing must be performed using advanced and often expensive equipment. In order to alleviate the cost of experimental testing, computational methods have been developed and have been proven to be quite accurate (Valavala & Odegard, 2005). Computational models enable researchers to conduct parametric studies of composites for design and application of composite structures in the real world.

1.2 Modelling of self-healing composites

Self-healing materials are important class of materials which have significant engineering interest (Zhang & Rong, 2012). They are polymers, metals, ceramics and their composites which can restore their original properties after sustaining damage (Roach et al., 2007; Wool, 2008). Most research in the domain of self-healing materials is focused on polymers and polymer composites as they are widely used in numerous applications such as electronics, aerospace, energy generation equipment, pressure vessels, marine structures, sporting goods, etc. (Wu, Meure, & Solomon, 2008). They are attractive as engineering materials as they have desirable physical properties. This research will focus mainly on capsule based self-healing composites. Encapsulation of healing agents can be done at micro-scale or nano-scale levels. These capsules can be then embedded into a matrix to form a self-healing composite. Hia et al., (2016) have encapsulated epoxy resin into alginate microcapsules and embedded those capsules into an epoxy resin. Thakur & Kessler (2015) have reviewed different methods such as emulsion electro spinning, emulsion solution blowing, and co-electro spinning for encapsulating self-healing liquid monomers into carbon nanotubes.

A better understanding of capsule based self-healing material behaviour will enable design optimization which will positively affect material safety, product performance and product lifetime (Wool, 2008). The most promising area of study when it comes to these systems encompasses the key properties of capsule based self-healing epoxy composites after fracture damage including healing frequency, healing efficiency and the healing and fracture mechanisms.

Self-healing materials mimic biological systems and have a huge potential for reducing the frequency for repair and maintenance of mechanical structures (Roach et al., 2007; Wool, 2008; Wu et al., 2008). One major drawback of polymers and their composites is that they are susceptible to internal crack formation from fatigue and fracture damage which severely deteriorates their mechanical properties (Zhong & Post, 2015). The elimination of this damage will have a significant impact in cases where the material's intended use does not permit damage assessment and repairs and also when the damage is internal and cannot be detected (Wool, 2008). Experimental studies of composite materials, especially the study of composites with micro/nano-scale reinforcements remains challenging due to the difficulty in observing how stresses are transferred and how the deformation occurs at such a small scale. Theoretical modelling and simulations can be used to fill in this gap. Computational models help provide insight into the composite behaviour (Al-Madani, Jarnaz, Alkharmaji, & Essuri, 2013; Lee, Buxton, & Balazs, 2004; Shokrieh & Rafiee, 2010).

This research is being proposed to create a foundation for the computational modelling of capsule based self-healing composite materials. It will help to obtain deeper insight into the interactions between the components of a capsule based self-healing composite under specified loading conditions. Consequently, computational methods will be used to create models and provide a guideline for optimized design of capsule based self-healing composites.

1.3 Problem Statement

The development of self-healing materials is still at its initial stages. As such, self-healing materials have a huge potential for applicability across many fields. There are many configurations of self-healing materials that use different healing mechanisms (such as in-situ healing, dual capsule systems, etc.) as well as different types of healing containers (such as embedded healing capsules, vascular networks, etc.).

As such, the main issues faced in self-healing materials research are as follows:

1. The interactions between the components of a self-healing composite are difficult to observe in an experimental set-up since the self-healing components are usually embedded inside the matrix and are at a microscopic scale.
2. Measurement of the internal stress distributions inside a capsule based self-healing composite is difficult in an experimental setup.
3. The time investment required for producing and testing all the material configurations in order to optimize the material for a given application or work environment is quite significant.

1.4 Objectives

1. To develop a basic finite element model for the rapid modelling and simulation of the mechanical response of capsule based self-healing composites.
2. To further develop the model to enable users to vary different parameters such as capsule distribution, capsule size variation, etc. This will enable the tailoring of parameters to obtain desired composite properties.

1.5 Aim

The aim of this project is to create a computational model that can simulate the mechanical behaviour of a capsule reinforced composite under small static strain. The model can be used as a basis for the design and modelling of capsule based self-healing composites. The model will allow the user to input parameters such as the properties of the matrix, capsules and capsule filler, thickness of the capsule wall, volume fraction of matrix and filler, strain, etc, and obtain the overall composite properties. Furthermore, it will reduce the need for researchers to experimentally create and test several composite configurations in order to find their desired composite property. Researchers will be able to converge towards their ideal composite configuration while saving time and experimental costs.

1.6 Hypothesis

The translation of the physical microstructure and the experimental results into a computational model of self-healing materials will enable the rapid modelling and testing of samples in a virtual environment under static tensile conditions with quick parameter variations. This will enable savings in terms of time and material costs and will provide a better insight on the material behaviour, the stress distribution in the composite and the interactions between the components of the composite material. The successful completion of this model will open the possibility for future research into fracture modelling and self-healing modelling.

1.7 Outline of thesis

Section 1 will provide a general introduction on the topic of capsule reinforced composites and the importance of Finite Element Modelling in this field. Section 2 will provide some background research relevant to this project. A broad range of research topics were reported from different self-healing mechanisms at different scales to the modelling approach of materials comprising of distinct phases/materials. The literature review enabled a better understanding of self-healing in capsule reinforced composites and how to initiate the modelling process. Section 3 will elaborate on the steps and the method used to create and analyse the finite element model. Section 5 will present the results and the discussion. Section 5 will be the conclusion and section 6 will be the future works.

2. Literature review

2.1 Self-healing mechanisms in nature

Self-healing occurs in nature in both plants and animals. This phenomenon is triggered by stimuli, both internal and external. Naturally occurring materials have evolved into complex, hierarchical structures that exhibit multifunctional behavior. Drawing inspiration from naturally occurring materials will enable scientists to improve material performance (Williams, Bond, & Trask, 2009). In plants and animals, tissue damage causes changes in the chemical balance at the damage site and causes the organism to send healing agents to heal the damage via complex internal transport networks of vessels. Natural self-healing systems are extremely complex and not fully understood; therefore, scientists have had to adopt a more simplified approach to mimic those systems (Williams et al., 2009).

2.2 Classification of healing mechanisms in synthetic materials

Researchers have attempted different ways to classify self-healing materials. Thakur & Kessler (2015) have categorized self-healing systems into several groups and sub-groups. The two major groups are autonomic and non-autonomic self-healing materials. Autonomic materials can heal by themselves without external intervention whereas non-autonomic materials require some form of intervention (White et al., 2001). The external interventions may be in different forms such as changes in temperature, lighting conditions, chemical or mechanical. Self-healing materials can also be further divided into extrinsic and intrinsic based on their healing mechanism (Thakur & Kessler, 2015). Extrinsic materials rely on the inclusion of storage vessels containing the healing agents into the polymer matrix. Extrinsic materials are generally composites as they are made up of two or more materials meaning that the matrix, the storage vessels and the healing agents are all different materials. Intrinsic materials can heal themselves naturally due to how their molecular bonding is set up.

On the other hand, some researchers have broadly classified self-healing systems into 3 categories as below (Grande et al., 2012; Shojaei, 2015):

1. Materials which incorporate microcapsules or micro-vascular networks in their matrix. The said micro features will contain the healing agents which get released upon crack propagation. The healing agent is usually a monomer which solidifies in the presence of a catalyst embedded in the matrix as illustrated in Figure 1 (Dementsov & Privman, 2008; Grande et al., 2012). These can be considered as autonomic self-healing composites (White et al., 2001).
2. Incorporation of solid healing agents which diffuses to crack surfaces upon their formation.
3. Innate healing capability in materials such as ionomers and materials with thermally reversible covalent bonds, shape memory alloys (SMAs) and shape memory polymers (SMPs). These can be considered as intrinsic self-healing materials.

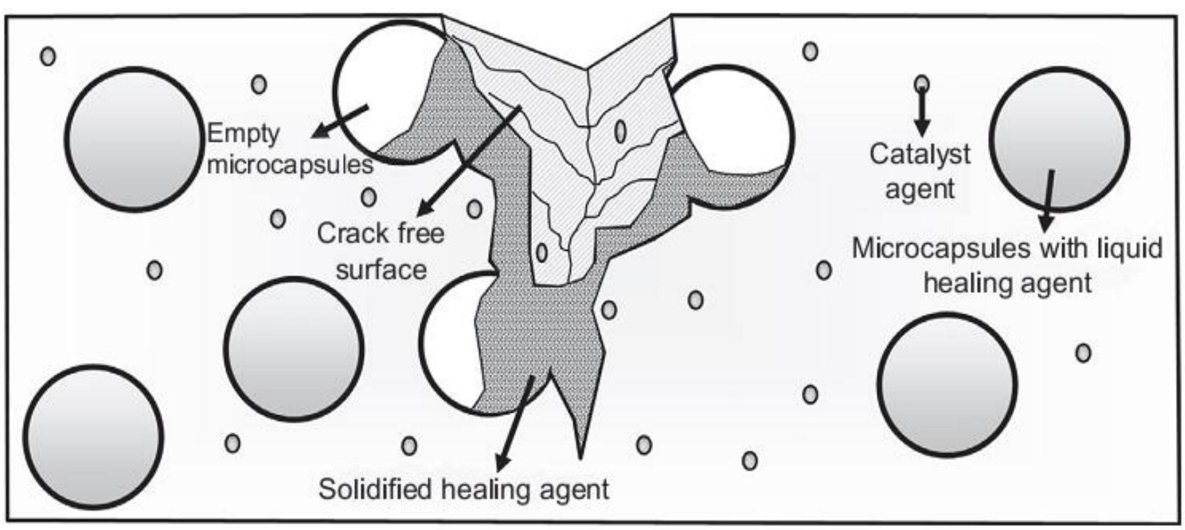

Figure 1. Self-healing mechanism of composites embedded with micro-caspsules (Shojaei, 2015).

2.3 Self-healing of polymer nano-composites

The use of polymers and polymer composite materials is widespread due to their overall desirable characteristics such as light weight, availability, flexibility, manufacturability, etc (Thakur & Kessler, 2015). On the downside, these materials have poor mechanical properties compared to metals and ceramics. They also degrade due to fatigue loading, thermal effects, environmental effects, impact, etc. (Lanzara, Yoon, Liu, Peng, & Lee, 2009). The incorporation of nano-materials into a polymer matrix will significantly improve their properties and result in a material that is highly homogeneous. Imparting self-healing capabilities into polymer nanocomposites would make them more sustainable, longer lasting and expand their range of applications (Lanzara et al., 2009; Thakur & Kessler, 2015). This is because polymers and their composites are susceptible to nano-scale damage which extends to the micro and the macro scale until catastrophic failure. The self-healing process in polymer composite materials has been studied using computational models and molecular dynamics simulations (Thakur & Kessler, 2015). From the idea that damage starts at a nano-scale level, Lanzara, Yoon et al., (2009) have created a conceptual model of a polymer nano-composite which uses Carbon Nanotubes (CNTs) as both matrix reinforcement and as containers for healing agents in polymer nano-composites. The model is illustrated in Figure 2. They have hypothesized that nano-scale damage will rupture the CNTs and cause the release of healing agents which will halt the damage progression at the initial stage itself. They have conducted molecular dynamics simulations whereby CNTs are used to store methane molecules and have found out that the healing agent release depends on the size of the crack on the CNT wall. The release of the healing agent is also temperature dependent and is prone to saturation which means that not all the healing agent molecules are released into the crack space. The results indicate that depending on the crack size, the percentage of methane molecules released ranges from 0.4-0.5%. Therefore, they have concluded that the number of released methane molecules can be controlled by varying the packing density of the methane inside the CNTs (Lanzara et al., 2009).

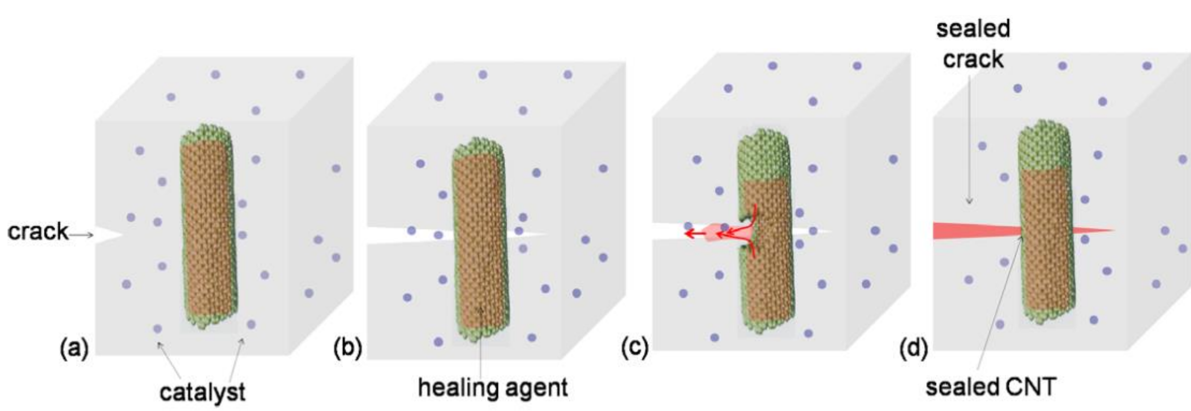

Figure 2. Concept of self-healing process using carbon nano-tubes (Lanzara et al., 2009).

2.4 Healing of fiber-reinforced polymers

Due to the planar nature of fiber reinforced composites, they have poor impact resistance and the extent of the damage cannot be assessed by visual inspection (Williams et al., 2009). Researchers have tried to take advantage of fiber reinforced composite hierarchical microstructures by incorporating self-healing capabilities into them. This was done by using hollow glass fibres as storage vessels for the healing agents and incorporating those fibres in a polymer matrix. When the polymer composite got damaged, the fibres were ruptured and released the healing agents which seeped into the cracks. This helped to recover some mechanical strength and prevents further crack propagation (Williams et al., 2009).

2.5 Non-autonomic healing of thermoplastic materials

There are several mechanisms by which thermoplastics can recover from damage. One mechanism exploits the thermoplastics' molecular chain mobility at temperatures above the glass transition temperature (T_g) (Wu et al., 2008). In other words, when the temperature of the thermoplastic exceeds the glass transition temperature, the polymer chains can move around and re-arrange themselves. This causes the crack surfaces to fuse together and restores the mechanical strength of the thermoplastic. This healing mechanism requires the application of heat to achieve temperatures above T_g and is illustrated in Figure 3.

Another healing mechanism is photo-induced healing. This requires the irradiation of the polymer with light of a certain wavelength (>280nm). This healing technique only works with polymers which have been specially prepared in the presence of light to polymerize (Wu et al., 2008).

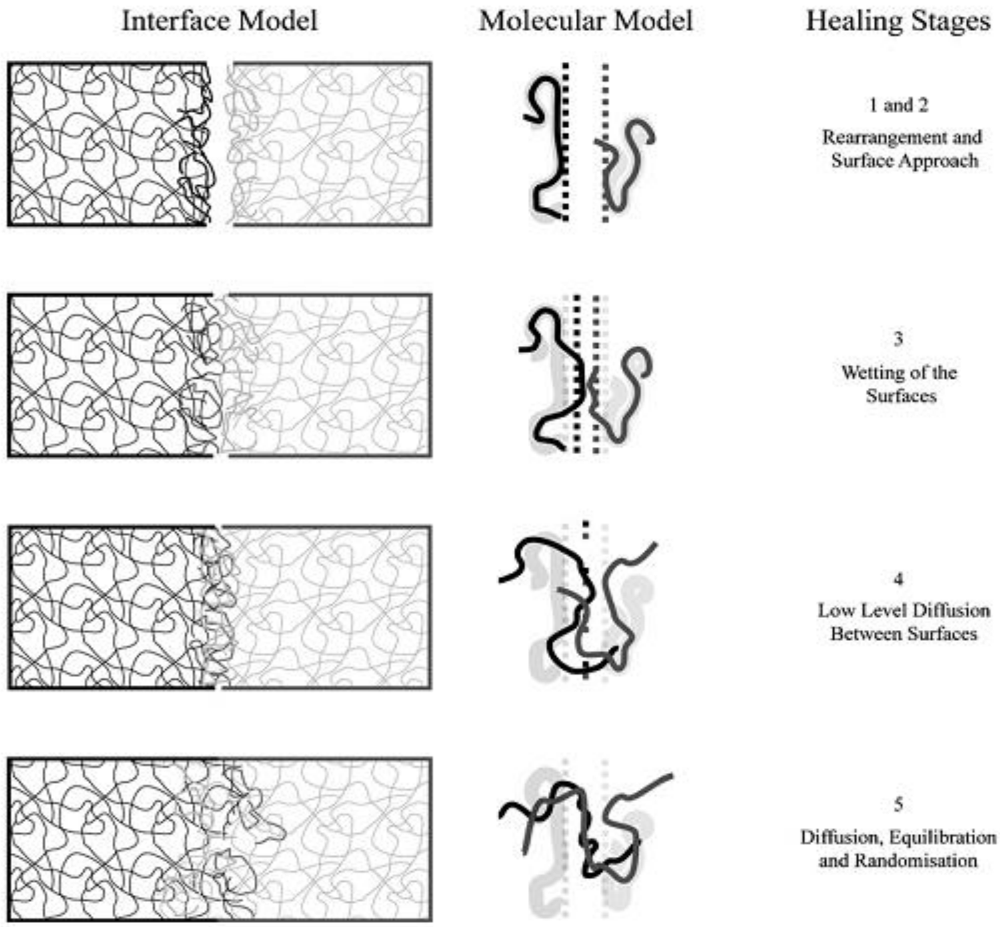

Figure 3. Illustration of molecular diffusion through crack interface (Wu et al., 2008).

2.6 Intrinsic self-healing materials

Ionomers are polymeric materials which can self-repair without any external intervention. However, their ability to self-heal is only limited to piercing damage under a very limited range of environmental and impact conditions such as the temperature, speed and shape of the projectile (Grande et al., 2012).

Shojaei (2015) has also mentioned a self-healing material proposed in previous works which combined two healing mechanisms by embedding SMP fibres and solid thermoplastic particles in the composite matrix. When a crack forms, the SMP fibres will pull the crack faces together and the application of heat will cause the solid thermoplastic particles to melt and heal the crack. This healing system is illustrated in Figure 4.

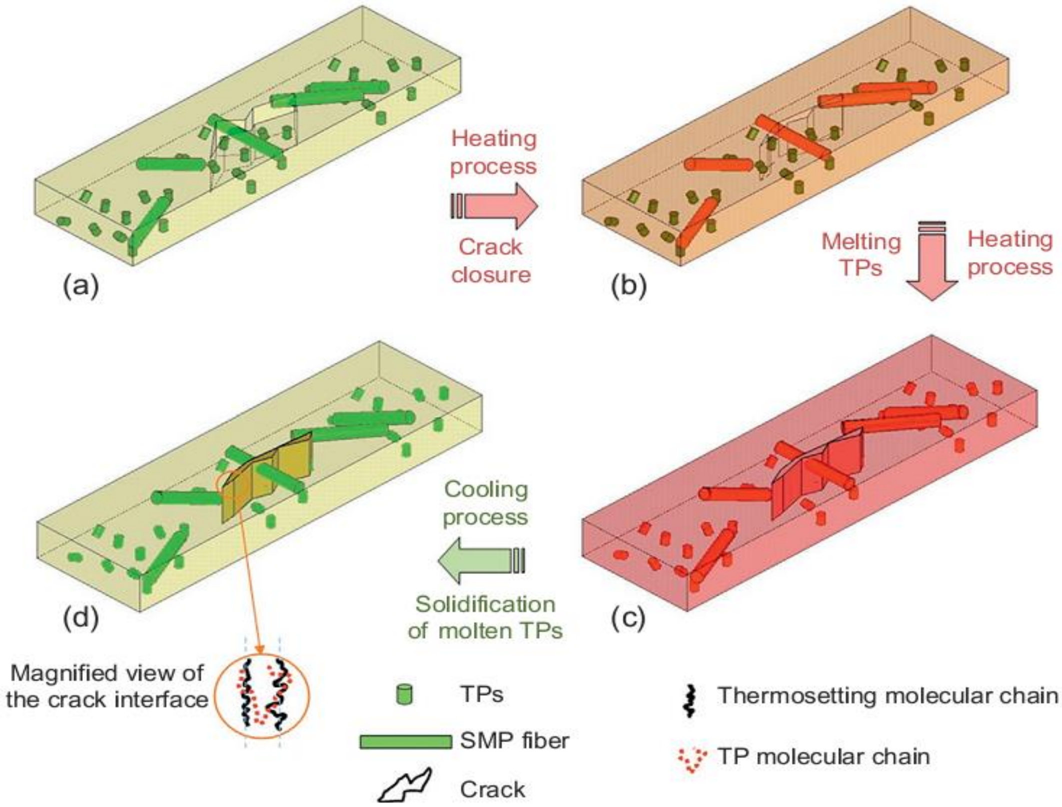

Figure 4. Illustration of the healing system proposed by Shojaei (2015) which incorporates SMP fibers and solid healing agents in the form of thermoplastic particles dispersed in a matrix. Figure 4(a) depicts a macroscopic crack in the material. Figure 4(b) shows the crack surfaces being brought together when the SMP fiber restores its shape. Figure 4(c) represents the heating process which melts the solid healing agent and allows it to fill up the crack. Figure 4(d) shows the healed material at room temperature (Shojaei, 2015).

The model illustrated in Figure 4 addresses an issue pertaining to the solid healing agents and the encapsulated liquid healing agents which is the run-off of liquid monomers from the crack sites before polymerization occurs. One of the main challenges is to create self-healing materials which can heal macro scale cracks repeatedly and efficiently.

2.7 Healing efficiency of self-healing composites

An important factor relating to self-healing composites is the healing efficiency. Healing efficiency is the percentage of strength restored after the composite has sustained damage and healed. In practice, it is the difference in load carrying capacity between the initial and the healed material

(Tsangouri, Aggelis, & Van Hemelrijck, 2015). Damage can be due to impact, extreme temperatures, radiation and fatigue and come in different forms such as warping, gashes, cracks, micro cracks and nano-cracks (Dementsov & Privman, 2008). The presence of micro cracks in the composite matrix will disrupt the load transfer mechanisms between capsules, fibres or any other containers used in the system and the matrix and it will ultimately lead to delamination and fracture of the container and the release of the healing agent (Wu et al., 2008).

Williams et al. (2009) have conducted low velocity impact tests on fibre reinforced composites that have been imparted with self-healing capabilities by embedding hollow glass fibres containing healing agents. They have obtained conclusive proof that the presence of resin filled glass fibres enabled the restoration of a significant proportion of the compressive strength of the host material without having a detrimental effect on the material strength. Healing cracks at the nano scale would be advantageous as mentioned in section 2.3 since this would delay material fatigue earlier than micro scale healing. One main drawback of current self-healing materials is their inability to heal cracks at a macroscopic scale for example for cracks from impact damage. These crack surfaces have to be brought together for the healing agent to act (Shojaei, 2015). In the case of micro encapsulated liquid healing agents, the healing of macro-cracks would require the incorporation of a large amount of healing agents which would significantly affect the mechanical properties of the structure. In the case of large capsules and fiber encapsulated healing agents, the empty spaces left behind after the healing agent is released are potential defect sites (Shojaei, 2015).

Most research on self-healing materials is focused on trial-and-error manufacturing processes to demonstrate their self-healing ability. However, to implement these materials into real world applications, the products need to be physically consistent. Since molecular level modelling techniques are difficult to implement computationally and experimentally, continuum level modelling approaches are the most widespread (Shojaei, 2015).

The strength restoration will depend on how efficiently these cracks are healed. It is therefore important to understand the underlying chemical processes of self-healing and how it affects the material strength. According to Dementsov & Privman (2008), theoretical and numerical modelling of self-healing composite behaviour is still at the initiation stage. Furthermore, there is a need for a coordinated effort to combine computational methods and spectroscopic methods to gain further understanding of how self-healing materials respond to stimuli (Urban, 2009).

2.8 Fracture study of polymer composites

It is important to study the fracture behaviour of polymer composites as it enables us to predict their response under daily work conditions. The ability of a polymer composite, employed in a structural application, to be able to absorb energy from strain or impact is crucial in many fields (Laurenzi, Pastore, Giannini, & Marchetti, 2013). It is therefore important to conduct experimental and computational studies to characterize its properties before using it in the field.

Fracture study of self-healing polymer composites is crucial when trying to determine the healing efficiency (Tsangouri et al., 2015). Since self-healing polymers form adhesive joint interfaces after healing, it is necessary to employ established testing regimes for monitoring of crack formation in adhesive composites (Tsangouri et al., 2015). The most commonly used fracture test to characterize self-healing material tensile strength are the tapered double cantilever beam (TDCB) tests and the single-edge notched beam tensile tests.

Researchers have identified 3 failure modes in polymers (illustrated in Figure 5.):

1. Crack opening where tensile forces perpendicular to the crack separate the crack surfaces.

2. Crack sliding where shear forces slide the crack surfaces on top of each other.

3. Crack tearing where shear forces pull the crack surfaces apart.

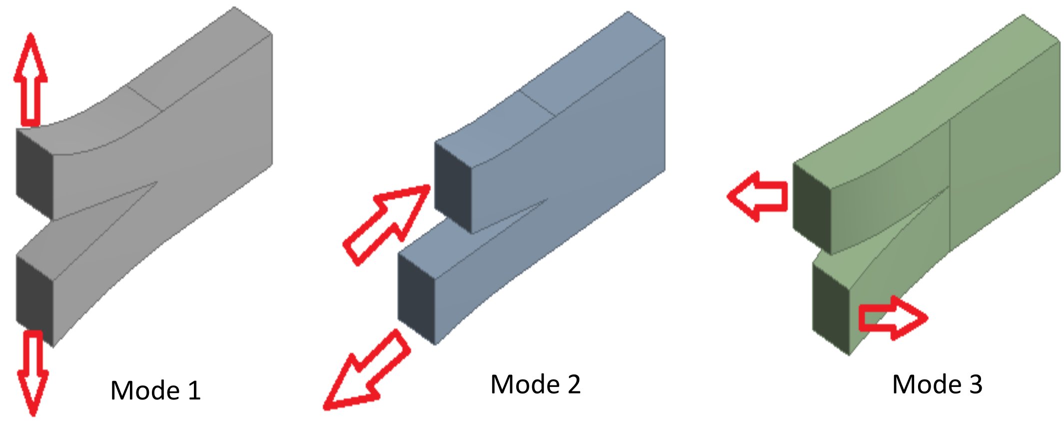

Figure 5. Damage modes whereby mode 1 is crack opening, mode 2 is crack sliding and mode 3 is crack tearing.

2.9 Computational modelling of materials

Generally, the intention of computational models is to attain computational efficiency when calculating the mechanical response of the material during damage without sacrificing the key physical aspects of the material microstructure, architecture and behaviour (Grujicic et al., 2010). Experimental studies require the manufacture of the material that needs to be analysed as well as costly material testing equipment. Computational models can help save in terms of time and the cost.

2.10 Finite element analysis of particle reinforced composites

It is generally agreed that the modelling of the mechanical response of particle reinforced composite materials is a very complex problem due to the large number of factors that can influence the behaviour. The factors include the size, distribution and shape of the inclusions (Chawla, Sidhu, & Ganesh, 2006; Sun, Shen, Song, & Du, 2012). In these cases, analytical and simple numerical models are not ideal since they do not always account for the factors that affect the behaviour at the microstructural level. Chawla, Sidhu & Ganesh (2006) have been able to obtain accurate results by using a 3D microstructure based approach to model particle reinforced material behaviour. They have found that 3D Finite Element Method is very effective at modelling multiphase materials and local deformations and damage characteristics can be easily visualized.

The experiment conducted by Chawla, Sidhu & Ganesh (2006) consisted of manufacturing pieces of aluminium alloy reinforced with various volume % of silicon carbide (SiC) particles and rendering the samples into 3D models for finite element analysis. The 3D rendering was done by taking a sample of the material, polishing the surface, taking a picture of the surface microstructure, shaving off thin slices off the surface while simultaneously taking pictures after each layer is removed. The pictures are then stacked together, and a 3D model is created. This process has enabled them to create very accurate representative volume elements. The process is illustrated in Figure 6.

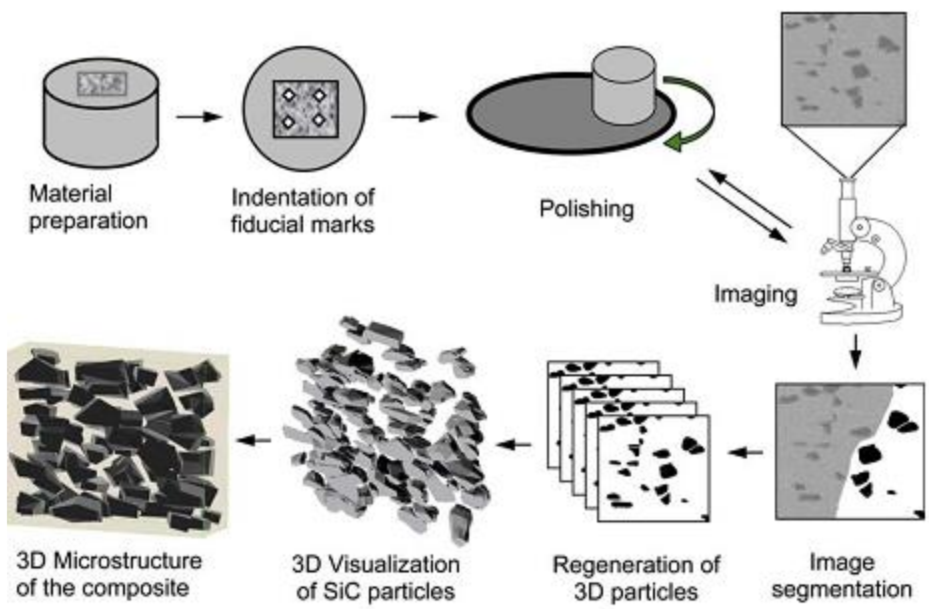

Figure 6. 3D modelling process of SiC reinforced Aluminum alloy (Chawla, Sidhu & Ganesh, 2006).

Once the realistic particle distribution was obtained, the shape of the inclusions could be modified to spherical or ellipsoidal (Figure 7) to investigate the effect of varying inclusion shapes on the composite properties without changing the particle distribution.

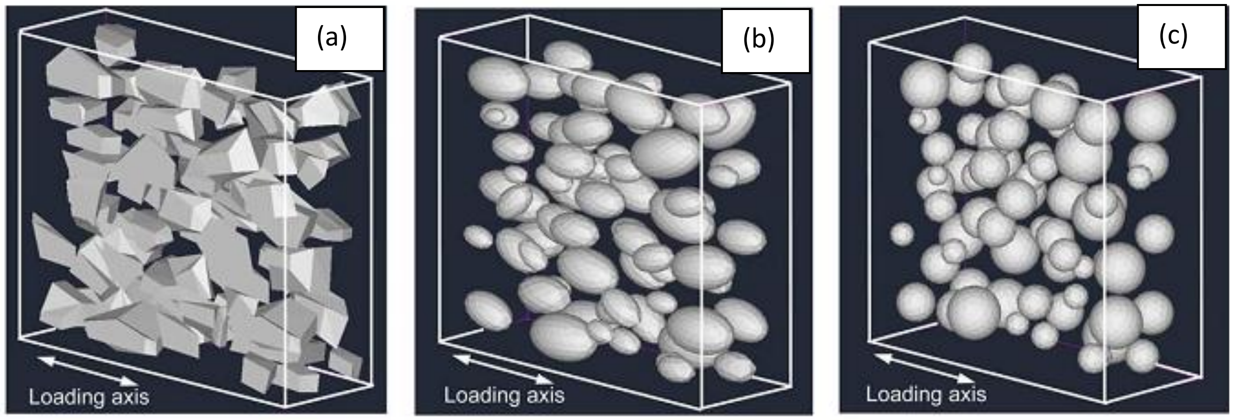

Figure 7. Illustration of differently shaped inclusions (a) sharp, angular (b) ellipsoidal (c) spherical (Chawla et al., 2006).

The ideas that can help to successfully create accurate finite element models of particle reinforced composites can be applied to model capsule reinforced composites. The main difference between modelling capsule reinforced composites and particle reinforced composites is that the particle will be modelled as a solid sphere or ellipsoid while the capsule will be modelled as a sphere with an internal radius and a wall thickness which can be either hollow or filled with a distinct material (healing agents).

2.11 Finite element analysis of metals comprised of 2 distinct phases

Guo, Ji et al., (2014) have conducted computational studies on the fracture behaviour of bimodal nano-structured (NS) metals. Bimodal NS metals consist of coarse grained (CG) and nano-grained (NG) phases. This combination of two distinct microstructures can significantly alter the material behaviour. The metal strength and ductility can be modified by adjusting the size, shape and distribution of the coarse grain inclusions. However, the direct experimental characterization of bimodal NS metal behaviour has limitations since the grain size distribution and shape cannot be easily reproduced and predicted. Their modelling approach can be applied to particle reinforced composites, however, the models with square and hexagonally packed particles are not suitable to predict material behaviour as these particle arrangements cannot be currently achieved in real life. Furthermore, 2D models tend to be overly simplified compared to 3D models.

The 2D models proposed by Guo et al., (2014) combine a mechanism-based strain gradient plasticity theory, a micromechanics composite model and the Johnson-Cook failure model. The model has been used to investigate the effect of the CG phase distribution and the shape of the CG phase on the fracture behaviour of bimodal nanostructured copper. The models display different microstructures as illustrated in Figure 8. Their models with differently shaped inclusions provided insights on how particles with sharp edges (square inclusions) affect the stress field as compared to particles with smooth edges (elliptical and spherical inclusions). They were also able to compare how regularly arranged inclusions can affect the mechanical response as opposed to randomly arranged inclusions.

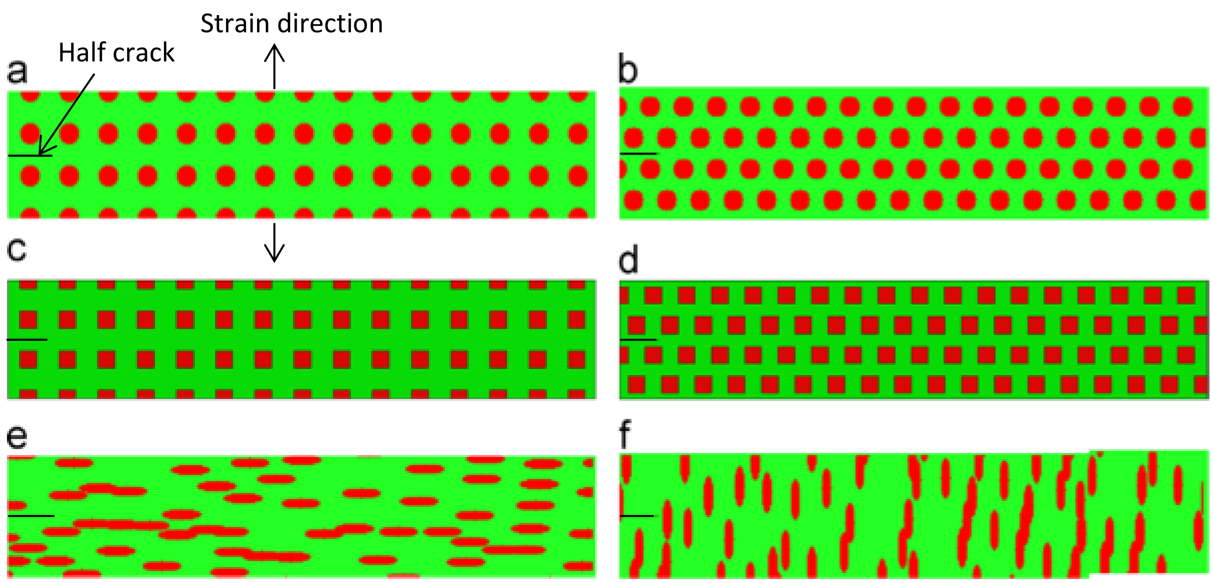

Figure 8. Illustration of different microstructures for the bimodal NS metal. The red structures represent the CG regions while the green area represents the NG region. The idealized microstructures are (a) spherical CG region with square packing (b) spherical CG region with hexagonal packing (c) square CG region with square packing (d) square CG region with hexagonal packing (e) randomly distributed elliptical CG region oriented parallel to the crack (f) randomly distributed elliptical region oriented perpendicularly to the crack (Guo, Ji, Weng, Zhu, & Lu, 2014).

Guo et al., (2014) have compared the load versus boundary displacement for different grain sizes, grain shapes and microstructures. They have also compared the virtual crack length versus boundary displacement for the same parameters as shown in Figures 9(a) and 9(b). They have found that there exists a critical volume fraction of CG inclusions where the fracture resistance is minimal, and this should be avoided when designing bimodal NS metals.

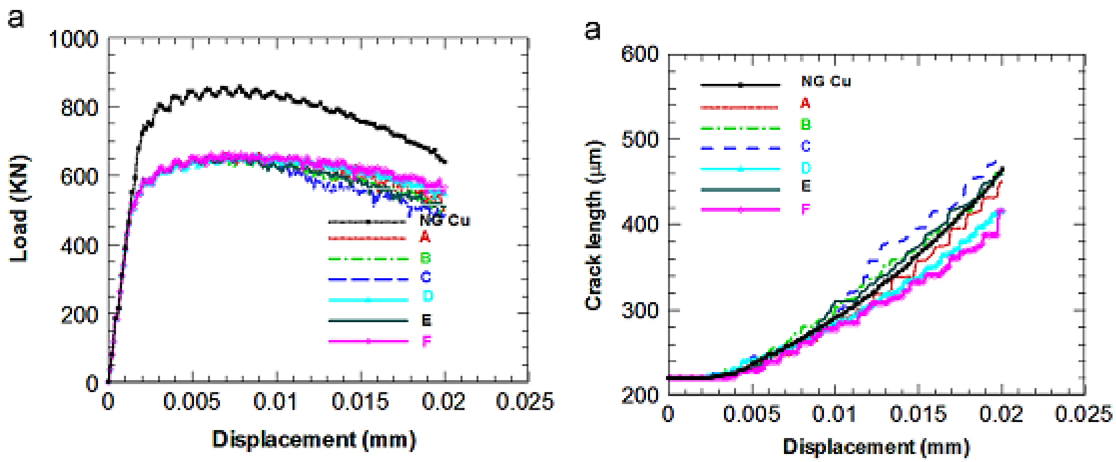

Figure 9. Results for microstructure with a CG grain size of 23nm where (a) shows the load vs boundary displacement with varying CG shapes and configurations and (b) shows the crack length vs boundary displacement with varying CG shapes and configurations (Guo et al., 2014).

In a subsequent research, Ouyang, Guo et al., (2016) have extended the research into 3D modelling and investigated more complex shaped CG inclusions with different orientations as illustrated in Figure 10.

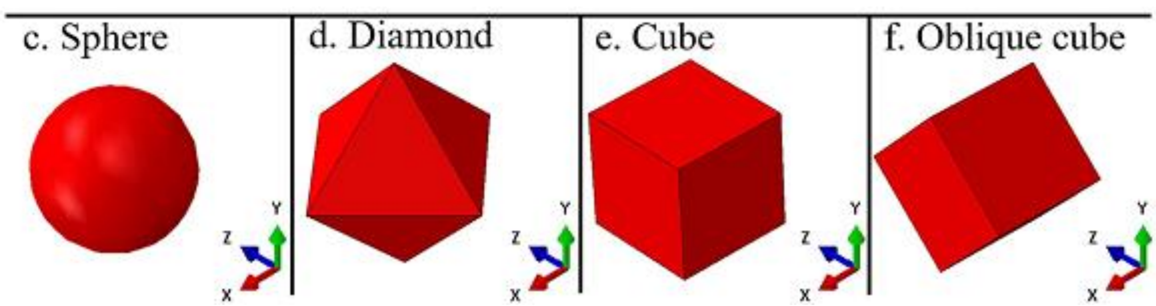

Figure 10. 4 different CG inclusions used in the 3D models (Ouyang, Guo, & Feng, 2016).

They have found that the presence of sharp edges on CG inclusions create areas of high stress concentration (see Figure 11) which are potential sites for crack initiation. This modelling approach is more suitable for modelling particle reinforced composites; however, these models are idealized and do not accurately reflect the arrangement of the inclusions inside the matrix.

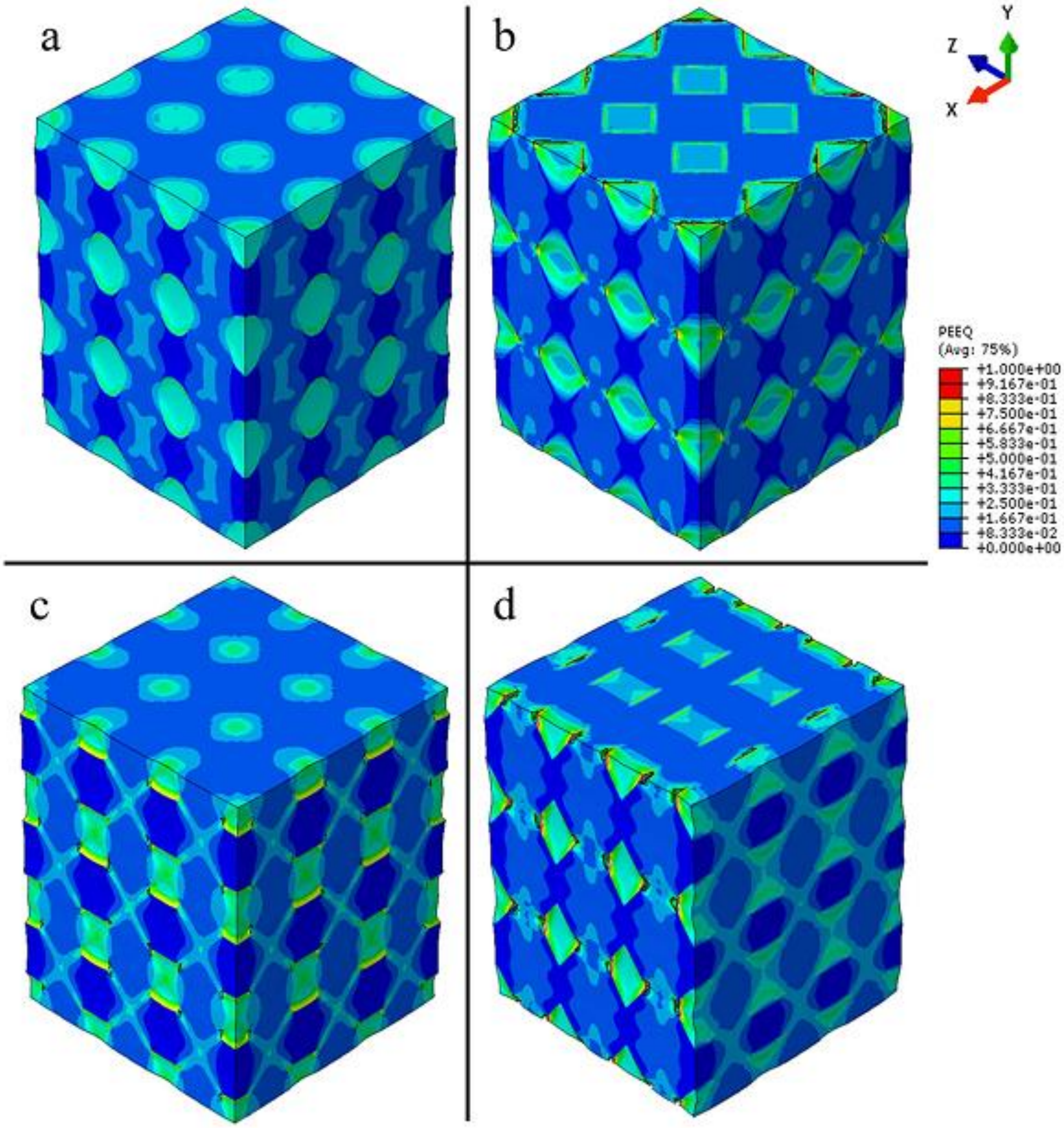

Figure 11. Equivalent plastic strain distribution in RVEs containing (a) spherical inclusions, (b) diamond inclusions, (c) cube inclusions and (d) oblique cube inclusions (Ouyang et al., 2016).

2.12 Influence of interface cohesive strength between reinforcement and matrix on the mechanical properties of the overall material

In further research on bimodal NS metals, Guo et al., (2016) have investigated the effect of the cohesive strength between the CG and NG phases on the strength and ductility of the material. They have found out that the strength of the interface is a crucial factor in the strength and ductility of bimodal metals. The cohesive finite element method (CFEM) has been used to investigate the fracture mechanism at this scale. The ratio of the cohesive strength of the CG to CG elements to the yield strength of the CG phase was denoted by n_{CG} while the ratio of cohesive strength of the NG to NG elements to the yield strength of the NG phase was denoted by n_{NG}. While investigating the different combinations of $n_{CG} - n_{NG}$, it was found that at a certain combination level, the bimodal NS metal will hit an upper limit in strength and ductility (Guo, Yang, & Weng, 2016). The finite element analysis of bimodal nano-structured metal by Guo et al., (2014), Guo, Yang & Weng (2016) and Ouyang et al., (2016) has shown that computational models can be used to accurately predict the mechanical behaviour of dual-phase materials comprising of a matrix with dispersed inclusions having different properties, shapes and distribution.

2.13 3D Progressive damage modelling of composite materials

Koumpias et al., (2014) have developed a progressive damage model (PDM) of a 3D fully interlaced woven composite material (illustrated in Figure 12).

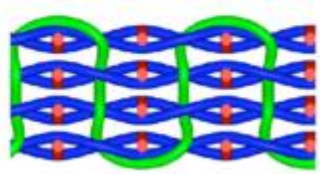

Figure 12. 3D model of a fully interlaced woven composite material (Koumpias, Tserpes, & Pantelakis, 2014).

The aim of the model was to simulate the mechanical response and predict the strength of the composite material. They have applied a Hashin-type failure criteria and the material property degradation was applied using a damage mechanics-based strain-softening law. Non-linear behaviour of the matrix was done by applying a multi-linear continuum damage model. Comprehensive response behaviour of the RVE was measured by loading it in uniaxial tension, compression in all three axes and shear in all three planes.

The PDM has integrated stress analysis, failure analysis and material property degradation by using an iterative algorithm which terminates when material failure is detected. This was performed using ANSYS APDL.

Sanada et al., (2015) have also developed a progressive damage model of a self-healing fibre reinforced composite on ANSYS. Their model assumed perfect bonding between the fibre and the matrix. The model was meshed with 20 node hexahedral elements using tetrahedral and pyramid options. They have carried out stress analyses under incremental loads to determine the damage location. The failure criterion used in this research was the Von-Mises criterion. The damage progression mode is shown in Figure 13.

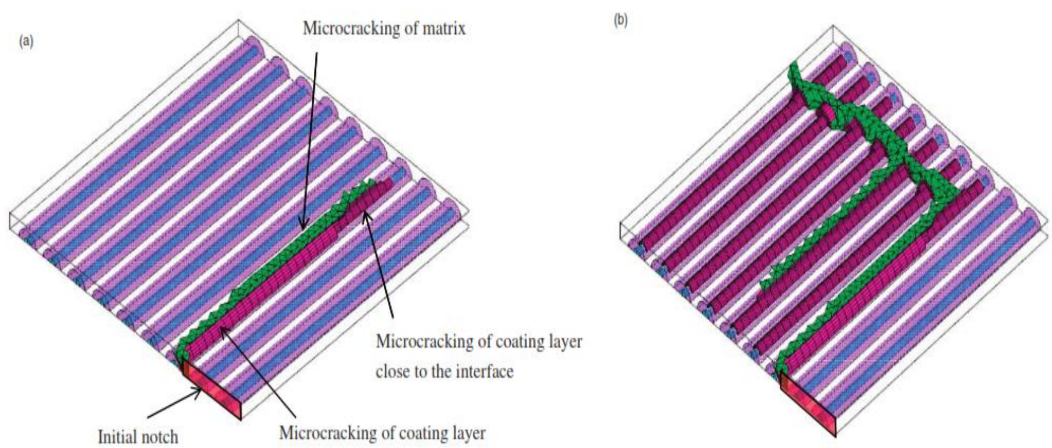

Figure 13. Illustration of progressive damage model of a self-healing fiber composite (Sanada, Mizuno, & Shindo, 2015).

There are different approaches to modelling self-healing composite behaviour and the creation of a Representative Volume Element (RVE) plays a major role in determining the mechanics of random heterogeneous materials (Chen, Ji, & Wang, 2013). Researchers may choose to either adopt a 2D RVE approach which is simple and less computationally demanding or use a 3D RVE which is more complex and closer to the actual situation (Chen et al., 2013). Despite the extensive research being done on self-healing materials in experiments, there is a distinct lack of theories that describe the complex multi-physics healing mechanisms at the microscopic level (Shojaei, Sharafi, & Li, 2015). Consequently, the modelling techniques which attempt to emulate the behaviour of self-healing systems are very limited and very few have been reported (Shojaei et al., 2015).

The modelling of elastic and inelastic responses of metallic, ceramic and polymeric materials is generally developed on several scales: nano-scale, micro-scale, meso-scale and macro-scale. Nano-scale mechanics face computational difficulties in terms of the time, temperature and length scales and still cannot address real engineering problems. The meso-scale approach is more computationally efficient and links the micro-scale to the macro-scale (Shojaei et al., 2015). In the case of polymers, micro models describe micro-scale features such as crosslinking, chain mobility, interface, motion and entanglement of polymer chains whereas the macro-scale models describe the material behaviour in terms of overall mechanical properties and the latter are appropriate for numerical and finite element methods (Baghani, Naghdabadi, Arghavani, & Sohrabpour, 2012). Continuum damage healing mechanics are used to connect the microscopic healing processes to the recovery of the overall material (Shojaei et al., 2015). In other words, the linking of micro and macro scale is done by using averaging techniques which take the micro-scale properties and provide internal state variables to the continuum models (Shojaei, 2015).

The main drawback of continuum models is the large number of material parameters that need to be determined experimentally and translated into simulations (Shojaei et al., 2015). To address this, modelling software packages provide material libraries which contain most of the necessary parameters needed. The user can also input their own material model based on their experimental results

Regardless of the nature of the material system, all the designs used for structural purposes will experience a wide range of damage mechanisms during their service life. Service life is categorized as mechanical damage and includes low/high cycle fatigue, ductile and impact damage. Micro cracks, voids and micro-cavities are examples of mechanical damage that occur at the micro scale during service life. Self-healing materials such as shape memory alloy (SMA) and shape memory polymer (SMP) experience an additional type of active damage mechanism which is specific to this class of materials. This damage is called thermo-mechanical damage and is associated with the process of programming and recovery of the material system. Continuum damage mechanics framework is used to formulate mechanical and thermo-mechanical damage (Shojaei et al., 2015).

While some believe that two independent damage variables are needed to describe isotropic mechanical damage, others have shown that the assumption of isotropic behaviour is sufficient to accurately predict load bearing capacity, number of cycles or time to local failure of components. Other researchers have developed a framework which superimposes mechanical and thermo-mechanical damage which enables designers to predict the entire range of active damage mechanisms in self-healing materials containing SMA and SMP components (Shojaei et al., 2015).

2.14 Fracture modelling using Finite Element Method

Chen et al., (2013) have investigated the effect of incorporating microcapsules containing healing agents into an epoxy matrix. They have done so by analysing the behaviour of a 3D RVE containing a single healing capsule. The microcapsule had made up 10% of the RVE volume. 2 models were created and analysed using extended Finite Element Method (XFEM). In one model, the crack was centred while in the other model, the crack was off centred as shown in Figure 14.

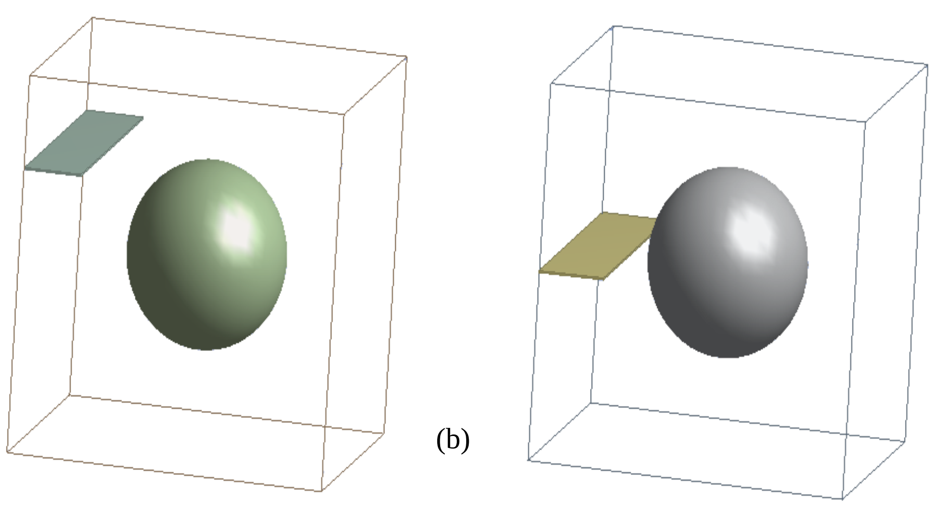

(a) (b)

Figure 14. RVE containing a single capsule with (a) off centred edge crack and (b) centred edge crack (Chen et al., 2013).

The RVE was subjected to a uniaxial tensile strain of 10% along the Y axis to induce mode 1 fracture. Using the rule of mixtures, it is generally agreed that composite properties are governed by the strength and volume fractions of their constituents. However, in their study, Chen et al. (2013) has found that the Young's Modulus of the microcapsules have negligible effects on the overall composite carrying capacity. They have verified the effect of the capsule elastic modulus on the RVE by varying the value from 3 to 5 GPa. It was also found that crack propagation in the matrix initiates crack formation in the microcapsule and facilitates the release of the healing agent into the crack. Consequently, in the off centred crack model, 2 parallel cracks were formed while in the crack centred model; the first crack turned and joined the secondary crack. Both phenomena are illustrated in Figure 14. In both cases, the crack propagation tends to be attracted towards the microcapsule.

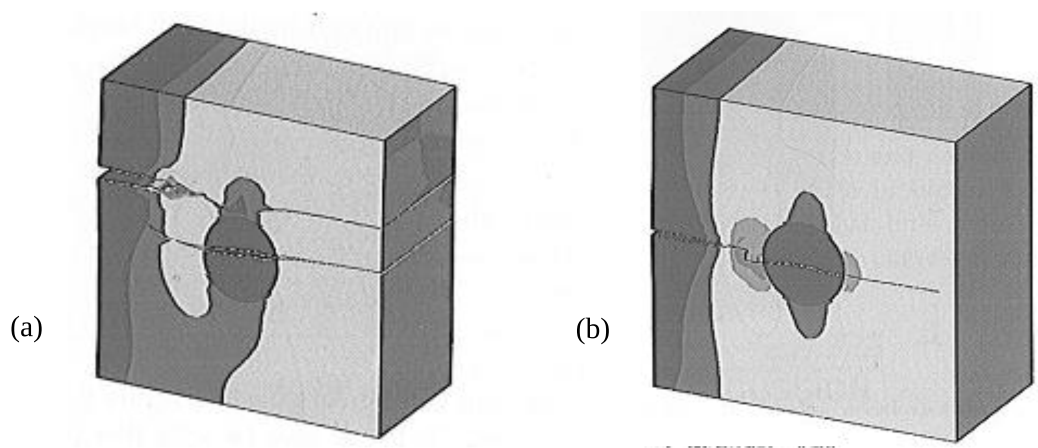

Figure 15. Crack propagation path in both models. It can be seen in (a) that two cracks are formed while in (b) the first crack turns and joins the secondary crack formed in the micro capsule (Chen et al., 2013).

2.15 Computational modelling of high speed deformation of materials

Plastic deformation in polymers is a multi-stage process and a physically consistent model needs to be able to re-create them. Polymers exhibit unusual elastic-plastic behaviour that classical plasticity constitutive models are unable to address. Many solid polymers undergo necking under both tensile and compressive stress. The finite element modelling of the ballistic impact behaviour of fabric armour carried out by Lim et al., (2003) has some important considerations worth mentioning. First, the detailed, high speed experimental analysis of impact would require difficult and costly high speed photographic measurements. Theoretical and finite element modelling provide cheaper alternatives to the aforementioned methods (Lim, Shim, & Ng, 2003).

Describing material behaviour under high speed damage is very complex. Modelling the material, its individual components and their interactions would require huge computational time and power. In the case of ballistic armour, those components would be the individual yarns and the interactions refer to the frictional, crimping, fraying and unravelling of the fibres (Lim et al., 2003). Due to the complexity of the fabric structure, the researchers were forced to resort to certain assumptions to simplify the analysis. The simplified finite element model for ballistic tests on fabric armour is illustrated in Figure 16. The results obtained from the simulation were compared to the experimental results (Lim et al., 2003).

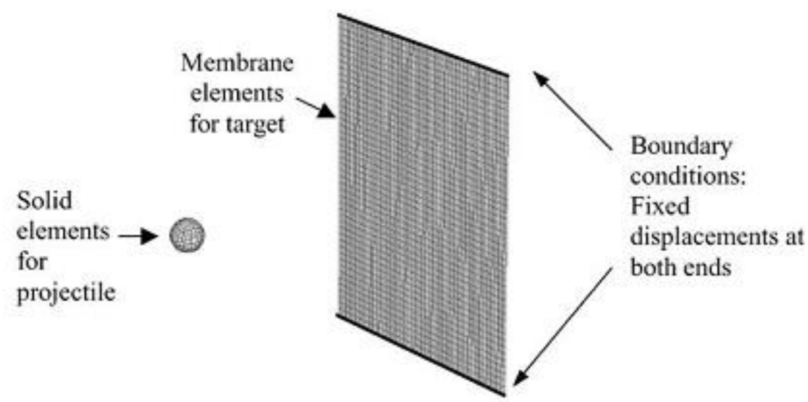

Figure 16. Finite element model of projectile and target (Lim et al., 2003).

The projectile was modelled using solid elements and the fabric was modelled using membrane elements. Both the projectile and the fabric were modelled in full to witness the ripple effects from the stress wave propagation through the fabric. The fabric was clamped on both ends and subject to impact by the projectile (Lim et al., 2003).

2.16 Multi-scale modelling of composite materials

Experimental studies of composite materials, especially the study of composites with micro/nano-scale reinforcements remain challenging due to the difficulty in observing how stresses are transferred and how the deformation occurs at such a small scale. Theoretical modelling and simulations can be used to fill in this gap. Computational models help provide insight into the composite behaviour (Shokrieh & Rafiee, 2010). Certain important considerations when modelling Carbon Nanotube Reinforced Polymers (CNTRP) are whether to model the CNT as a solid fibre or model the full lattice structure. Another consideration is how to model the interphase between the reinforcing material and the matrix.

2.17 Modelling the flow of resin in self-healing composites

Hall et al., 2015 have studied the flow of the healing agents through cracks in self-healing composites. They have found that it is important to deliver the correct amount of resin to the correct location and therefore, it is essential to understand how the liquid healing agent flows to the damage site from a single point or multiple points. They have created a model of the fluid flow leaving the healing storage and into the crack under the influence of a pressure gradient and/or capillary action. The flows involve complicated geometries, which may still be moving with respect to each other, free surface behaviour and chemical changes in the fluid.

They have also determined the relationship between the local pressure differential across the crack and the flow rate through it using Smooth Particle Hydrodynamics (SPH) SPH is a meshless Langrangian numerical method for fluid dynamics.

However, they did not simulate crack formation through the healing agent storage and the subsequent outflow of healing agent through the crack. Instead, they have simulated the flow of fluids of varying viscosities being forced through a crack (Figure 17) using a pressure gradient.

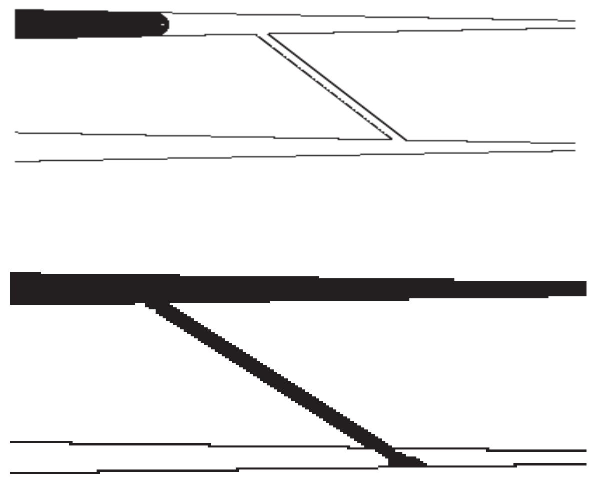

Figure 17. Geometry through which the healing agent is forced. The black area represents the fluid while the white, enclosed area represents the crack (Hall, Qamar, Rendall, & Trask, 2015).

They have found that a high fluid viscosity leads to a lower volume fraction filled. The relationship between the Reynolds number and the volume fraction filled during a fixed time is shown in the following chart:

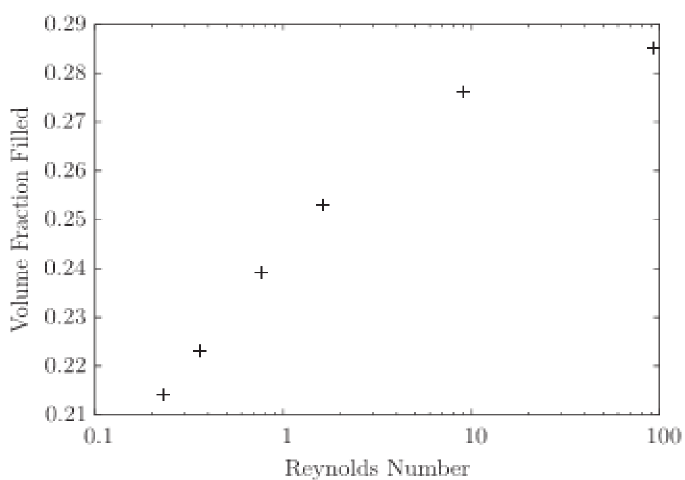

Figure 18. Figure showing the volume fraction filled vs Reynolds number of healing fluid at a fixed time of t = 1.258 x 10^{-4}s (Hall et al., 2015).

This means that a resin with a low viscosity will travel faster and fill both cracks more efficiently while a resin with high viscosity will travel slower and will not fill the adjacent lower crack to the same extent. This research could be useful when modelling the flow of self-healing agents in fractured self-healing composites.

3. Methodology

For this project, ANSYS Mechanical APDL 16.2 was used to develop a finite element model of a capsule reinforced composite material. Finite Element Analysis (FEA) was chosen over experimental methods as the former presents several advantages over the latter.

Experimental methods tend to be costly and time consuming and require the use of specialized equipment. Finite Element methods are very useful when time and resources are scarce. It is possible to create parametric representative models, run many simulations and obtain results relatively fast depending on the complexity of the analysis.

3.1 Overview of the Finite Element Method

The Finite Element Method (FEM) is an established numerical method which is used when analytical methods are too difficult to implement. The finite element method approximates exact solutions at discrete points called nodes. The geometric model must be divided into small, discrete regions known as elements. Adjacent elements are joined by nodes and collectively, they form a mesh. The elements must obey certain element boundary conditions while obeying regional boundary conditions to be compatible with each other.

A plane elasticity problem is used to illustrate the FE method (from Rockey et al., 1975).

Figure 19 shows (a) a continuum divided into triangular elements and (b) a triangular element. Each element node has 2 degrees of freedom indicated by U and V. There are three nodes per element, therefore each element has 6 degrees of freedom.

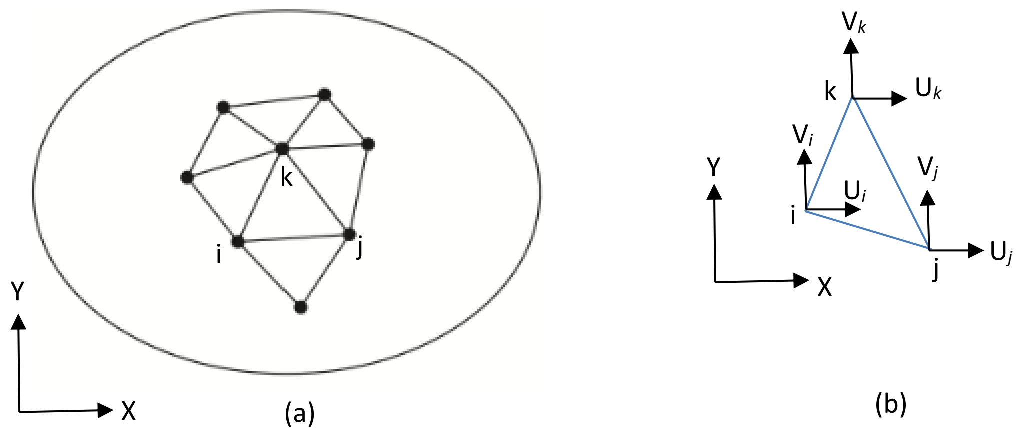

Figure 19. Figure showing (a) a continuum divided into triangular elements and (b) a triangular element.

Let the symbols *U(X,Y)* and *V(X,Y)* indicate displacement in the *X* and *Y* directions respectively at any point *(X,Y)* in the element. Assume *U(X,Y)* and *V(X,Y)* are linear in *X* and *Y* over the entire continuum domain. Therefore,

$$\left.\begin{aligned} U(X,Y) &= \alpha_1 + \alpha_2 X + \alpha_3 Y \\ V(X,Y) &= \beta_1 + \beta_2 X + \beta_3 Y \end{aligned}\right\} \quad - [1]$$

Where α and β are constants and are known as generalised co-ordinates. They are determined by solving eq [1] at the nodal coordinates (X_i, Y_i), (X_j, Y_j) and (X_k, Y_k) simultaneously where i, j and k are designated nodes for an element (see figure 19 (b)).

The displacement components *U(X,Y)* and *V(X,Y)* account for the internal displacement at any point in the element based on the nodal displacement vector $\overrightarrow{\delta_e}$, which is expressed as

$$\overrightarrow{\delta_e}^T = \left(U_i, V_i, U_j, V_j, U_k, V_k\right) \quad - [2]$$

(U(X,Y), V(X,Y)) is related to $\overrightarrow{\delta_e}$ via matrix, N, expressed as:

$$\begin{pmatrix} U(X,Y) \\ V(X,Y) \end{pmatrix} = N\overrightarrow{\delta_e} \qquad - [3]$$

This equation is derived from equations 1 and 2. N contains entries known as shape functions or interpolation functions which describe global coordinates of the nodes, i.e. (X_i, Y_i), (X_j, Y_j) and (X_k, Y_k) and any point *(X,Y)*, within the element.

In the plane stress and strain problems, the strain components, $\varepsilon_{xx}, \varepsilon_{yy}$ and γ_{xy} at any point in an element within the FE model can be represented as a single column matrix which is related to $\overrightarrow{\delta_e}$, via a strain-displacement matrix, **B**, expressed by:

$$\begin{pmatrix} \varepsilon_{xx} \\ \varepsilon_{yy} \\ \gamma_{xy} \end{pmatrix} = \mathbf{B}\overrightarrow{\delta_e} \qquad - [4]$$

B contains entries expressed in terms of global coordinates of the nodes in the element.

The stress components σ_{xx}, σ_{yy} and τ_{xy}, at any point in an element can also be represented as a single column matrix, **D**, expressed by:

$$\begin{pmatrix} \sigma_{xx} \\ \sigma_{yy} \\ \tau_{xy} \end{pmatrix} = \mathbf{D}\begin{pmatrix} \varepsilon_{xx} \\ \varepsilon_{yy} \\ \gamma_{xy} \end{pmatrix} \qquad - [5]$$

The element stiffness matrix can be determined by the expression:

$$\mathbf{k}_e = \int_s \mathbf{B}^{\mathrm{T}}\mathbf{D}\mathbf{B}\mathrm{d}s \qquad - [6]$$

Integrated over the volume, S, of the model. **B** and **D** are the strain-displacement (eq 4) and elasticity (eq 5) matrices respectively.

$\mathbf{k}_e$ related the element nodal force vector, $\overrightarrow{\mathrm{Q}_e}$ (which is the sum of body force and surface traction on the element), to the displacement within the element by the following equation:

$$\mathbf{k}_e\overrightarrow{\delta_e} = \overrightarrow{\mathrm{Q}_e} \qquad - [7]$$

By superposing $\mathbf{k}_e$ from all the elements within the FE model, we can obtain the global stiffness matrix, **K**, expressed by:

$$\mathbf{K} = \sum \mathbf{k}_e \qquad - [8]$$

The global stiffness matrix, **K**, is related to the global nodal displacement vector $\vec{\delta}$ and the applied nodal force vector, $\vec{Q}$, by the expression:

$$\mathbf{K}\vec{\delta} = \vec{Q} \qquad - [9]$$

$\vec{\delta}$ and $\vec{Q}$ are derived by superposing $\overrightarrow{\delta_e}$ and $\overrightarrow{\mathrm{Q}_e}$ respectively over all elements. $\vec{\delta}$ can then be determined by inverting **K**. From $\vec{\delta}$, $\overrightarrow{\delta_e}$ can then be found at every element in the model. From $\overrightarrow{\delta_e}$, strain components can be found at any point in the FE model by using equation [4] and the stress components can be determined using equation [5].

There are 3 stages in the finite element method:

- Pre-processing involves creating and meshing the model and applying stresses and boundary conditions. The model is divided into discrete stress elements during meshing. The material properties and element types are also chosen during pre-processing.
- Solving involves using the default solver to calculate the stresses in each stress element.
- Post-processing involves reading the data and processing the data into meaningful results.

A Representative Volume Element (RVE) consisting of random capsules embedded in a block matrix was developed to explore the viability of modelling a composite which contains a randomly scattered reinforcement phase. An initial model was created to establish dimensions and optimum meshing to be used in further models. The purpose of this model was also to ensure that the results are concurrent with the expected results for the range of properties tested. The mesh was refined and simplified at each step of the modelling process to ensure computational efficiency as well as result accuracy. Models with different types of random distribution in terms of capsule size and capsule distributions were created and will be further explained in the next section.

The variables frequently used in the following sections are listed and described below:

L_x and L_y denote the width and the height of the model along the X and Y axes. L_z denotes the length of the model along the Z axis (illustrated in Figure 19). r_o denotes the outer radius of the capsules, r_i is the inner radius and *t* is the capsule wall thickness. *N* is the number of capsules. E_m and v_m are the matrix modulus and matrix Poisson's ratio respectively. E_c and v_c are the capsule modulus and capsule Poisson's ratio respectively. E_{fill} and v_{fill} are the filler modulus and filler Poisson's ratio respectively. ε is the strain applied on the model and *S* is the displacement applied on one face of the model.

3.2 Description of models

Initially, a macro-scale model was developed. However, due to computational restrictions, it was not possible to simulate the behaviour of a piece of composite material with potentially thousands of micro-capsules. Therefore, it was decided to create a meso-scale model with a small number of capsules (<100). A meso-scale model is an intermediate scale model between the macro and micro scale models. The different scale models are illustrated in Figure 20.

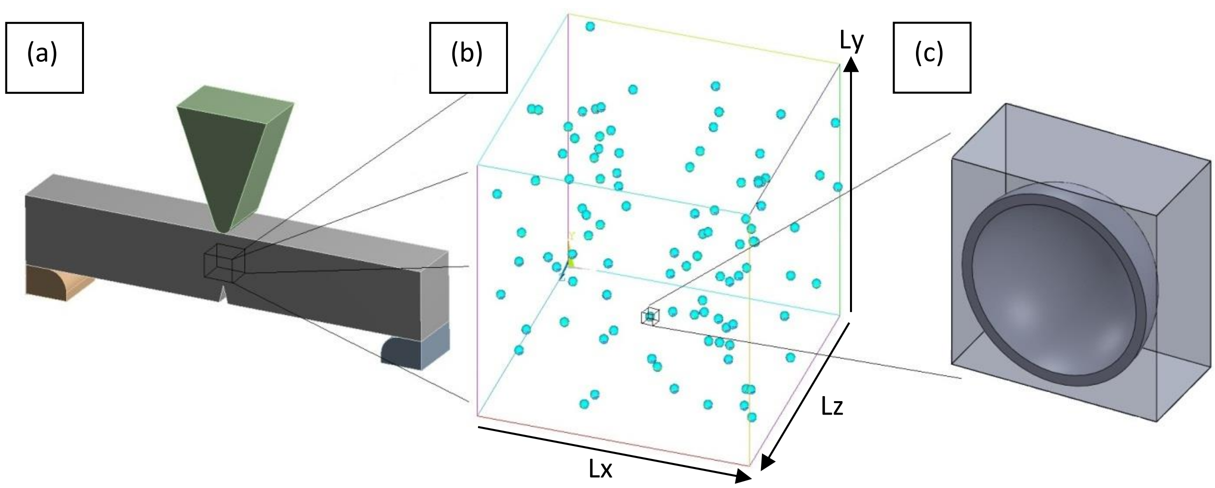

Figure 20. Illustration of the different scale models showing the (a) macro-scale model (b) meso-scale model (c) micro-scale model.

In our case, an example of a macro-scale model would be the full test sample and the micro-scale model would be a single capsule embedded in a block matrix. The meso or intermediate scale model would be multiple capsules embedded in a block matrix.

The models created are 3-dimensional RVE of a capsule reinforced composite material. They consist of randomly distributed capsules embedded in block matrices. The user can define the number of capsules, N, the capsule modulus, E_c, the capsule Poisson's ratio, v_c, the matrix modulus, E_m, the matrix Poisson's ratio, v_m, the capsule filler modulus, E_{fill}, and the capsule filler Poisson's ratio, v_{fill}. The user can also choose between 4 distinct capsule distribution models: dispersion, agglomeration, single agglomeration + dispersion and multiple agglomerations + dispersion. The different capsule distribution models are illustrated in Figure 21 and detailed in the next section.

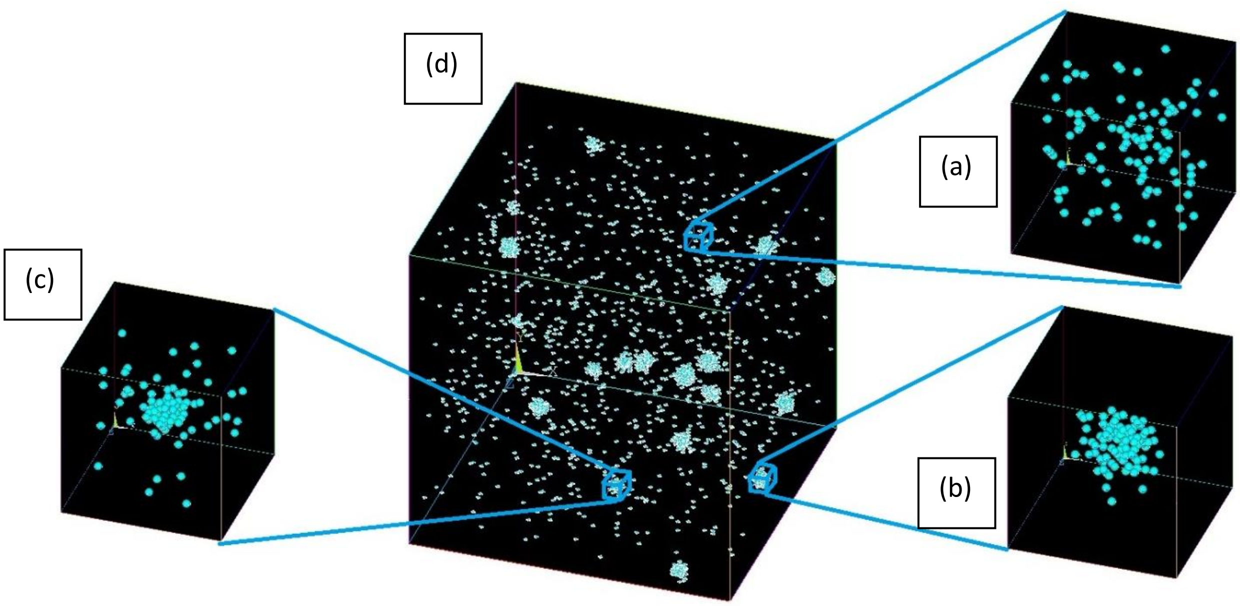

Figure 21. Illustration of the different capsule distribution models: (a) dispersion model (b) agglomeration model (c) single agglomeration + dispersion model and (d) multiple agglomerations + dispersion model.

The reason for having these different distribution models is when particle/capsule reinforced composites are manufactured; the particles/capsules are not uniformly distributed through the matrix. The particles tend to cluster up as observed in FESEM images of fracture surfaces by co-workers (Hia, Pasbakhsh, Chan, & Chai, 2016). There will be areas where capsules will cluster up and other areas where individual capsules will be randomly distributed as well as areas without capsules. The particle/capsule distribution is known to affect the properties of the composite and must be taken into consideration when creating 3D FEA models (Chawla et al., 2006; Wang et al., 2011). The multiple agglomeration + dispersion model is part of an effort to create simulations that are more accurate to real life composites. The different distribution models in Fig. 21 (a), (b) and (c) help us analyse each distribution individually and the final model in Fig. 21(d) help us analyse all the distributions combined.

Capsules are spherical in shape and can be either hollow or full. The user can define the capsule filler material properties by specifying the elastic modulus and the Poisson's ratio. The capsule has an inner radius of r_i and an outer radius of r_o. The capsule wall thickness is uniform and has a thickness: $t = r_o - r_i$. A single capsule embedded in a block matrix along with a sectional view is illustrated in Figure 22.

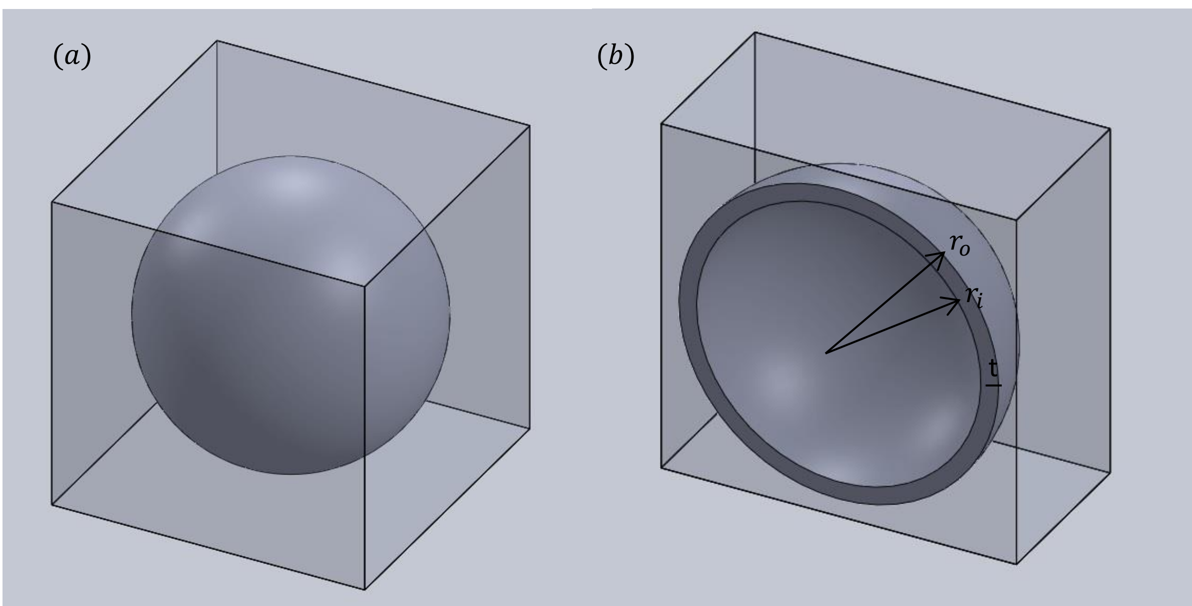

Figure 22. Illustration of (a) single, hollow capsule embedded in block matrix and (b) cross section of single, hollow capsule embedded in block matrix.

A basic damage model was also created to observe how the damage progresses inside of the different capsule distribution models.

3.2.1 Capsule dispersion model

In the first and simplest model, the capsules are randomly distributed inside the matrix. The capsules do not overlap or get into contact. There is always a minimum distance in the *x*,*y* and *z* directions between all capsules. Capsules do not overlap with the boundaries of the block matrix either. The reason for the spacing is that the software is unable to mesh and solve the model if the capsules overlap or are in contact. Models with different numbers of randomly scattered capsules with uniform distribution are illustrated in Figures 23(a) – 23(d).

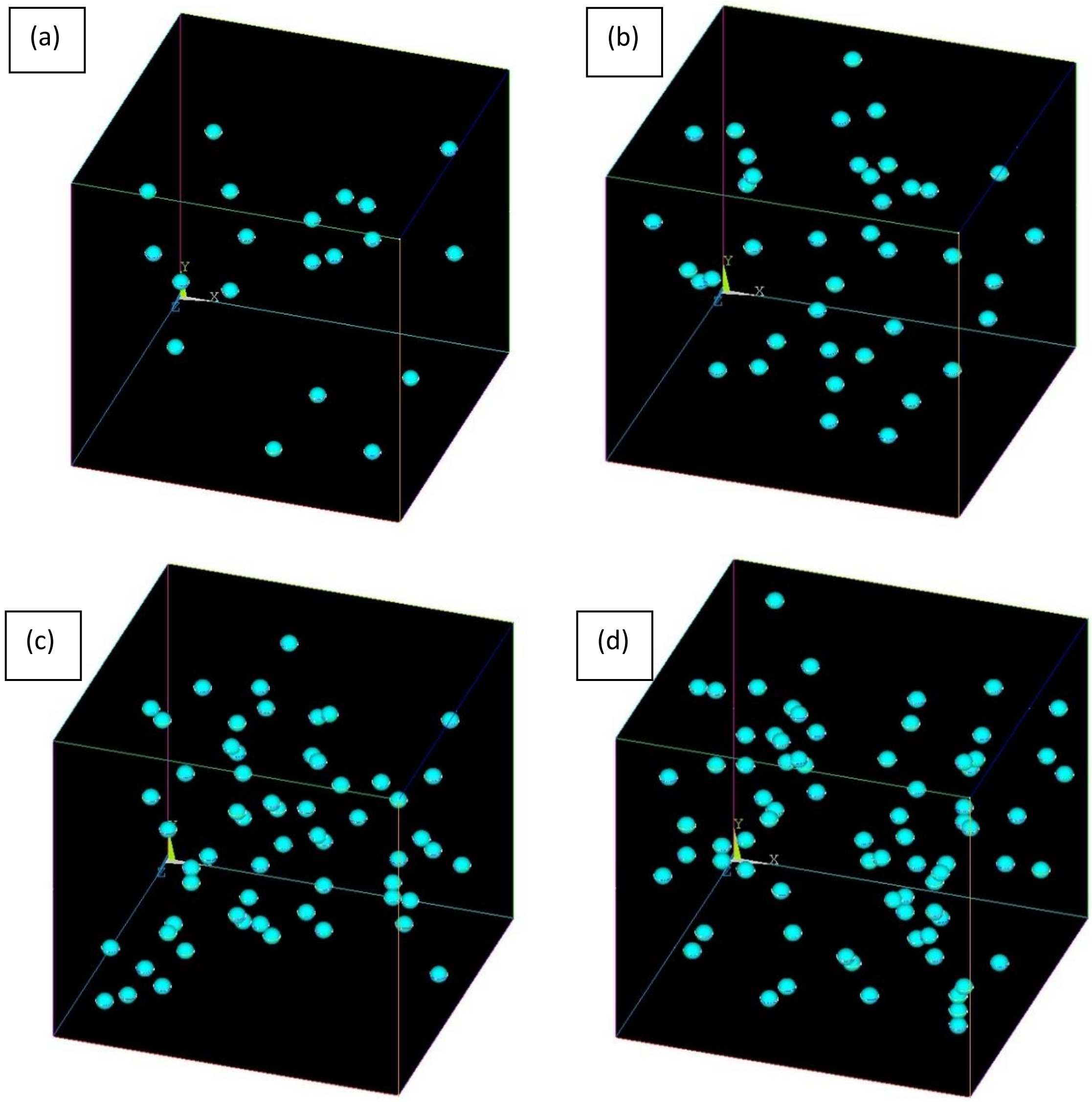

Figure 23. RVE with (a) 20 (b)40 (c) 60 (d) 80 capsules showing capsule dispersion.

3.2.2 Capsule agglomeration model

In the second model, the capsules are randomly scattered and follow a normal distribution.

The user can specify the mean point where the capsules will be concentrated as well as the standard deviation. The standard deviation dictates the degree to which the capsules are concentrated about the mean point. This capability will enable us to explore how various degrees of capsule agglomeration affect the mechanical properties of the model. Some of the models are illustrated in Figure 24(a) – (d).

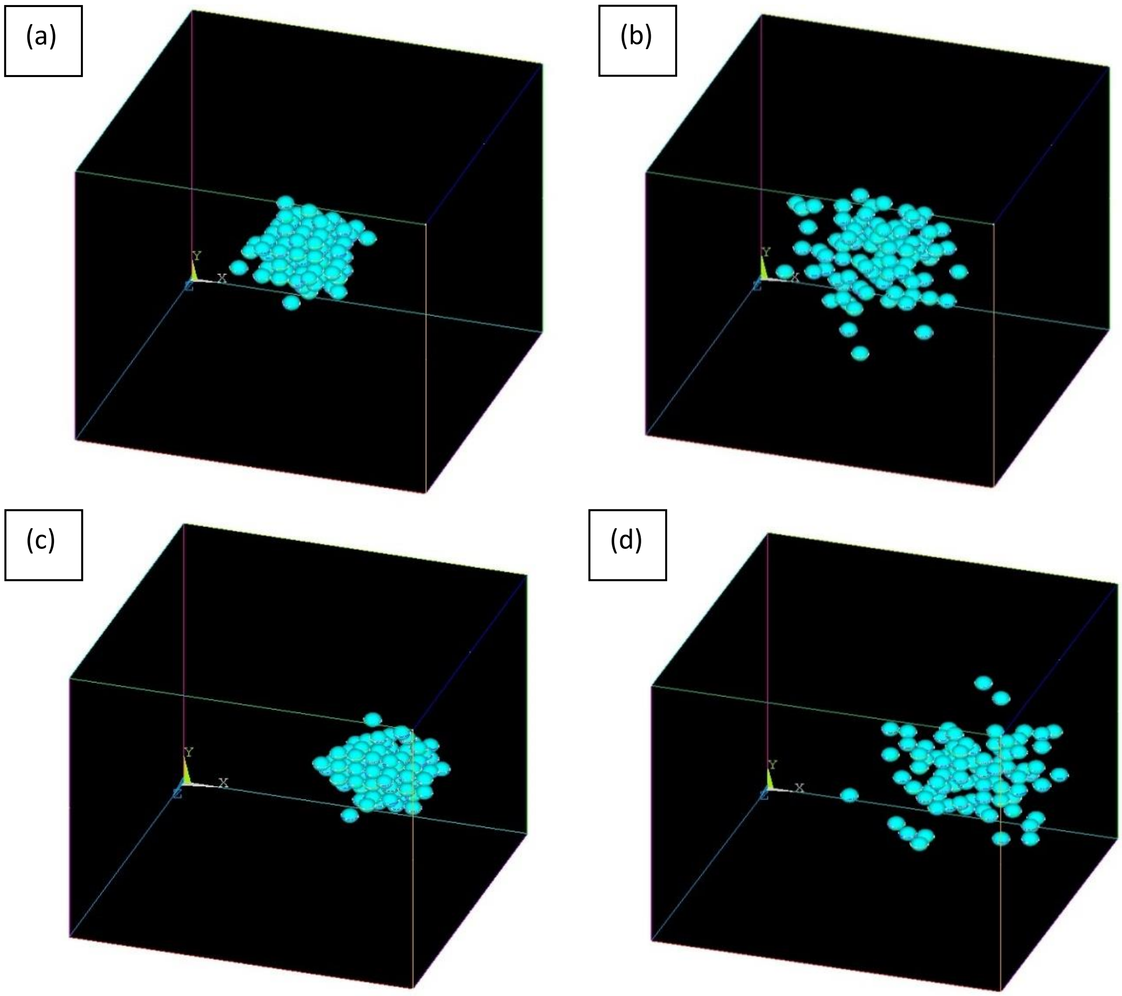

Figure 24. Figure illustrating various capsule agglomerations achievable by the model (a) mean centred around the (0.5Lx, 0.5Ly,0.5Lz) with std deviation = 1 (b) mean centered around (0.5Lx, 0.5Ly,0.5Lz) with std deviation = 2 (c) mean centred around (0.75Lx,0.5Ly,0.5Lz) with std deviation = 1 (c) mean centred around (0.75Lx,0.5Ly,0.5Lz) with std deviation = 2.

3.2.3 Single agglomeration + dispersion model

In the third model (Figure 25(a) – (d)), the capsules follow both normal and uniform distribution.

Like the agglomeration model, the user can specify the mean point where the capsules will be concentrated as well as the standard deviation. The user can also specify the number of capsules and the proportion of capsules that are agglomerated.

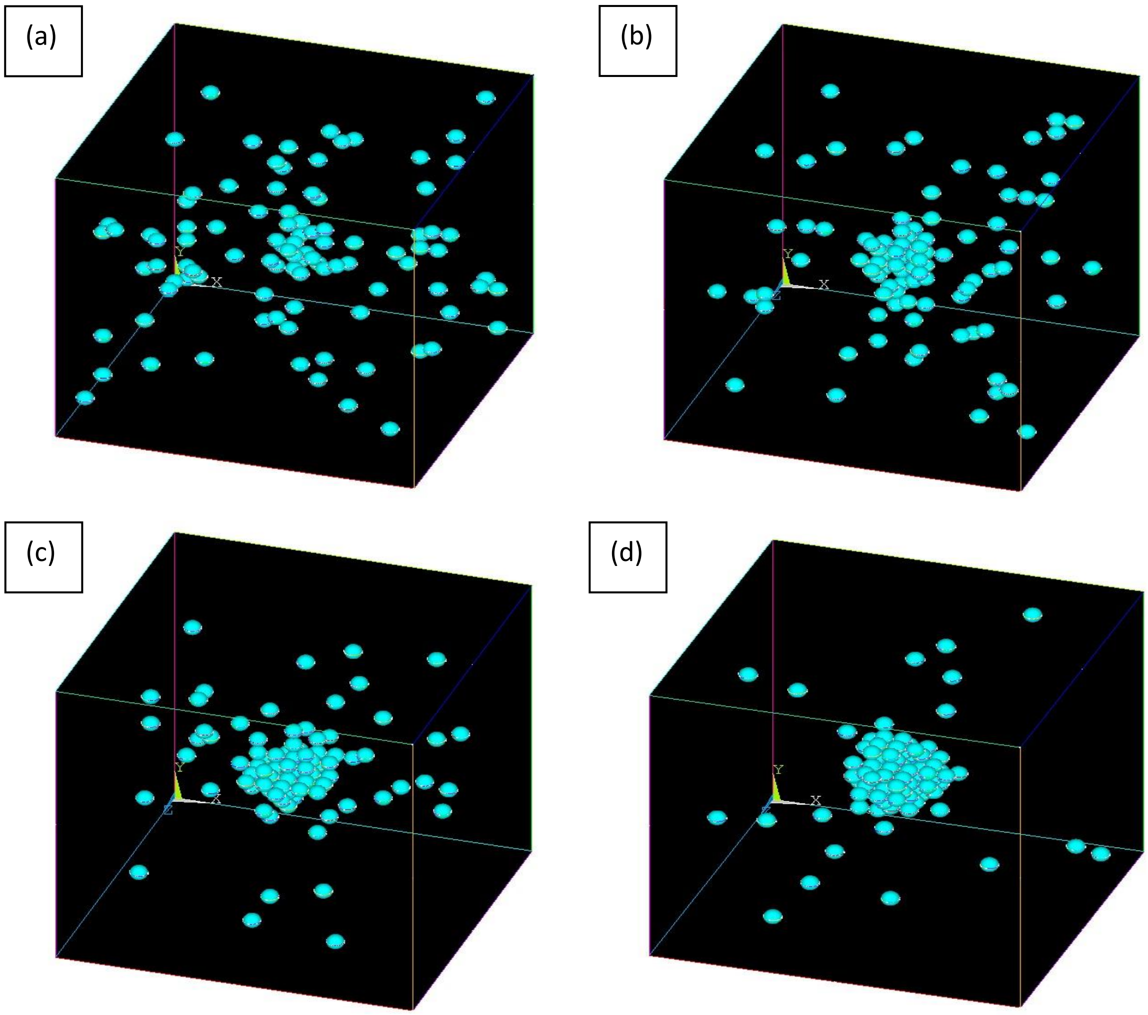

Figure 25. Figure illustrating the various percentages of agglomerations that can be achieved by the model. In this case the agglomeration is at the center of the matrix. The agglomeration can be placed anywhere inside the matrix. The Figures illustrate 100 capsules with (a) 20% (b) 40% (c) 60% (d) 80% agglomeration.

3.2.4 Multiple agglomerations + dispersion model

The final model combines all the previous models; however, the user has no control over specific parameters.

Unlike the previous two models, the agglomerations are randomly located and contain a random number of particles each. The user can specify the number of capsules, the number of agglomerations and the standard deviation. The model is illustrated in Figure 26(a) – (j).

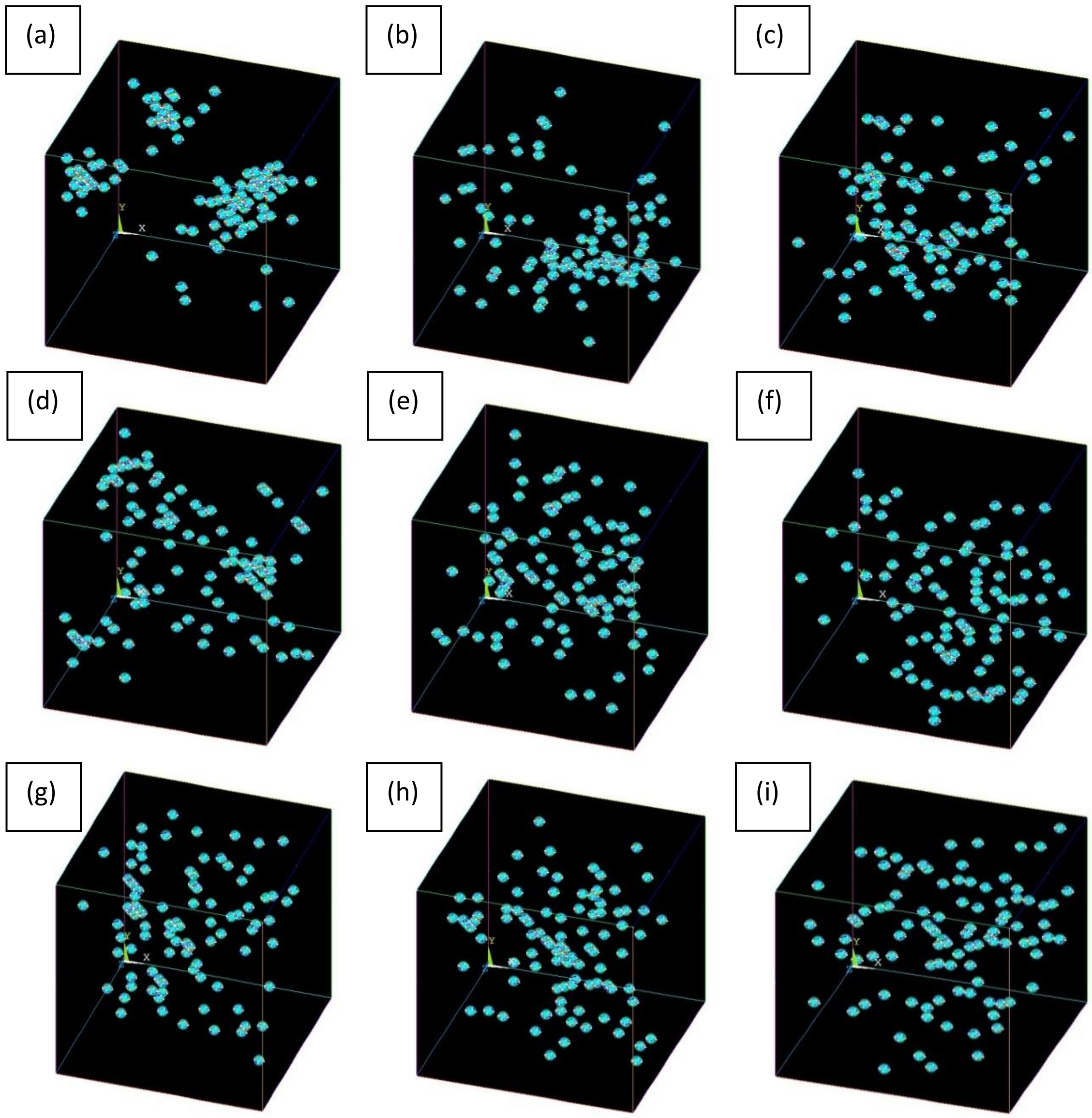

Figure 26. Illustration of multiple agglomerations+dispersion model. All models contain 100 capsules. The different models shown have the following parameters (a) 5 agglomerations, std dev = 1 (b) 5 agglomerations, std dev = 2 (c) 5 agglomerations, std dev = 3 (d) 10 agglomerations, std dev = 1 (e) 10 agglomerations, std dev = 2 (f) 10 agglomerations, std dev = 3 (g) 15 agglomerations, std dev = 1 (h) 15 agglomerations, std dev = 2 (i) 15 agglomerations, std dev = 3.

It can be observed that, for a constant number of capsules, as the number of agglomerations increases, the particles tend to look dispersed similar to the simple dispersion model in section 3.1.1. The same can be observed when the standard deviation is increased.

3.3 Material properties

Material properties of the matrix and capsules are listed in table 1. The material properties of Poly(urea-formaldehyde) were obtained from (Keller & Sottos, 2006).

Table 1. Material properties of components.

	Elastic modulus (Gpa)	Poisson ratio
Epoxy	3.5	0.34
Poly(urea-formaldehyde)	3.9	0.33

3.4 Material strength limits

Material strength limits of the matrix and capsules for the damage model are listed in table 2.

Table 2. Strength limit of material components.

	Tensile strength (Mpa)	Compressive strength (MPa)	Shear strength (MPa)
Epoxy	85	190	112
Poly(urea-formaldehyde)	0.07	0.14	0.1

3.5 Boundary conditions

The boundary conditions are as follows (illustrated in Figure 27):

u(BCFG) = 0
v(ABGH) = 0
w(HGFE) = 0
v(DCFE) = S

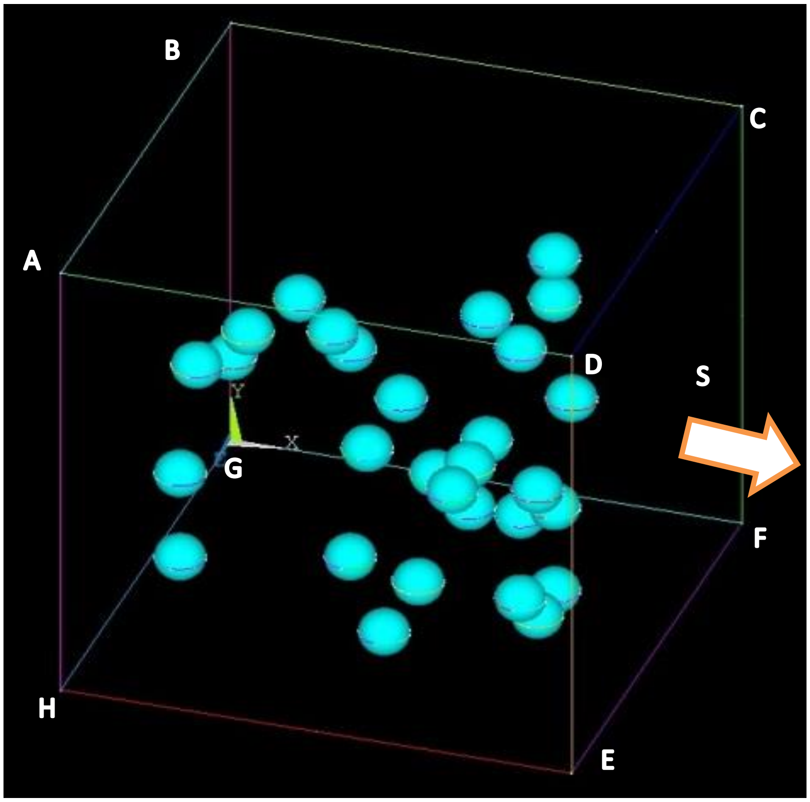

Figure 27. Illustration of boundary conditions.

Letters A-G mark the corners of the RVE, u, v and w denote the displacement in the x, y and z directions respectively and S is the displacement applied on face DCFE. Faces BCFG, ABGH and HGFE are restricted from moving in a perpendicular direction from the respective planes.

3.6 Meshing

Tetrahedral elements with 4 nodes (SOLID285) were used to mesh the entire model. Due to the irregular internal shape of the model, brick elements could not be used. The meshed model is illustrated in Figure 28.

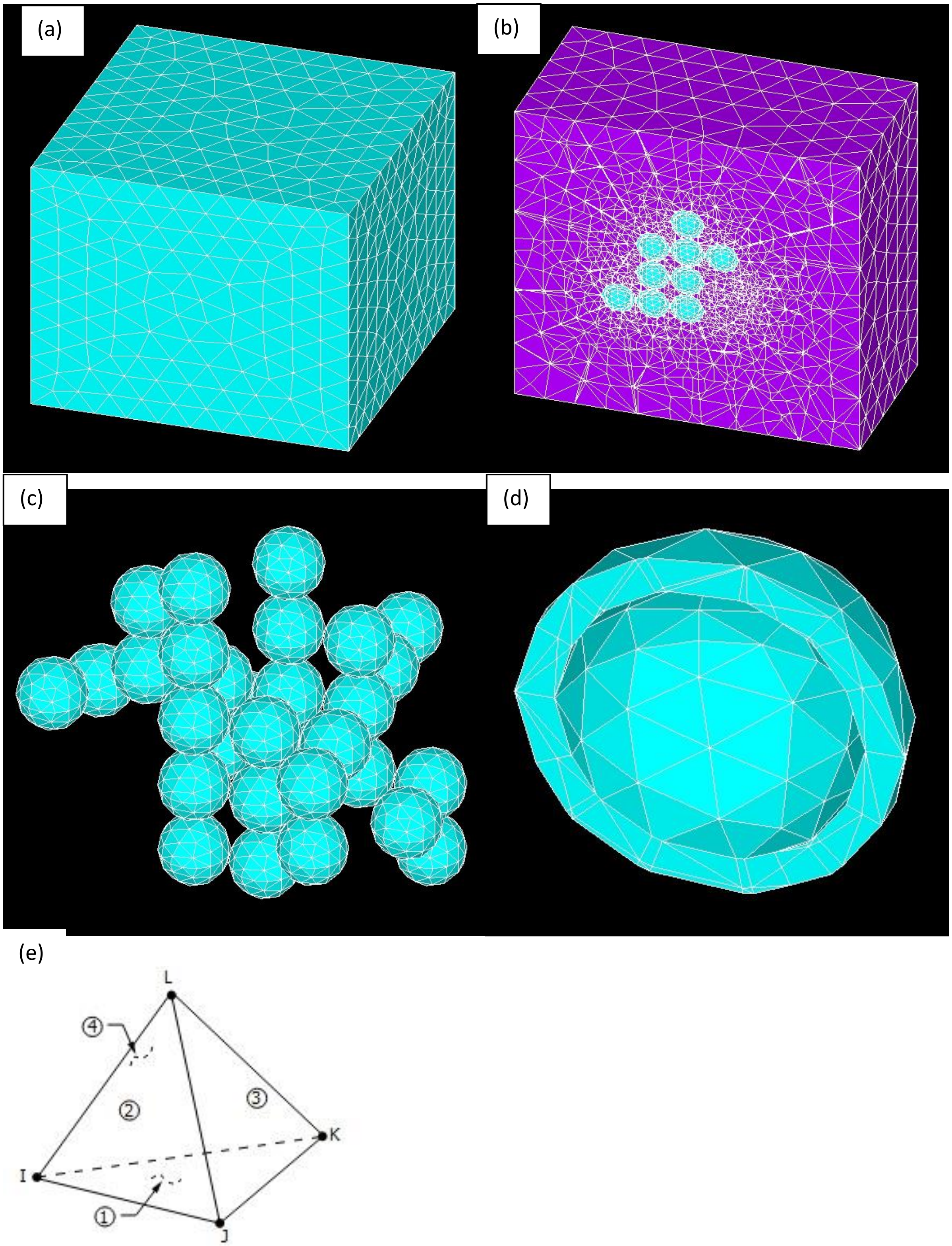

Figure 28. Illustration of RVE mesh showing (a) the matrix mesh (b) sectional view of the matrix showing embedded capsules (c) close-up of meshed capsules (d) sectional view of single meshed capsule (e) 4-Node Tetrahedral element (SOLID 285).

3.7 Instruction manual

This section will provide instructions on how to specify parameters, run the code and obtain results.

Step 1: Open the code file and specify the material and geometric parameters. For each model, the parameters that can be specified will be slightly different and will be highlighted.

a. **Dispersion model:**

For the dispersion model, the following parameters can be specified: (a) material properties, (b) geometric values such as RVE dimensions and capsule external and internal radii, (c) number of capsules, (d) strain, (e) mesh parameters such as line divisions and element type.

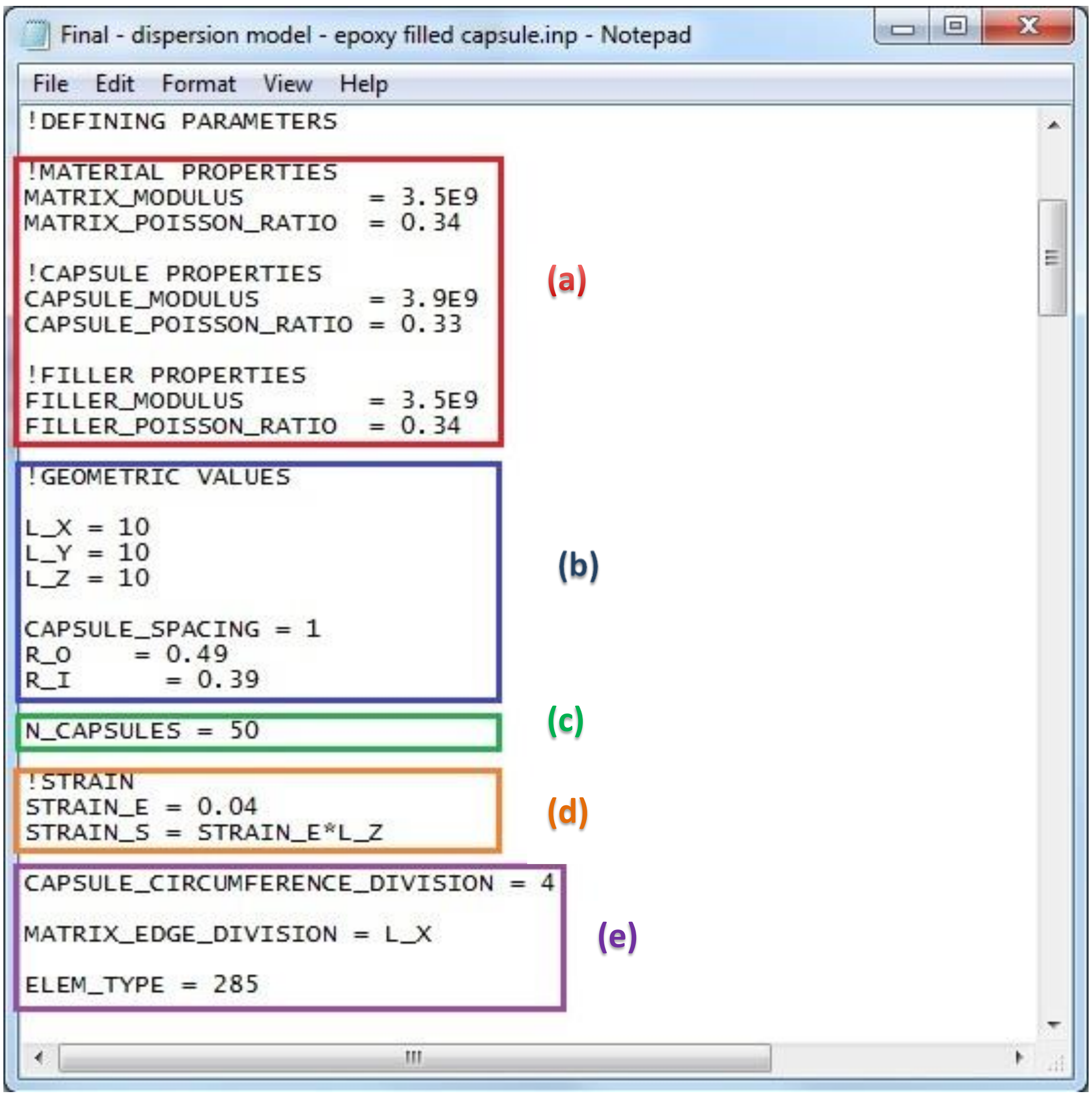

b. Agglomeration model:

In addition to the parameters that can be specified in the previous model, the user can specify the (a) normal distribution parameters whereby the center of the agglomeration and the standard distribution in each plane can be specified.

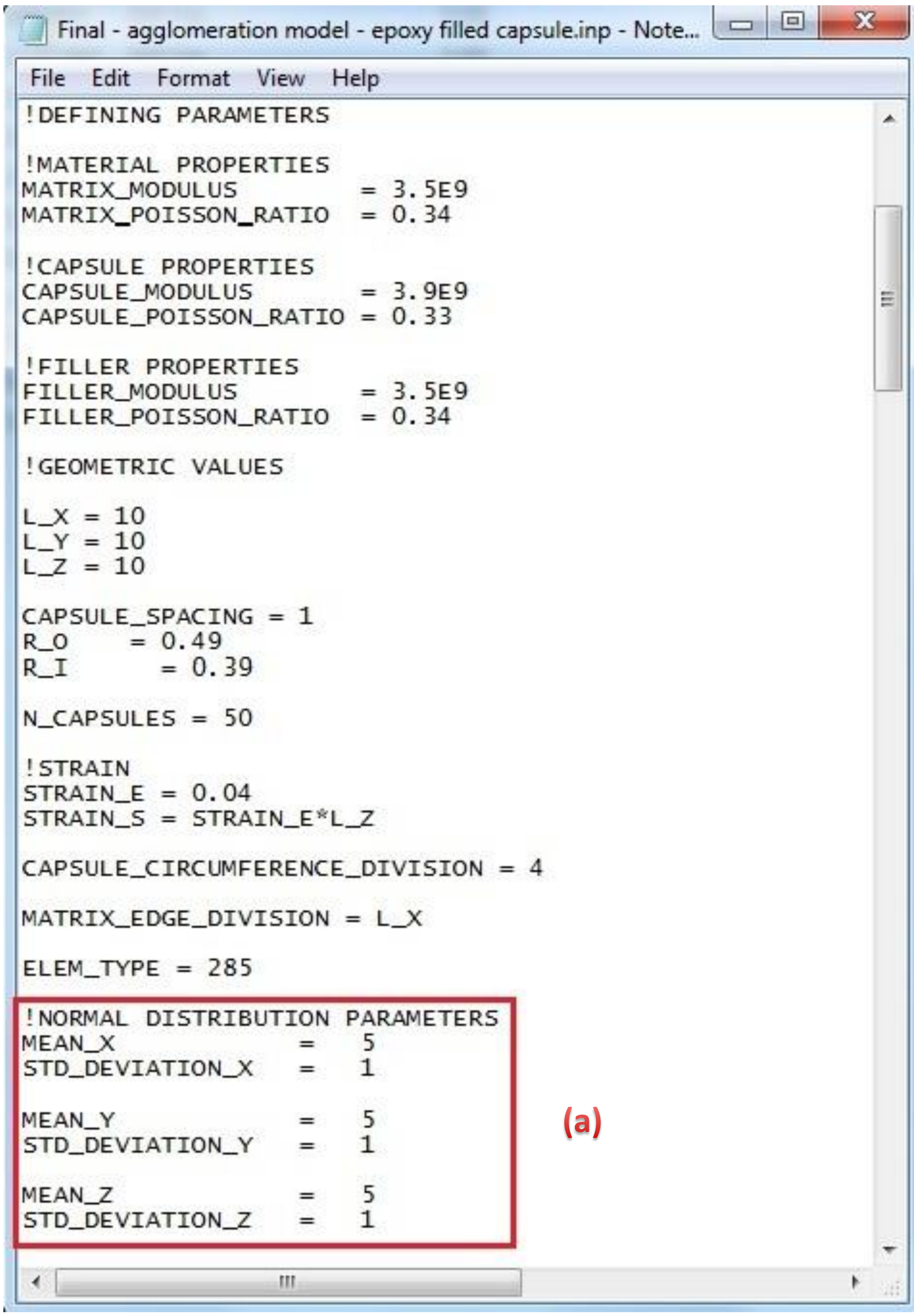


```
!DEFINING PARAMETERS

!MATERIAL PROPERTIES
MATRIX_MODULUS        = 3.5E9
MATRIX_POISSON_RATIO  = 0.34

!CAPSULE PROPERTIES
CAPSULE_MODULUS       = 3.9E9
CAPSULE_POISSON_RATIO = 0.33

!FILLER PROPERTIES
FILLER_MODULUS        = 3.5E9
FILLER_POISSON_RATIO  = 0.34

!GEOMETRIC VALUES

L_X = 10
L_Y = 10
L_Z = 10

CAPSULE_SPACING = 1
R_O    = 0.49
R_I      = 0.39

N_CAPSULES = 50

!STRAIN
STRAIN_E = 0.04
STRAIN_S = STRAIN_E*L_Z

CAPSULE_CIRCUMFERENCE_DIVISION = 4

MATRIX_EDGE_DIVISION = L_X

ELEM_TYPE = 285

!NORMAL DISTRIBUTION PARAMETERS
MEAN_X           =    5
STD_DEVIATION_X  =    1

MEAN_Y           =    5
STD_DEVIATION_Y  =    1

MEAN_Z           =    5
STD_DEVIATION_Z  =    1
```

c. Single agglomeration + dispersion model:

In addition to the parameters that can be specified in the previous models, the user can specify (a) the ratio of capsules that are agglomerated.

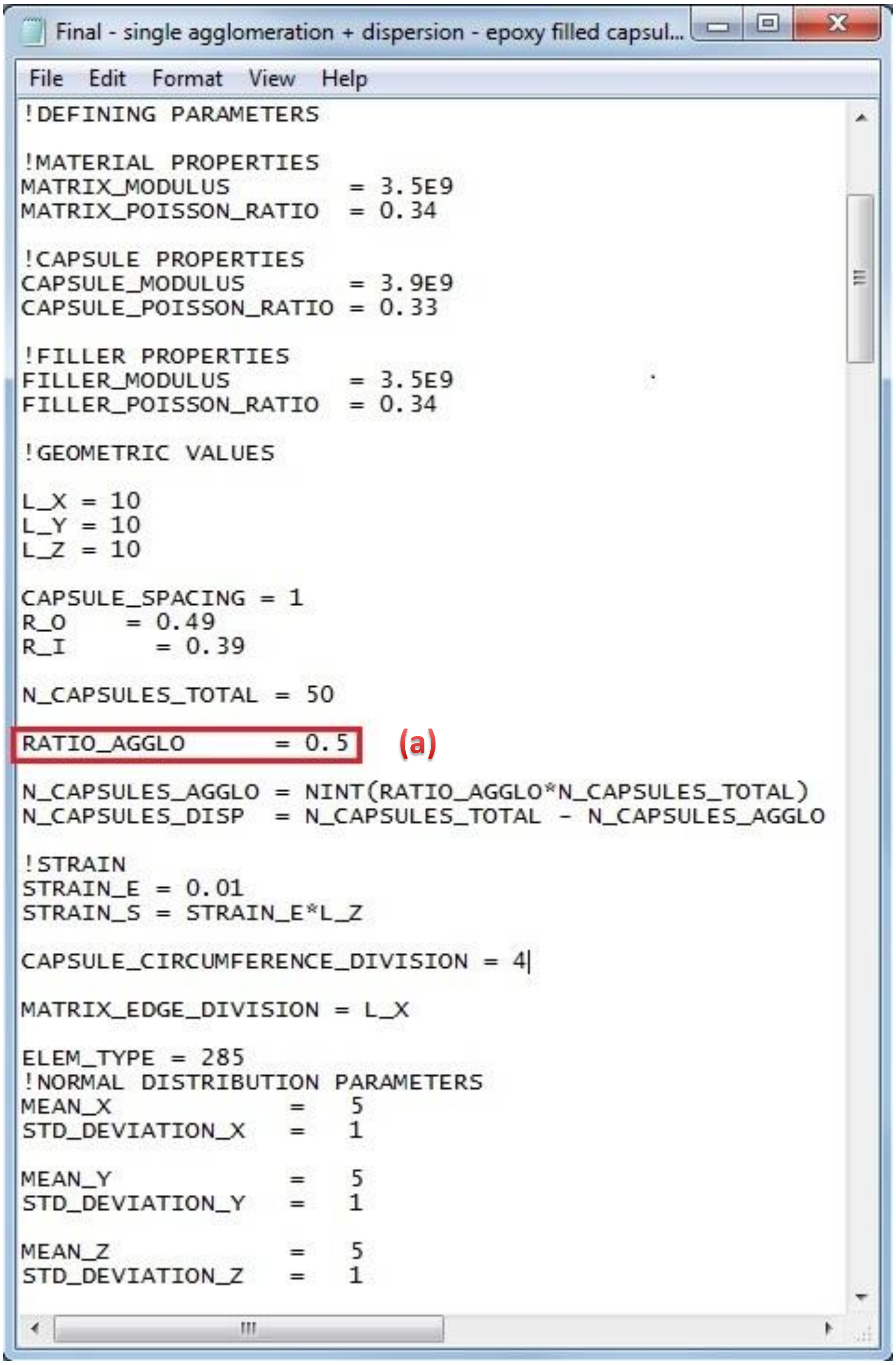

Final - single agglomeration + dispersion - epoxy filled capsul...

File Edit Format View Help

```
!DEFINING PARAMETERS

!MATERIAL PROPERTIES
MATRIX_MODULUS         = 3.5E9
MATRIX_POISSON_RATIO   = 0.34

!CAPSULE PROPERTIES
CAPSULE_MODULUS        = 3.9E9
CAPSULE_POISSON_RATIO  = 0.33

!FILLER PROPERTIES
FILLER_MODULUS         = 3.5E9
FILLER_POISSON_RATIO   = 0.34

!GEOMETRIC VALUES

L_X = 10
L_Y = 10
L_Z = 10

CAPSULE_SPACING = 1
R_O     = 0.49
R_I       = 0.39

N_CAPSULES_TOTAL  = 50

RATIO_AGGLO         = 0.5

N_CAPSULES_AGGLO  = NINT(RATIO_AGGLO*N_CAPSULES_TOTAL)
N_CAPSULES_DISP   = N_CAPSULES_TOTAL - N_CAPSULES_AGGLO

!STRAIN
STRAIN_E = 0.01
STRAIN_S = STRAIN_E*L_Z

CAPSULE_CIRCUMFERENCE_DIVISION = 4

MATRIX_EDGE_DIVISION = L_X

ELEM_TYPE  = 285
!NORMAL DISTRIBUTION PARAMETERS
MEAN_X              =    5
STD_DEVIATION_X     =    1

MEAN_Y              =    5
STD_DEVIATION_Y     =    1

MEAN_Z              =    5
STD_DEVIATION_Z     =    1
```

(a)

d. Multiple agglomerations + dispersion model:

In this model, the user can specify (a) the number of agglomerations and (b) the standard deviation that dictates how tightly packed the capsules are. However, unlike the previous 2 agglomeration models, the user cannot specify the location of the agglomerations are those are random.

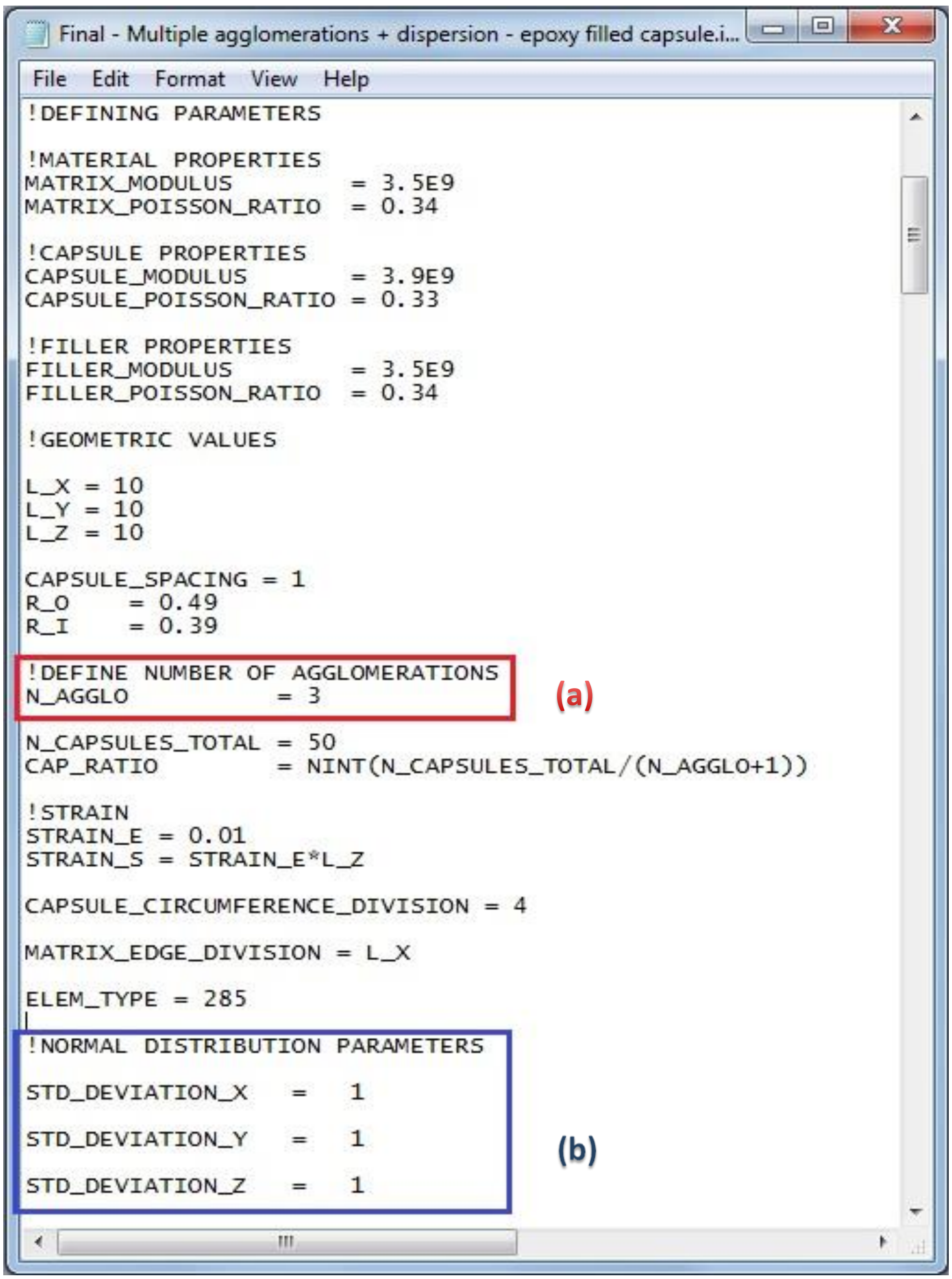


```
!DEFINING PARAMETERS

!MATERIAL PROPERTIES
MATRIX_MODULUS         = 3.5E9
MATRIX_POISSON_RATIO   = 0.34

!CAPSULE PROPERTIES
CAPSULE_MODULUS        = 3.9E9
CAPSULE_POISSON_RATIO  = 0.33

!FILLER PROPERTIES
FILLER_MODULUS         = 3.5E9
FILLER_POISSON_RATIO   = 0.34

!GEOMETRIC VALUES

L_X = 10
L_Y = 10
L_Z = 10

CAPSULE_SPACING = 1
R_O     = 0.49
R_I     = 0.39

!DEFINE NUMBER OF AGGLOMERATIONS
N_AGGLO              = 3

N_CAPSULES_TOTAL  = 50
CAP_RATIO            = NINT(N_CAPSULES_TOTAL/(N_AGGLO+1))

!STRAIN
STRAIN_E = 0.01
STRAIN_S = STRAIN_E*L_Z

CAPSULE_CIRCUMFERENCE_DIVISION = 4

MATRIX_EDGE_DIVISION = L_X

ELEM_TYPE = 285

!NORMAL DISTRIBUTION PARAMETERS

STD_DEVIATION_X    =    1

STD_DEVIATION_Y    =    1

STD_DEVIATION_Z    =    1
```

Step 2: Scroll down in the code and specify the output parameters.

(a) Select the location where nodal data is to be extracted, specify the stress component to be extracted and retrieve the nodal stress.

(b) Specify the output file name and file extension.

(c) Specify the target folder where the file will be written.

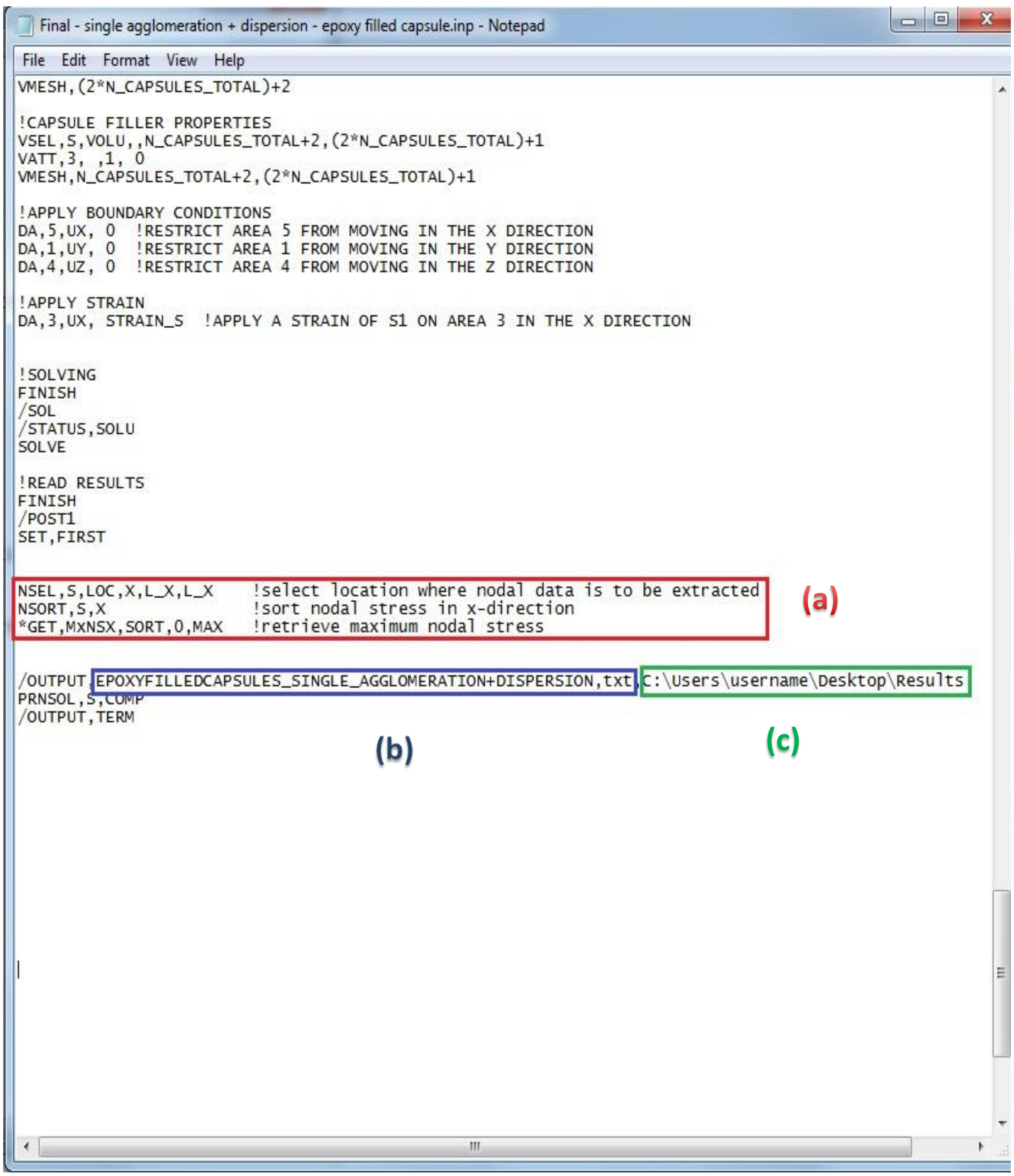


```
VMESH,(2*N_CAPSULES_TOTAL)+2

!CAPSULE FILLER PROPERTIES
VSEL,S,VOLU,,N_CAPSULES_TOTAL+2,(2*N_CAPSULES_TOTAL)+1
VATT,3, ,1, 0
VMESH,N_CAPSULES_TOTAL+2,(2*N_CAPSULES_TOTAL)+1

!APPLY BOUNDARY CONDITIONS
DA,5,UX, 0  !RESTRICT AREA 5 FROM MOVING IN THE X DIRECTION
DA,1,UY, 0  !RESTRICT AREA 1 FROM MOVING IN THE Y DIRECTION
DA,4,UZ, 0  !RESTRICT AREA 4 FROM MOVING IN THE Z DIRECTION

!APPLY STRAIN
DA,3,UX, STRAIN_S  !APPLY A STRAIN OF S1 ON AREA 3 IN THE X DIRECTION


!SOLVING
FINISH
/SOL
/STATUS,SOLU
SOLVE

!READ RESULTS
FINISH
/POST1
SET,FIRST

NSEL,S,LOC,X,L_X,L_X     !select location where nodal data is to be extracted
NSORT,S,X                !sort nodal stress in x-direction
*GET,MXNSX,SORT,0,MAX    !retrieve maximum nodal stress

/OUTPUT,EPOXYFILLEDCAPSULES_SINGLE_AGGLOMERATION+DISPERSION,txt,C:\Users\username\Desktop\Results
PRNSOL,S,COMP
/OUTPUT,TERM
```

Step 3: Open APDL, (a) click File → read input from.

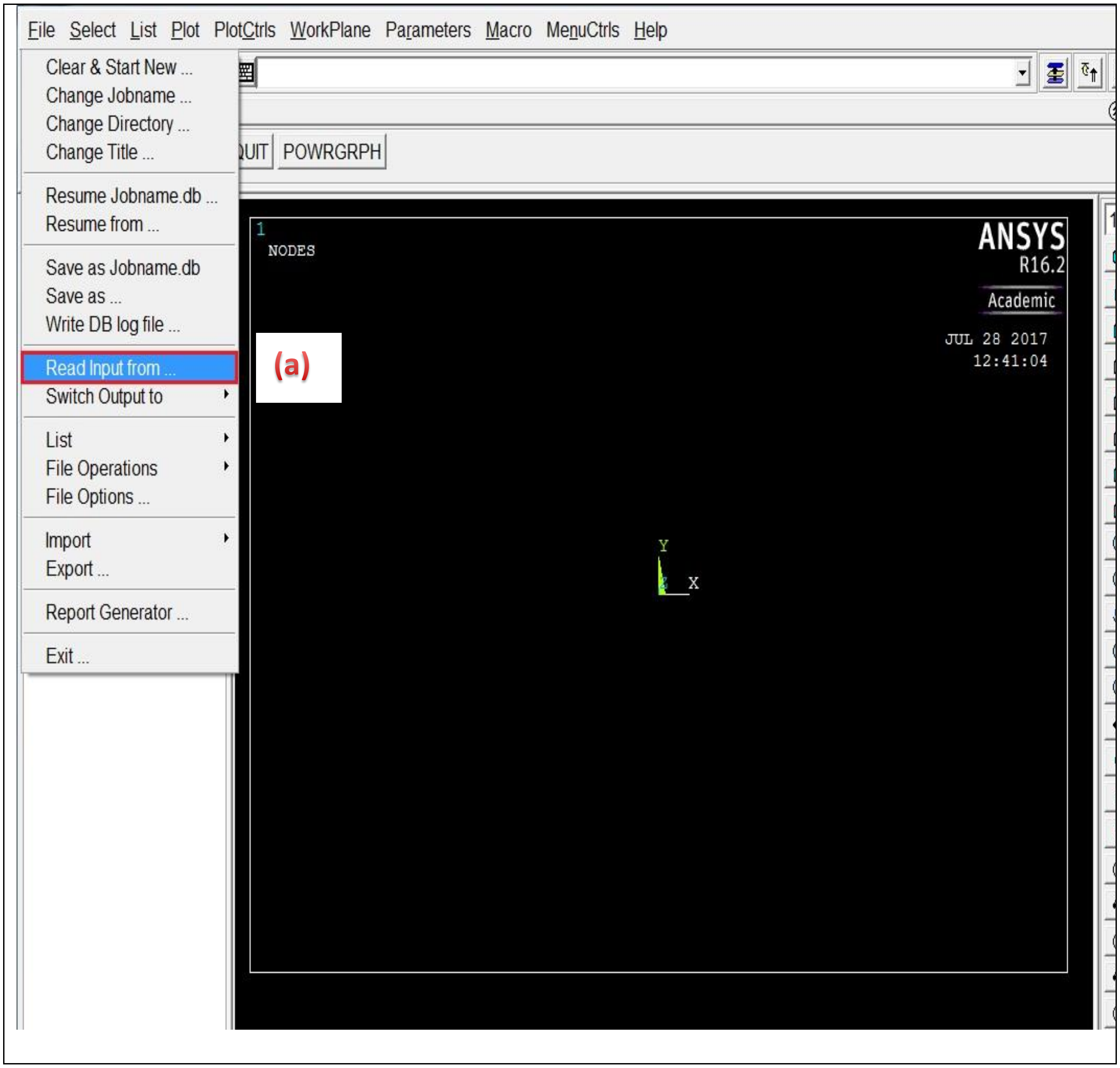

Step 4: Select (a) the folder where the file is located and (b) the code file to be read.

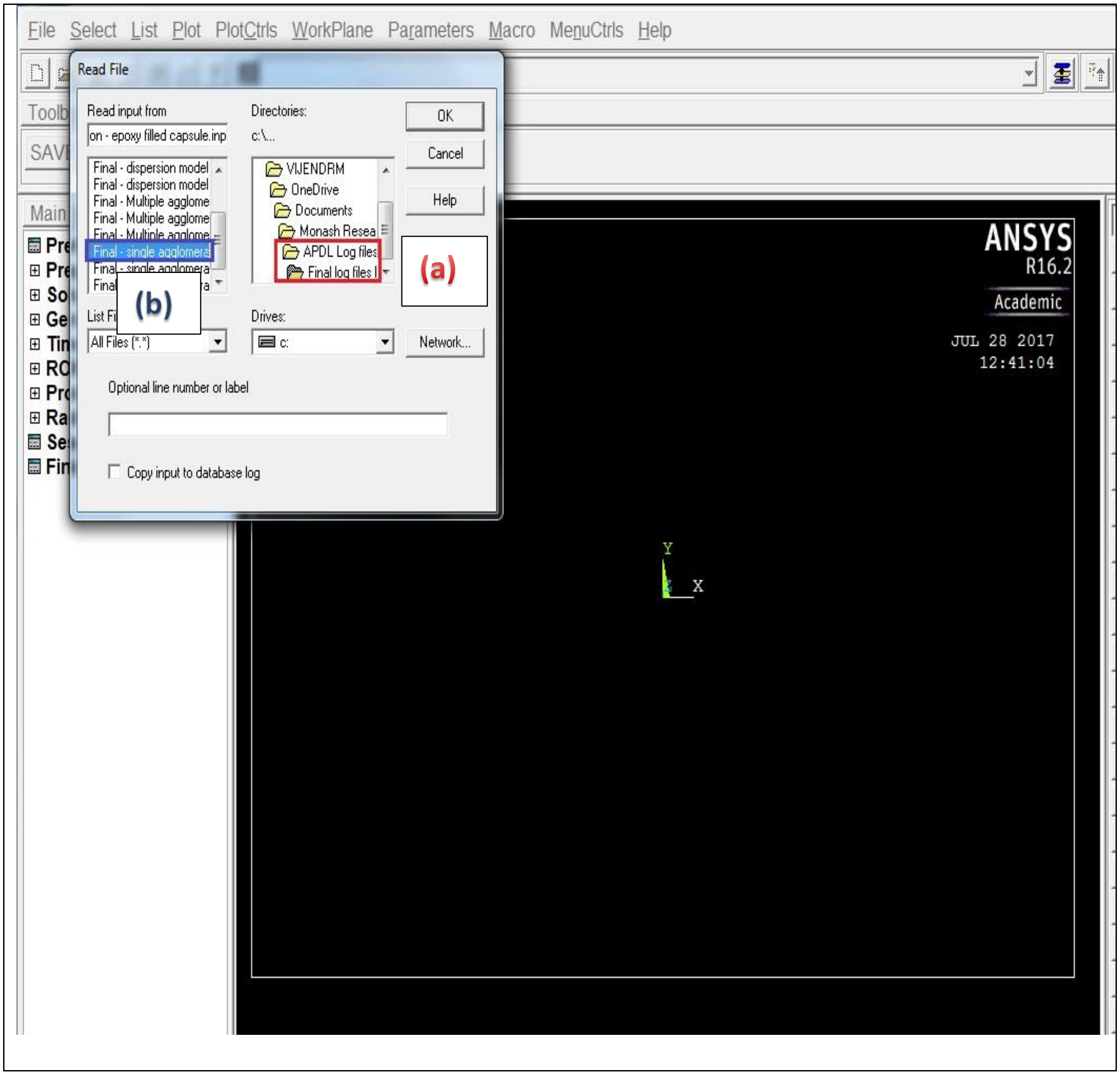

Step 5: Viewing and processing the output file.

The output file will look like this:

```
File  Edit  Format  View  Help

PRINT S     NODAL SOLUTION PER NODE

 ***** POST1 NODAL STRESS LISTING *****

 LOAD STEP=     1  SUBSTEP=     1
  TIME=    1.0000      LOAD CASE=   0

 THE FOLLOWING X,Y,Z VALUES ARE IN GLOBAL COORDINATES

   NODE     SX          SY          SZ          SXY         SYZ         SXZ
   3269  0.14064E+09 -17953.      -3477.6      3299.9     -15283.      8847.7
   3271  0.14063E+09  5626.5      107.22     -18999.     -15940.      7826.1
   3270  0.14061E+09 -3487.6      15817.      -7078.6     -25760.     -15602.
   3264  0.14059E+09  4360.0      49340.       6911.5     -8376.3      26835.
   3272  0.14057E+09 -239.52      16560.     -14741.     -10727.     -22542.
   3262  0.14053E+09  14787.      8392.1      17150.     -25913.      8218.0
   3268  0.14050E+09  36269.     -4442.4     -31559.      9413.1     -19272.
   3265  0.14047E+09  44101.      17713.     -33197.     -28173.      18479.
   3263  0.14045E+09 -15238.      487.59      5240.4     -43414.     -12170.
   3266  0.14043E+09 -29757.      23029.     -1793.6     -12952.     -12393.
   3261  0.14043E+09  6200.9      32953.      19207.      20006.      22348.
   3249  0.14042E+09  10453.      94075.     -7938.0     -21197.      41427.
   3248  0.14035E+09 -4967.8     0.10490E+06  7493.0      20841.      37421.
   3244  0.14035E+09  22380.     -21849.      12720.     -35401.      11634.
   3258  0.14034E+09 0.12567E+06  11489.     -44550.     -1095.4     -2174.7
   3267  0.14034E+09  34202.      33790.     -28246.      30535.     -13114.
   3245  0.14030E+09  8521.4      2286.9      4238.4     -59504.     -5578.0
   3243  0.14030E+09  22606.     -666.20      12331.      7353.4      14351.
   3253  0.14029E+09 -20687.      41524.     -5791.1     -16839.     -9964.8
   3250  0.14027E+09  55708.      98433.     -13880.     -44112.      28889.
   3254  0.14026E+09 -10322.      45717.     -16089.      21812.     -16601.
   3257  0.14025E+09 0.10644E+06  28757.     -32643.     -38231.      13126.
   3259  0.14025E+09 0.11218E+06  12548.     -27066.      31476.     -4154.6
   3247  0.14025E+09  20419.      96529.      3050.2      44162.      20265.
   3220  0.14023E+09  26948.     -21297.      7166.6     -7385.6      11535.
   3221  0.14023E+09  9240.8     -31012.      733.07     -42611.      4012.1
   3242  0.14023E+09  32711.      37303.      12278.      38829.      16286.
   3252  0.14023E+09 -32303.      8980.3      752.54     -51987.     -10826.
   3226  0.14023E+09 -8034.3     0.15958E+06 -6139.7      5870.8      29663.
   3255  0.14017E+09  53443.      42227.     -9682.9      49727.      2491.7
   3246  0.14017E+09 -7290.2      4310.2     -1271.9     -63342.      1753.5
   3225  0.14017E+09  7478.9     0.15003E+06 -208.37      35420.      16605.
   3260  0.14016E+09  96404.      36341.     -15373.      50851.     -1210.2
   3237  0.14015E+09 0.16441E+06  9577.9     -15382.     -15623.      7501.0
   3222  0.14015E+09 -16973.     -28415.     -3306.6     -65476.     -2493.0
   3227  0.14014E+09  13539.     0.16304E+06 -8820.1     -28968.      23657.
   3231  0.14013E+09 -53291.      15376.     -7758.2     -24622.      1295.2

 ***** POST1 NODAL STRESS LISTING *****

 LOAD STEP=     1  SUBSTEP=     1
  TIME=    1.0000      LOAD CASE=   0

 THE FOLLOWING X,Y,Z VALUES ARE IN GLOBAL COORDINATES

   NODE     SX          SY          SZ          SXY         SYZ         SXZ
   3251  0.14013E+09  90453.      71801.     -20748.     -52554.      14466.
```

It can be viewed using Notepad and the information can be extracted and plotted on Microsoft Excel or Matlab.

Non-linear damage model:

The progressive damage model is considered as a non-linear model because the stiffness of the model will change as the analysis progresses. In this model, the damage initiation criteria and the damage evolution law are specified. Note that progressive damage refers to how the damage progresses spatially throughout the model.

The damage initiation criteria are specified by entering the material strength limits listed in table 2 into the code. The damage evolution law is then specified. The damage evolution law dictates how damage progresses through the model. In this model, we have chosen the material property degradation (MPDG) method as the damage evolution law. This means that, once the stress (tensile, compressive or shear) of an element reaches the strength limit of the material specified for that element, the element will undergo an instant stiffness reduction (both tensile and compressive). In this case, an arbitrary stiffness reduction of 70% was chosen.

For this model, steps 1-3 in the linear section should be followed and the material strength limits must be specified as follows:

(a) Assign values to the variables: Matrix tensile strength, matrix compressive strength, matrix shear strength, capsule tensile strength, capsule compressive strength, capsule shear strength, filler tensile strength, filler compressive strength, filler shear strength. The solid epoxy filled capsule RVE is used as an example.

```
File  Edit  Format  View  Help

/Filename,non_linear_Epoxy Filled_99 capsules_strain01,0        !define model name
/Title,non_linear_Epoxy Filled_99 capsules_strain01


!DEFINING PARAMETERS

!MATERIAL PROPERTIES
MATRIX_MODULUS        = 3.5E9
MATRIX_POISSON_RATIO  = 0.34

!CAPSULE PROPERTIES
CAPSULE_MODULUS       = 3.9E9
CAPSULE_POISSON_RATIO = 0.33

!FILLER PROPERTIES
FILLER_MODULUS        = 3.5E9
FILLER_POISSON_RATIO  = 0.34

!MATERIAL STRENGTH LIMITS
MATRIX_TENSILE_STR = 85E6
MATRIX_COMP_STR    = -190E6
MATRIX_SHEAR_STR   = 112E6

CAPSULE_TENSILE_STR = 0.07E6
CAPSULE_COMP_STR    = -0.14E6
CAPSULE_SHEAR_STR   =  0.1E6

FILLER_TENSILE_STR = 0.07E6
FILLER_COMP_STR    = -0.14E6
FILLER_SHEAR_STR   =  0.1E6
```

(a)

(b) Specify the failure criteria for each material by using the TB and TBDATA commands The TB command activates a data table to input special material properties. The TBDATA command enables us to input the data in the table invoked by the previous TB command (refer to ANSYS online help manual for further details on how to use TB and TBDATA).

(c) Specify the damage evolution law for each material by using the TB and TBDATA commands.

(d) Assign the respective strength limits by using the TB and TBDATA commands.

File Edit Format View Help

```
!CAPSULE FAILURE CRITERIA
!SPECIFY DAMAGE INITIATION CRITERIA FOR MATERIAL 1
TB,DMGI,1,1,4,FCRT
TBDATA,1,2,2,2,2
```

(a)

```
!SPECIFY DAMAGE EVOLUTION LAW FOR MATERIAL 1
TB,DMGE,1,1,4,MPDG
TBDATA,1,0.7,0.7,0.7,0.7
```

(b)

```
!SPECIFY MATERIAL STRENGTH LIMITS FOR MATERIAL 1
TB,FCLI,1,1, ,1
TBDATA,1,CAPSULE_TENSILE_STR,CAPSULE_COMP_STR,CAPSULE_TENSILE_STR,CAPSULE_COMP_STR,
CAPSULE_TENSILE_STR,CAPSULE_COMP_STR,CAPSULE_SHEAR_STR,CAPSULE_SHEAR_STR,CAPSULE_SHEAR_STR
```

(c)

```
!MATRIX FAILURE CRITERIA
!SPECIFY DAMAGE INTIATION CRITERIA FOR MATERIAL 2
TB,DMGI,2,1,4,FCRT
TBDATA,1,2,2,2,2
```

(a)

```
!SPECIFY DAMAGE EVOLUTION LAW FOR MATERIAL 2
TB,DMGE,2,1,4,MPDG
TBDATA,1,0.7,0.7,0.7,0.7
```

(b)

```
!SPECIFY MATERIAL STRENGTH LIMITS FOR MATERIAL 2
TB,FCLI,2,1, ,1
TBDATA,1,MATRIX_TENSILE_STR,MATRIX_COMP_STR,MATRIX_TENSILE_STR,MATRIX_COMP_STR,
MATRIX_TENSILE_STR,MATRIX_COMP_STR,MATRIX_SHEAR_STR,MATRIX_SHEAR_STR,MATRIX_SHEAR_STR
```

(c)

```
!FILLER FAILURE CRITERIA
!SPECIFY DAMAGE INTIATION CRITERIA FOR MATERIAL 3
TB,DMGI,3,1,4,FCRT
TBDATA,1,2,2,2,2
```

(a)

```
!SPECIFY DAMAGE EVOLUTION LAW FOR MATERIAL 3
TB,DMGE,3,1,4,MPDG
TBDATA,1,0.7,0.7,0.7,0.7
```

(b)

```
!SPECIFY MATERIAL STRENGTH LIMITS FOR MATERIAL 3
TB,FCLI,3,1, ,1
TBDATA,1,FILLER_TENSILE_STR,FILLER_COMP_STR,FILLER_TENSILE_STR,FILLER_COMP_STR,
FILLER_TENSILE_STR,FILLER_COMP_STR,FILLER_SHEAR_STR,FILLER_SHEAR_STR,FILLER_SHEAR_STR
```

(c)

4. Results & discussion

4.1 Linear analysis

This section will compare the FEA results with theoretical results obtained by using the Voigt and Reuss models for rule of mixtures (ROM) to assess the model. The Voigt model for rule of mixtures for composites is as follows:

$$E_C = E_m V_m - E_p V_p \quad \text{- [1]}$$

The Reuss model for rule of mixtures for composites is as follows:

$$E_C = [\frac{V_m}{E_m} - \frac{V_p}{E_p}]^{-1} \quad \text{- [2]}$$

Where E_C is the elastic modulus of the composite, E_m is the elastic modulus of the matrix, V_m is the volume fraction of the matrix, E_p is the elastic modulus of the capsule and V_p is the volume fraction of the particles. Both ROM models apply for continuous, unidirectional fiber composites. In the case of the Voigt model, the stress is applied in a direction parallel to the fiber direction to evaluate the effective elastic modulus of the composite while for the Reuss model, the stress is applied in a direction perpendicular to the fiber alignment (Kim, 2000). Since reinforcement by spherical inclusions will be much less effective than aligned fiber reinforcement, it is expected that the resulting elastic moduli will be much lower than the results obtained from both ROM models.

The following sub-sections will compare the expected ROM results with the simulated FEA results for hypothetical composites reinforced with hollow capsules, PUF capsules filled with solid PUF and capsules containing solid epoxy under different strain values. The strain values will be 0.1%, 0.4% and 0.7%. This is to ensure that the model will function properly through a range of strains that the material might be subjected to in real life. The same results of elastic modulus are expected for all strain values, however, when modelling, it is important to assess the sensitivity of the model to different parameters. There will also be a comparison between composites with different capsule distributions namely: dispersion, agglomeration, single agglomeration + dispersion and multiple agglomerations + dispersion. The single agglomeration + dispersion model will have a 50% capsule agglomeration ratio. The multiple agglomerations + dispersion model will have 3 agglomerations and will simply be labelled as “multiple agglomerations” in the graphs. The following table (table 3) summarizes all the strains applied, the capsule configurations and the capsule distributions.

Table 3. Summary of strain and RVE configurations used in this project.

Strain	Capsule configuration	Capsule distribution
0.1%	Hollow Solid PUF capsule Solid epoxy filled PUF capsule	Pure dispersion Pure agglomeration Single agglomeration + dispersion Multiple agglomerations (3) + dispersion
0.4%	Hollow Solid PUF capsule Solid epoxy filled PUF capsule	Pure dispersion Pure agglomeration Single agglomeration + dispersion Multiple agglomerations (3) + dispersion
0.07%	Hollow Solid PUF capsule Solid epoxy filled PUF capsule	Pure dispersion Pure agglomeration Single agglomeration + dispersion Multiple agglomerations (3) + dispersion

Below is a table (table 4) listing the number of capsules vs. the different volume fractions of each component for hollow capsules, solid PUF capsules and solid epoxy filled capsules.

Table 4. Number of capsules and corresponding volume fraction for different material configurations.

Number of capsules	Hollow capsule		Epoxy filled capsule		Solid PUF capsule	
	V_m	V_p	V_m	V_p	V_m	V_p
10	0.99755	0.00245	0.99756	0.00244	0.99507	0.00493
20	0.99509	0.00491	0.99511	0.00489	0.99014	0.00986
30	0.99261	0.00739	0.99267	0.00733	0.98522	0.01478
40	0.99013	0.00987	0.99023	0.00977	0.98029	0.01971
50	0.98763	0.01237	0.98778	0.01222	0.97536	0.02464
60	0.98512	0.01488	0.98534	0.01466	0.97043	0.02957
70	0.98259	0.01741	0.98290	0.01710	0.96550	0.03450
80	0.98006	0.01994	0.98045	0.01955	0.96058	0.03942
90	0.97751	0.02249	0.97801	0.02199	0.95565	0.04435
99	0.97520	0.02480	0.97581	0.02419	0.95121	0.04879

The resulting elastic modulus will be plotted against the % volume of capsules. The following table lists the number of capsules and the corresponding volume percentage of capsules.

Table 5. Number of capsules and corresponding % volume for different material configurations

Number of capsules	Hollow capsule	Epoxy filled capsule	Solid PUF capsule
	$\%V_p$	$\%V_p$	$\%V_p$
10	0.24	0.24	0.49
20	0.49	0.49	0.99
30	0.74	0.73	1.48
40	0.99	0.98	1.97
50	1.24	1.22	2.46
60	1.49	1.47	2.96
70	1.74	1.71	3.45
80	1.99	1.95	3.94
90	2.25	2.20	4.44
99	2.48	2.42	4.88

4.1.1 Solid PUF capsules (0.1% strain)

A 0.1% strain is applied on the RVE and the resulting elastic moduli are compared for the different capsule distributions. The capsules are filled with solid PUF.

Figure 29 shows the variation of elastic modulus vs. the % volume of capsules for the different capsule distributions for the case of solid PUF capsules.

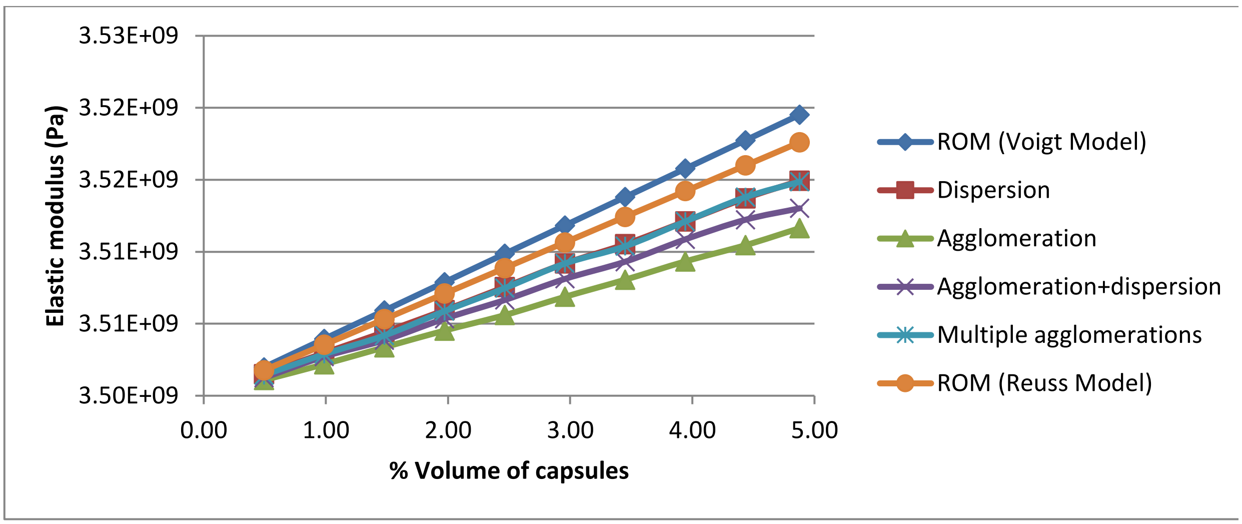

Figure 29. Elastic modulus vs % volume of solid PUF capsules for RVE under 0.1% for; ROM, Voight (♦), ROM, Reuss (●), dispersion model (■), agglomeration model (▲), single agglomeration + dispersion model (×) and multiple agglomerations + dispersion model (*).

In this case, the elastic modulus of the RVE increases as the number of capsules increases. The increase in elastic modulus is greatest for the pure dispersion and the multiple agglomerations + dispersion models. The pure agglomeration model shows the least increase in elastic modulus while the single agglomeration + dispersion model falls in between the pure dispersion and the pure agglomeration models.

4.1.2 Solid epoxy filled capsules (0.1% strain)

A 0.1% strain is applied on the RVE and the resulting elastic moduli are compared for the different capsule distributions. The capsules are filled with solid epoxy in this case.

Figure 30 shows the variation of elastic modulus vs. % volume of capsules for the different capsule distributions for the case of solid epoxy filled.

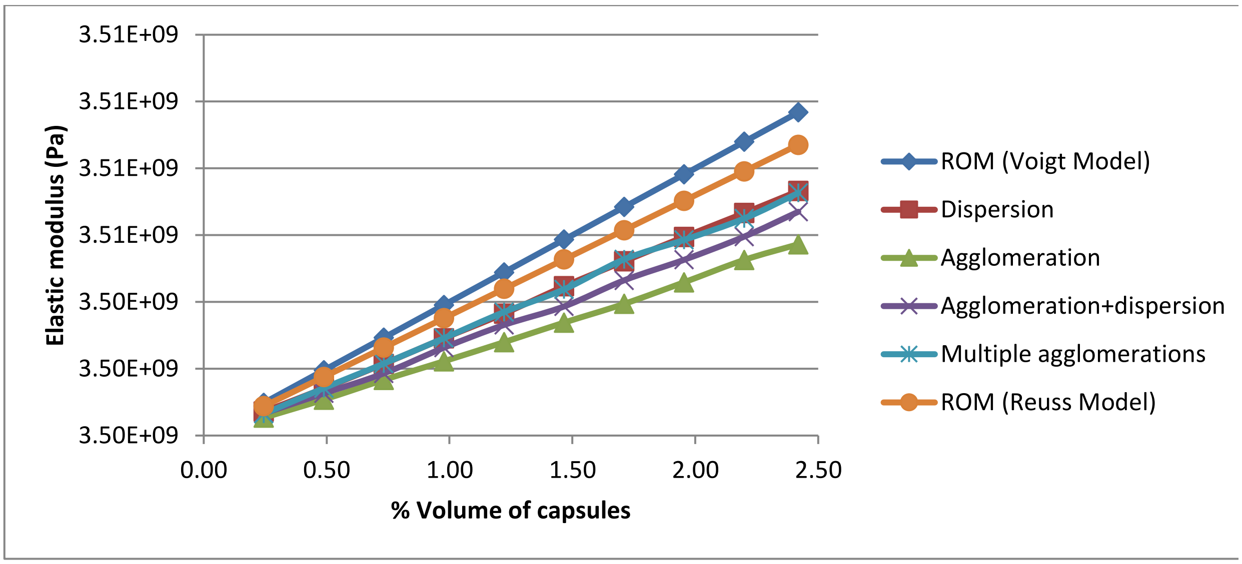

Figure 30. Elastic modulus vs % volume of capsules of epoxy filled capsules for RVE under 0.1% for; ROM, Voight (♦), ROM, Reuss (●), dispersion model (■), agglomeration model (▲), single agglomeration + dispersion model (×) and multiple agglomerations + dispersion model (*).

Like the solid PUF particles case, for the solid epoxy filled capsules model, the elastic modulus of the RVE increases as the number of capsules increases. The increase in elastic modulus is greatest for the pure dispersion and the multiple agglomerations + dispersion models. The pure agglomeration model shows the least increase in elastic modulus while the single agglomeration + dispersion model falls in between the pure dispersion and the pure agglomeration models.

4.1.3 Solid PUF capsules (0.4% strain)

A 0.4% strain is applied on the RVE and the resulting elastic moduli are compared for the different capsule distributions. The capsules are filled with solid PUF.

Figure 31 shows the variation of elastic modulus vs. the % volume of capsules of capsules for the different capsule distributions for the case of solid PUF particles.

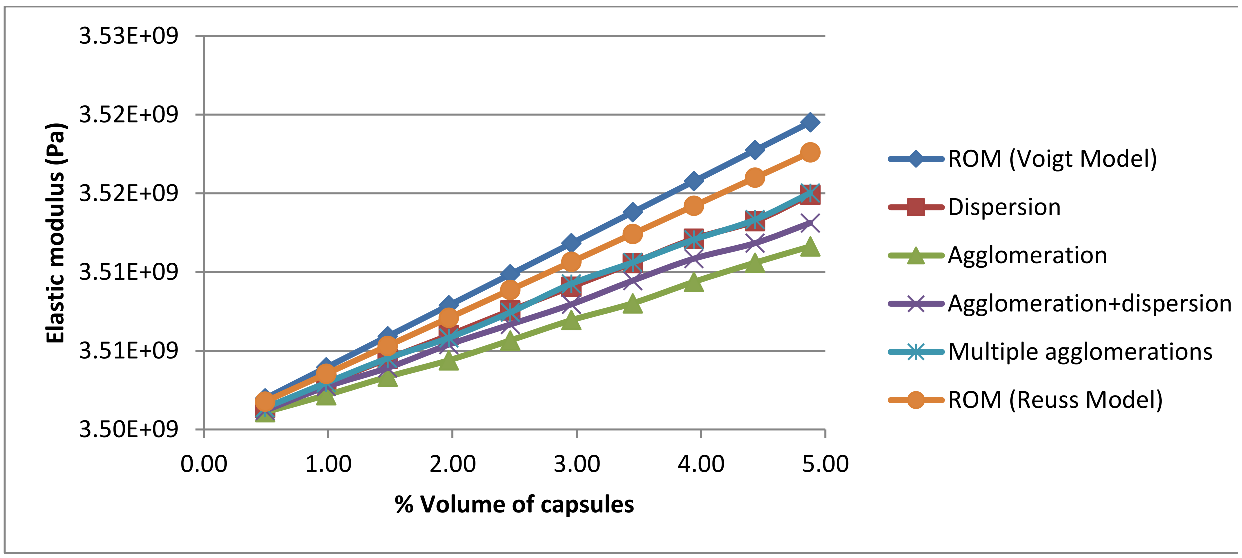

Figure 31. Elastic modulus vs % volume of capsules of solid PUF capsules for RVE under 0.4% for; ROM, Voight (♦), ROM, Reuss (●), dispersion model (■), agglomeration model (▲), single agglomeration + dispersion model (×) and multiple agglomerations + dispersion model (*).

The solid PUF particles case subject to 0.4% strain shows similar results to the 01% strain case. The elastic modulus of the RVE increases as the number of capsules increases. The increase in elastic modulus is greatest for the pure dispersion and the multiple agglomerations + dispersion models. The pure agglomeration model shows the least increase in elastic modulus while the single agglomeration + dispersion model falls in between the pure dispersion and the pure agglomeration models.

4.1.4 Epoxy filled capsules (0.4% strain)

A 0.4% strain is applied on the RVE and the resulting elastic moduli are compared for the different capsule distributions. The capsules are filled with solid epoxy in this case.

Figure 32 shows the variation of elastic modulus vs. the % volume of capsules of capsules for the different capsule distributions for the case of solid epoxy filled capsules.

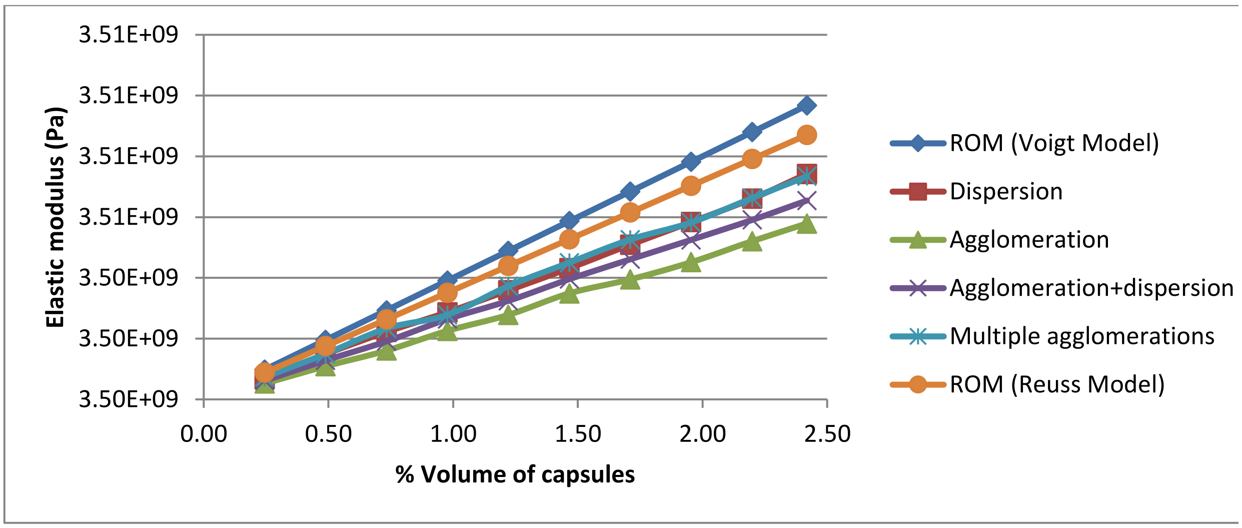

Figure 32. Elastic modulus vs % volume of capsules of epoxy filled capsules for RVE under 0.4% for; ROM, Voight (♦), ROM, Reuss (●), dispersion model (■), agglomeration model (▲), single agglomeration + dispersion model (×) and multiple agglomerations + dispersion model (*).

The solid epoxy filled capsules case subject to 0.4% strain shows similar results to the 01% strain case. The elastic modulus of the RVE increases as the number of capsules increases. The increase in elastic modulus is greatest for the pure dispersion and the multiple agglomerations + dispersion models. The pure agglomeration model shows the least increase in elastic modulus while the single agglomeration + dispersion model falls in between the pure dispersion and the pure agglomeration models.

4.1.5 Solid PUF capsules (0.7% strain)

A 0.7% strain is applied on the RVE and the resulting elastic moduli are compared for the different capsule distributions. The capsules are filled with solid PUF.

Figure 33 shows the variation of elastic modulus vs. the % volume of capsules of capsules for the different capsule distributions for the case of solid PUF particles.

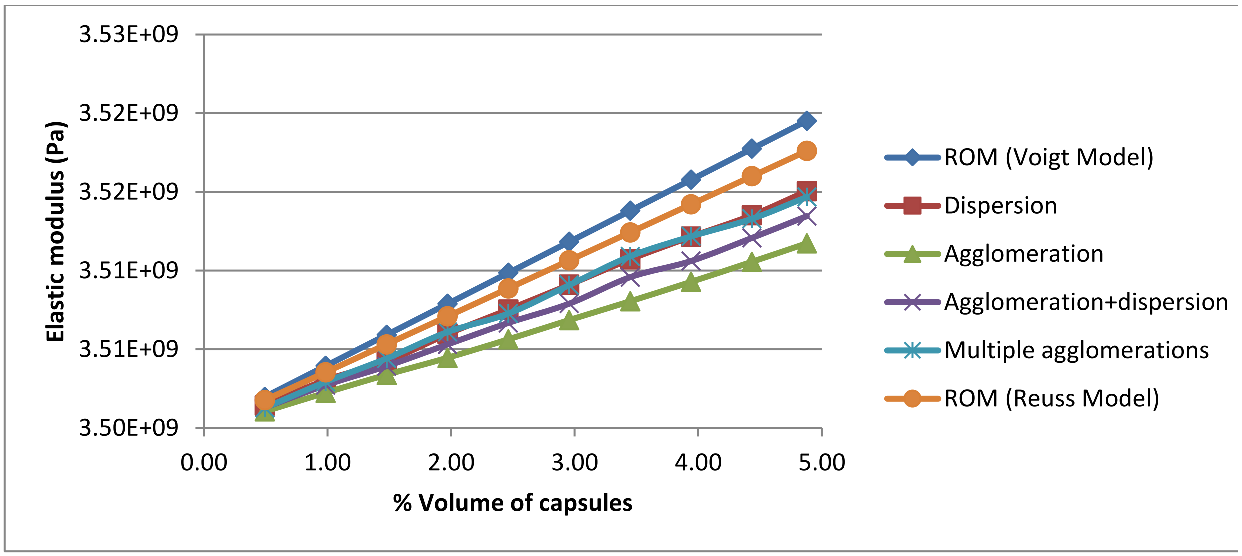

Figure 33. Elastic modulus vs % volume of capsules of solid PUF capsules for RVE under 0.7% for; ROM, Voight (♦), ROM, Reuss (●), dispersion model (■), agglomeration model (▲), single agglomeration + dispersion model (×) and multiple agglomerations + dispersion model (*).

When the RVE containing solid PUF particles is subject to 0.7%, it shows a similar trend as the two previous cases (solid PUF particles RVE under 0.1% & 0.4% strain). The elastic modulus of the RVE increases as the number of capsules increases. The increase in elastic modulus is greatest for the pure dispersion and the multiple agglomerations + dispersion models. The pure agglomeration model shows the least increase in elastic modulus while the single agglomeration + dispersion model falls in between the pure dispersion and the pure agglomeration models.

4.1.6 Epoxy filled capsules (0.7% strain)

A 0.7% strain is applied on the RVE and the resulting elastic moduli are compared for the different capsule distributions. The capsules are filled with solid epoxy in this case.

Figure 34 shows the variation of elastic modulus vs. the % volume of capsules of capsules for the different capsule distributions for the case of solid epoxy filled capsules.

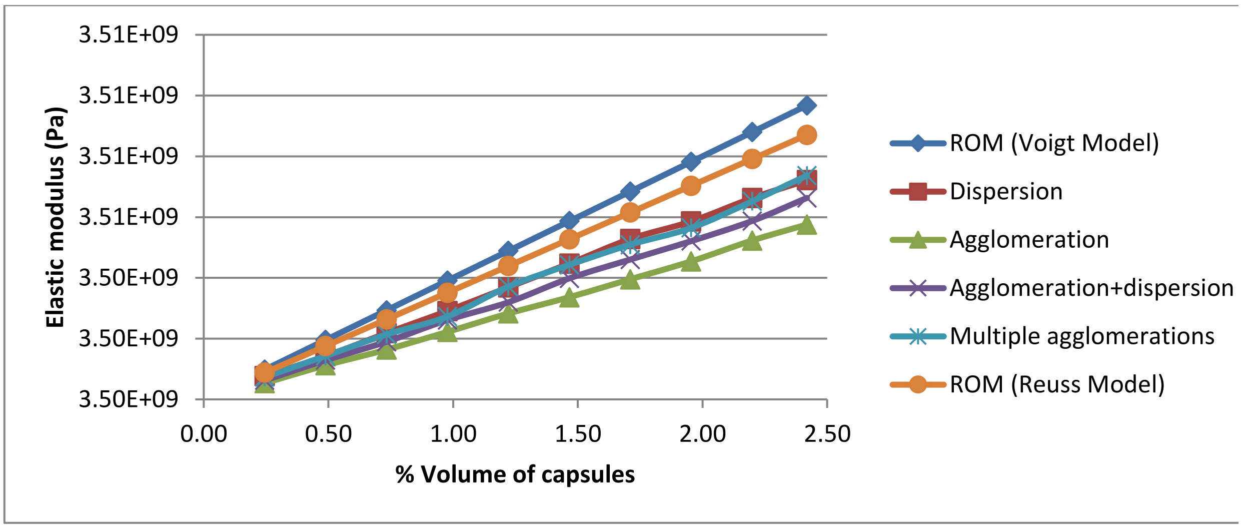

Figure 34. Elastic modulus vs % volume of capsules of epoxy filled capsules for RVE under 0.7% for; ROM, Voight (♦), ROM, Reuss (●), dispersion model (■), agglomeration model (▲), single agglomeration + dispersion model (×) and multiple agglomerations + dispersion model (*).

The solid epoxy filled capsules case subject to 0.7% strain shows similar results to the 0.1% and 0.4% strain cases. The elastic modulus of the RVE increases as the number of capsules increases. The increase in elastic modulus is greatest for the pure dispersion and the multiple agglomerations + dispersion models. The pure agglomeration model shows the least increase in elastic modulus while the single agglomeration + dispersion model falls in between the pure dispersion and the pure agglomeration models.

In the case of solid PUF particles and solid epoxy filled capsules, it was observed that the elastic modulus tends to increase as the number of capsules increases (Figure 35). This increase in elastic modulus is higher in the case of solid PUF particles as compared to the epoxy filled capsule case.

This is because PUF has a higher elastic modulus than epoxy and a higher volume fraction of PUF particles will increase the elastic modulus of the RVE more.

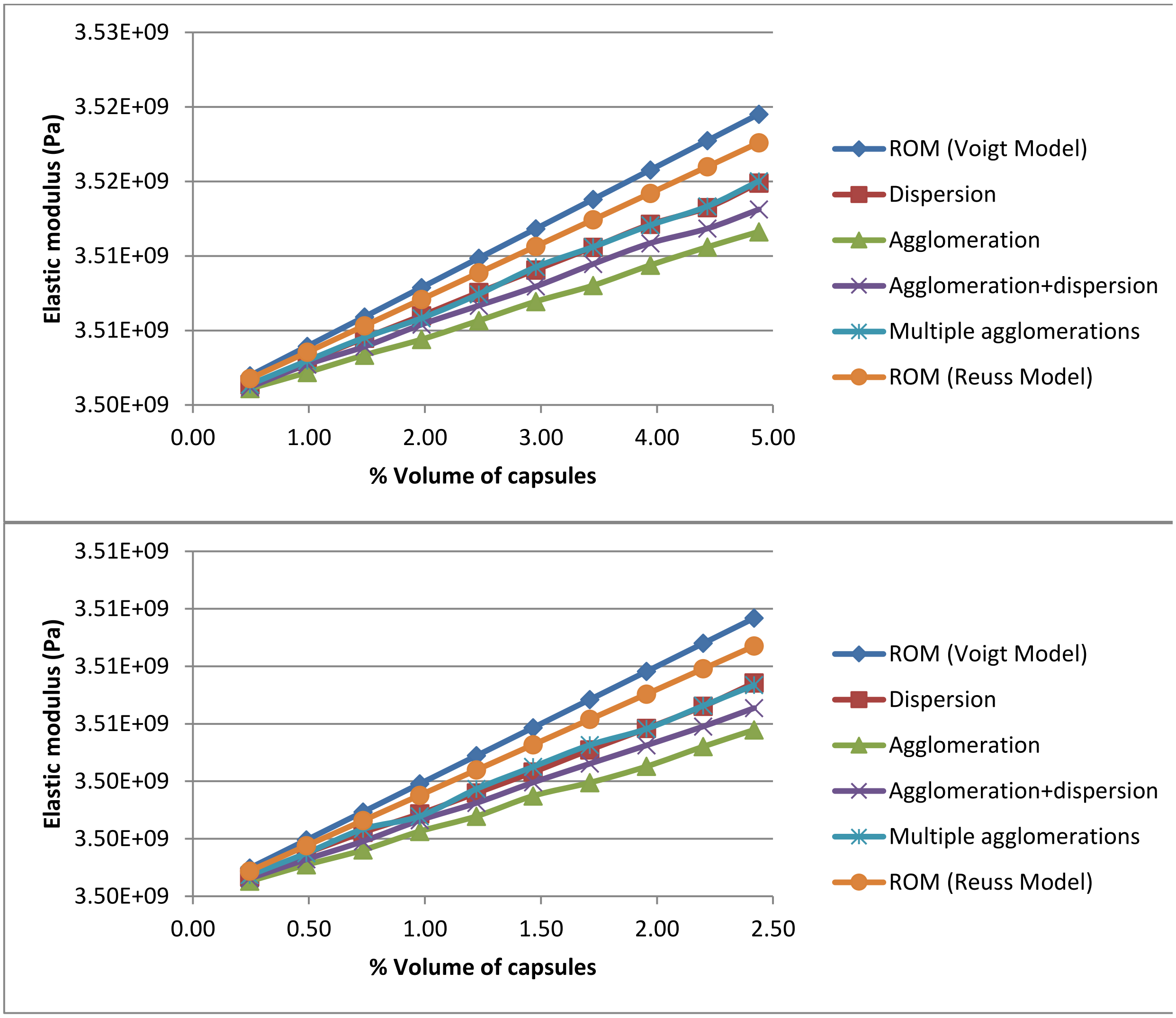

Figure 35. Illustration of the differences in the elastic modulus vs. % volume of capsules of capsules trends between (a) solid PUF particles and (b) solid, epoxy filled capsules for the case of 0.4% strain.

It can also be observed that the different capsule distributions produce elastic moduli trend lines with different gradients. The trend line for the ROM calculations has the steepest gradients. The dispersion and multiple agglomerations + dispersion models produce similar trend lines with the second steepest gradients. The trend line for the single agglomeration has a lower gradient while the trend line for pure agglomeration has the lowest gradient.

Epoxy Filled capsules	Solid PUF particles

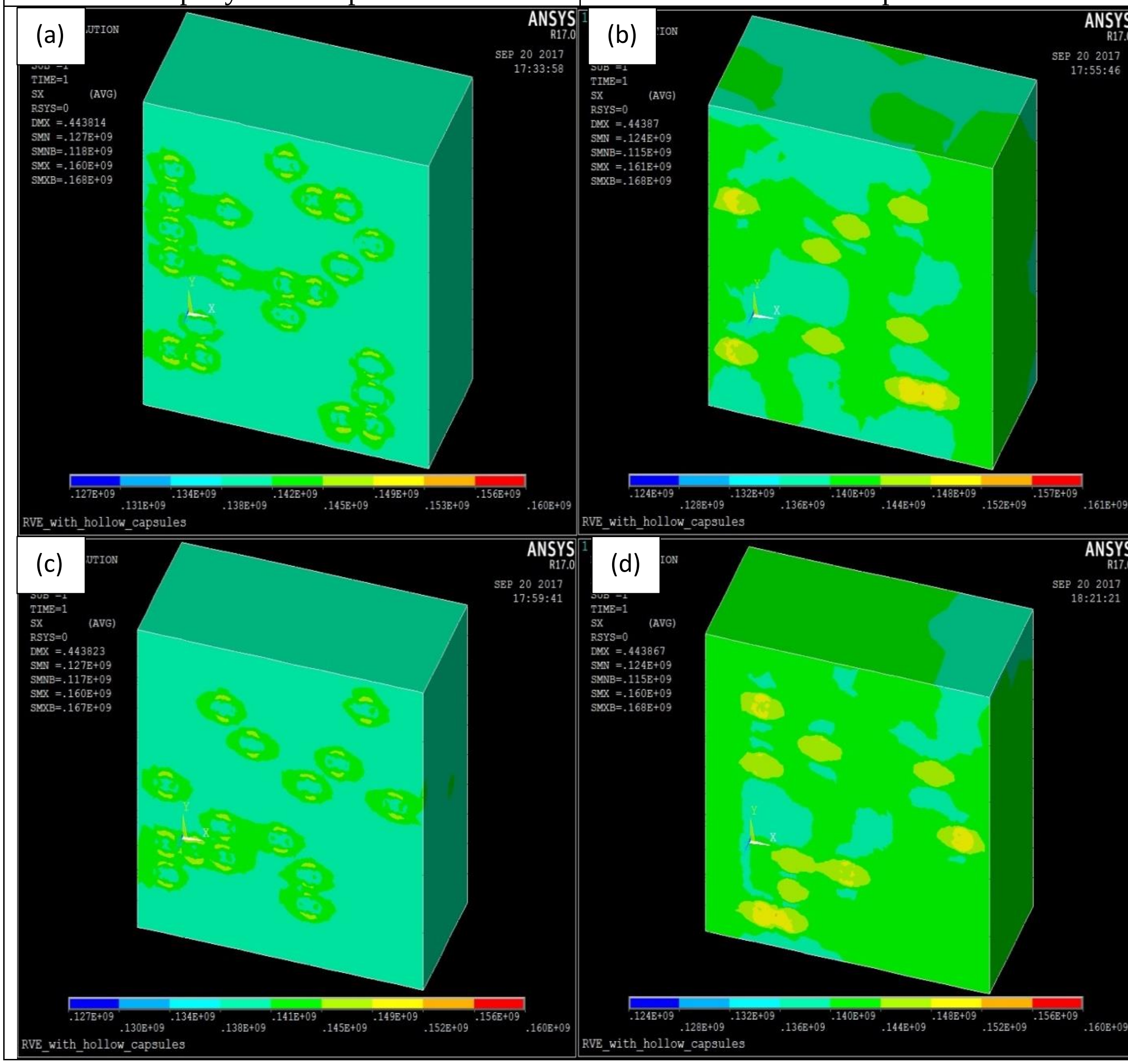

Figure 36. Comparison of cross sectional views showing stress contours inside the RVE for the following configurations (a) epoxy filled capsules – dispersion, (b) Solid PUF particles – dispersion, (c) Epoxy filled capsules – multiple agglomerations + dispersion and (d) Solid PUF capsules – multiple agglomerations + dispersion.

As it can be seen from the stress contour plots (Figures 36 & 37), the solid PUF particles create some widespread higher stress regions inside the matrix while for the epoxy filled capsule scenario and the higher stress regions are concentrated around the capsule shell which is made of PUF. This could explain the higher elastic modulus caused by the solid PUF particles.

Epoxy Filled capsules	Solid PUF particles

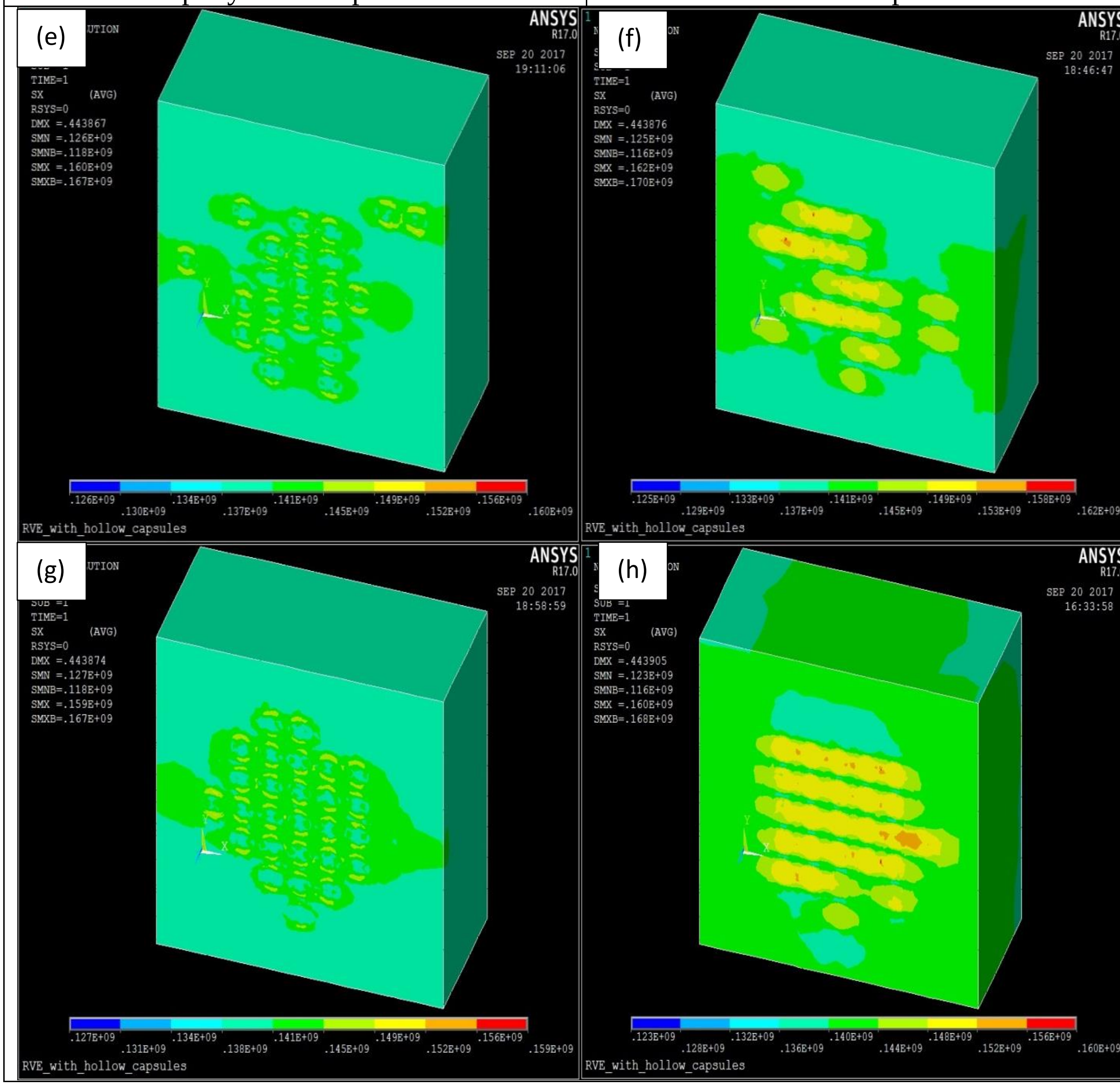

Figure 37. Comparison of cross sectional views showing stress contours inside the RVE for the following configurations (a) epoxy filled capsules – single agglomeration + dispersion, (b) Solid PUF particles – single agglomeration + dispersion, (c) Epoxy filled capsules – pure agglomeration and (d) Solid PUF capsules –pure agglomeration.

Comparing the stress contour plots based on capsule distributions, the dispersion and multiple agglomerations + dispersion models produce very similar stress contours. The agglomeration model and the single agglomeration + dispersion models also produce similar stress contours. It can be concluded that pure agglomeration causes minimal reinforcement of the RVE and as the capsules get more dispersed, the reinforcement becomes more effective. Therefore, the capsule distribution can have a major impact on the composite elastic modulus.

4.1.7 Hollow capsules (0.1% strain)

In the following sub-sections, a 0.1% strain is applied on the RVE and the resulting elastic moduli are compared for the different capsule distributions. The capsules are hollow in this case.

Figure 38 shows the variation of elastic modulus vs. the number of capsules for the different capsule distributions for the case of hollow capsules.

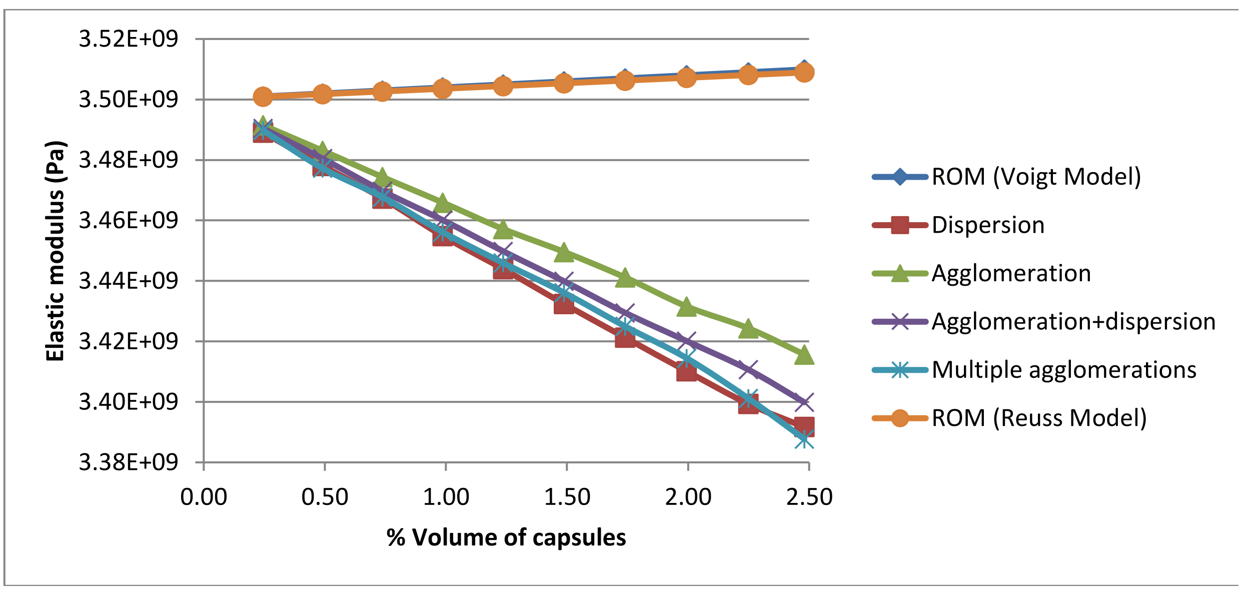

Figure 38. Elastic modulus vs number of hollow capsules for RVE under 0.1% strain for; ROM, Voight (♦), ROM, Reuss (●), dispersion model (■), agglomeration model (▲), single agglomeration + dispersion model (×) and multiple agglomerations + dispersion model (*).

It can be observed that the elastic modulus decreases as the number of hollow capsules in the RVE increases. The pure dispersion and multiple agglomerations + dispersion models display similar behaviour and suffer the most significant decrease in elastic modulus while the pure agglomeration model has the least decrease in elastic modulus. The decrease in elastic modulus in the pure agglomeration model is also closest to the ROM calculations. The single agglomeration + dispersion model falls in between the pure agglomeration and pure dispersion models.

4.1.8 Hollow capsules (0.4% strain)

In the following sub-section, a 0.4% strain is applied on the RVE containing hollow capsules and the resulting elastic moduli are compared for the different capsule distributions.

Figure 39 shows the variation of elastic modulus vs. the number of capsules for the different capsule distributions for the case of hollow capsules.

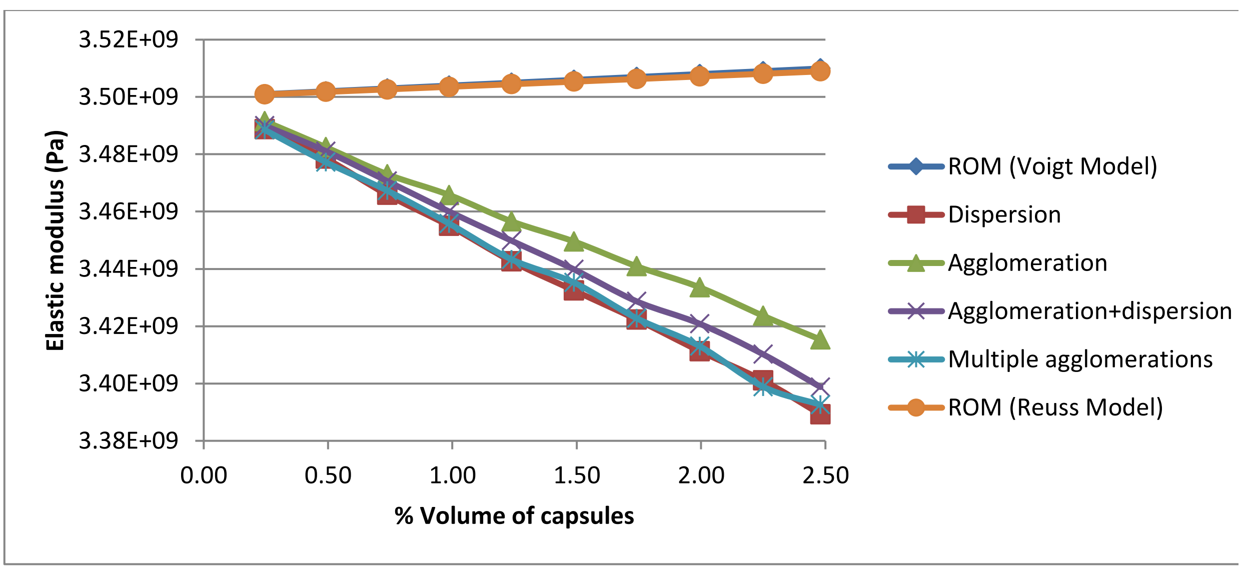

Figure 39. Elastic modulus vs number of hollow capsules for RVE under 0.4% for; ROM, Voight (♦), ROM, Reuss (●), dispersion model (■), agglomeration model (▲), single agglomeration + dispersion model (×) and multiple agglomerations + dispersion model (*).

When the RVE is subjected to 0.4% strain, the elastic modulus results are the same as the 0.1% case. The pure dispersion and multiple agglomerations + dispersion models display similar behaviour to each other and suffer the most significant decrease in elastic modulus while the pure agglomeration model has the least decrease in elastic modulus. The decrease in elastic modulus in the pure agglomeration model is also closest to the ROM calculations. The single agglomeration + dispersion model falls in between the pure agglomeration and pure dispersion models.

4.1.9 Hollow capsules (0.7% strain)

In the following sub-sections, a 0.7% strain is applied on the RVE and the resulting elastic moduli are compared for the different capsule distributions. The capsules are hollow in this case.

Figure 40 shows the variation of elastic modulus vs. the number of capsules for the different capsule distributions for the case of hollow capsules.

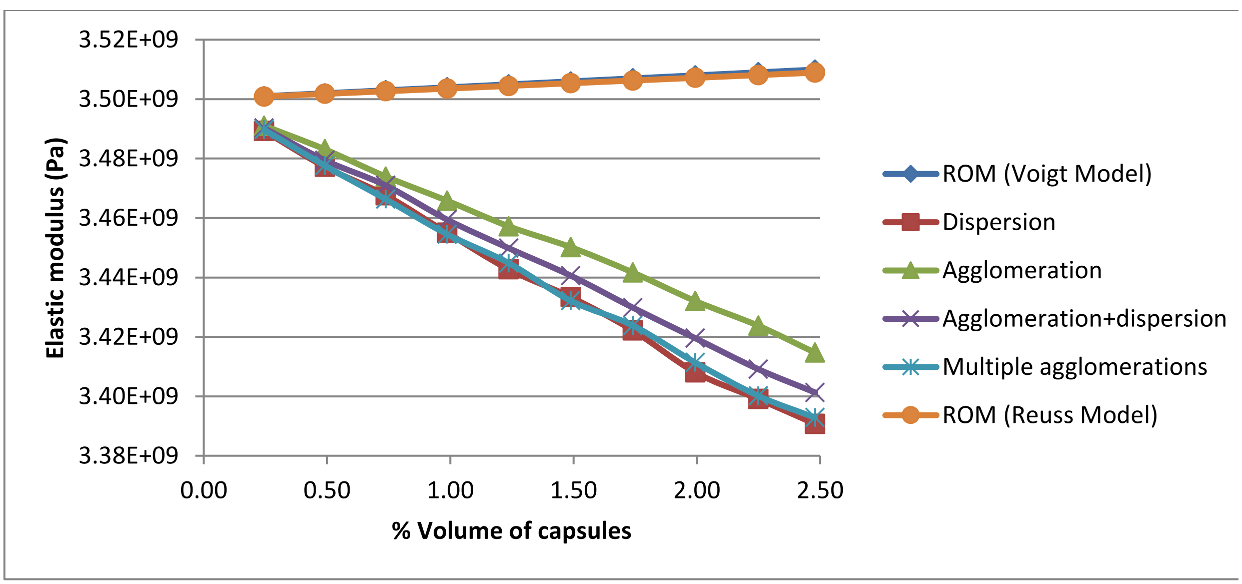

Figure 40. Elastic modulus vs number of hollow capsules for RVE under 0.7% for; ROM, Voight (♦), ROM, Reuss (●), dispersion model (■), agglomeration model (▲), single agglomeration + dispersion model (×) and multiple agglomerations + dispersion model (*).

When the RVE containing hollow capsules is subject to 0.7%, it shows a similar trend as the two previous cases (hollow capsule cases subject to 0.1% & 0.4% strain). The elastic modulus of the RVE decreases as the number of hollow capsules increases. The pure dispersion and the multiple agglomerations + dispersion cases show the greatest decrease in elastic modulus. The pure agglomeration model shows the least decrease in elastic modulus and is very close to the ROM calculations. The single agglomeration + dispersion case results falls in between pure agglomeration and pure dispersion.

For the case of hollow capsules, the trend in elastic modulus vs. number of capsules is very different (Figures 38-40). The elastic modulus decreases as the number of capsules increases. This is because the hollow capsules can be considered as voids and they tend to weaken the matrix. It can be observed that the dispersion and multiple agglomerations + dispersion models produce the largest decrease in elastic modulus as the number of capsules increases. The agglomeration + dispersion model shows a lesser decrease in elastic modulus while the pure agglomeration model shows the least decrease in elastic modulus.

Looking at the stress contour plots for the case of hollow capsules (Figure 41), the highest stress concentrations are located at the capsule walls, perpendicular to the direction of the strain applied. It can also be observed that capsules that horizontally adjacent to each other tend to create low stress in between them whereas capsules that are vertically adjacent to each other tend to create regions of high stress. It can be inferred that cracks will propagate in a direction perpendicular to the direction in which strain is applied. If the capsule is filled with healing agents, this will facilitate the release of healing agents into the crack.

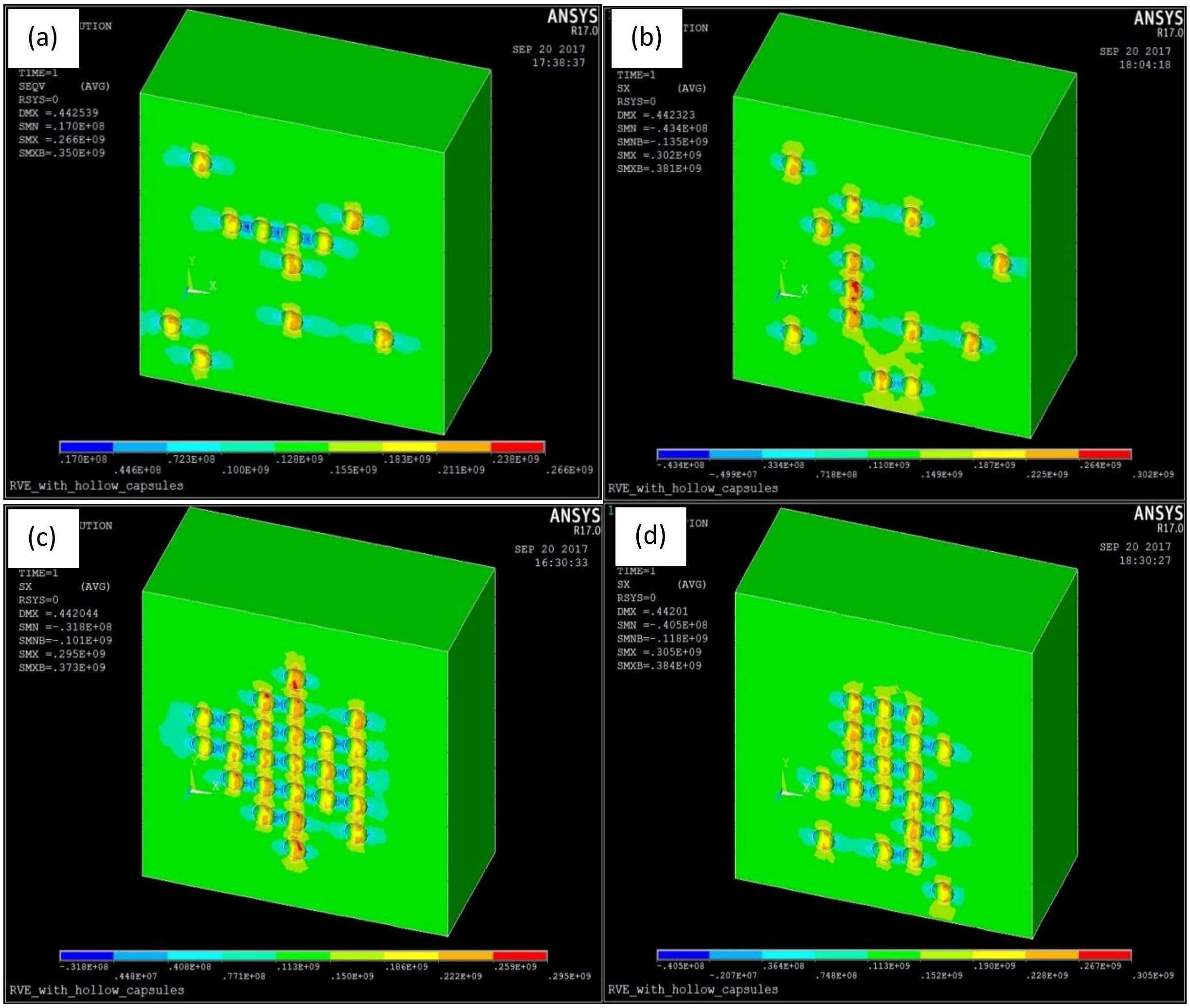

Figure 41. Cross sectional views for the RVE containing hollow capsules for the following capsule distributions (a) dispersion (b) multiple agglomerations + dispersion (c) agglomeration (d) single agglomeration + dispersion.

It must also be noted that the calculated changes of elastic modulus vs % volume of capsules are less than 0.05 GPa which is below the typical uncertainty of 0.1 GPa when the elastic modulus of polymers and composites is measured.

4.2 Non-linear analysis (damage model)

This section presents the damage progression in the RVE when material strength limits are specified. All the diagrams are cross sectional views of the RVEs. All RVEs contain 99 capsules. Each sub-section will display results for the different types of capsule distribution. In ANSYS

APDL, the damage status is represented by 3 numbers: 0 – undamaged, 1 – partially damaged and 2 – completely damaged. The colour chart on each diagram will vary depending on the maximum damage in each individual RVE. This software feature is still being developed in ANSYS and not much information is available on what the software considers as ‘partially damaged’. However, it can be inferred that since the material strength limits have to be specified in the code, the element is considered ‘damaged’ once the element stress exceeds the material strength limit associated with this element.

4.2.1 Epoxy filled capsules, pure agglomeration: 1% strain to 2% strain

This section presents the damage progression for the RVE containing 99 epoxy filled PUF capsules which are agglomerated at the centre of the RVE (Figure 42). These cross sections have been obtained by inserting a cutting plane parallel to the x-y plane in the centre of the RVE.

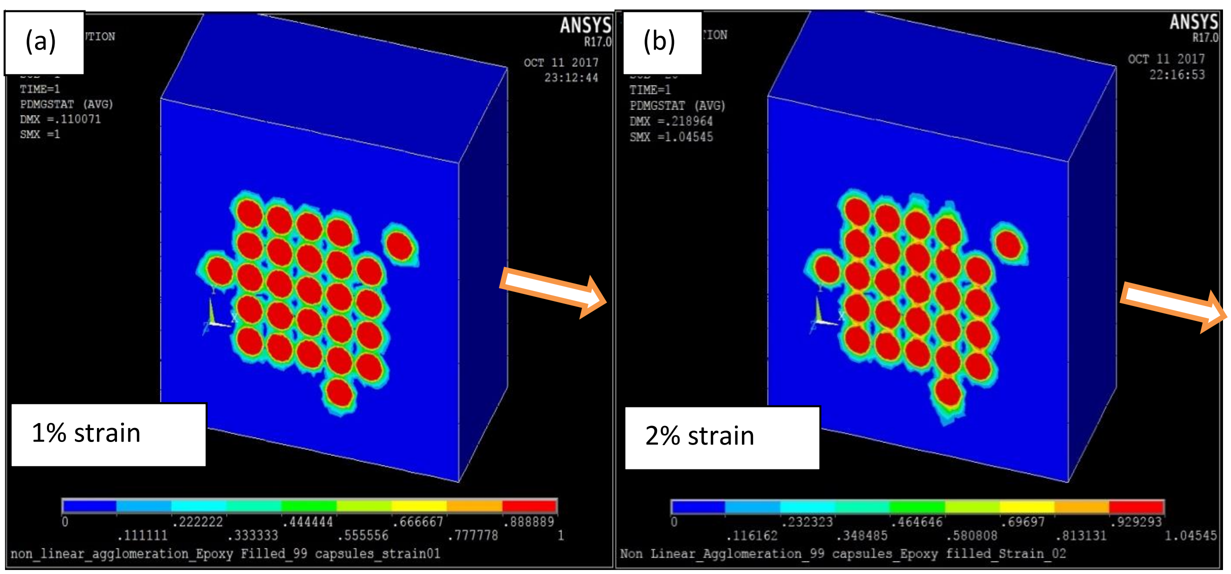

Figure 42. Comparison of damage between (a) 1% strain and (b) 2% strain for RVE containing 99 solid epoxy filled PUF capsules which are agglomerated at the centre of the RVE.

In Figure 41 and 41(b), the blue areas represent undamaged elements while the red areas represent partially damaged elements. When the RVE is subject to 1% strain, the capsules are seen to get partially damaged with areas surrounding the capsule varying between undamaged and partially damaged. When the strain is increased to 2%, the partially damaged areas are seen spreading vertically through the matrix in between the capsules.

4.2.2 Epoxy filled capsules, single agglomeration + dispersion: 1% strain to 2% strain

This section presents the damage progression for the RVE containing 99 epoxy filled PUF capsules where 50% of the capsules are agglomerated at the centre of the RVE and the remaining capsules are dispersed in the rest of the matrix (Figure 43). These cross sections have been obtained by inserting a cutting plane parallel to the x-y plane in the centre of the RVE.

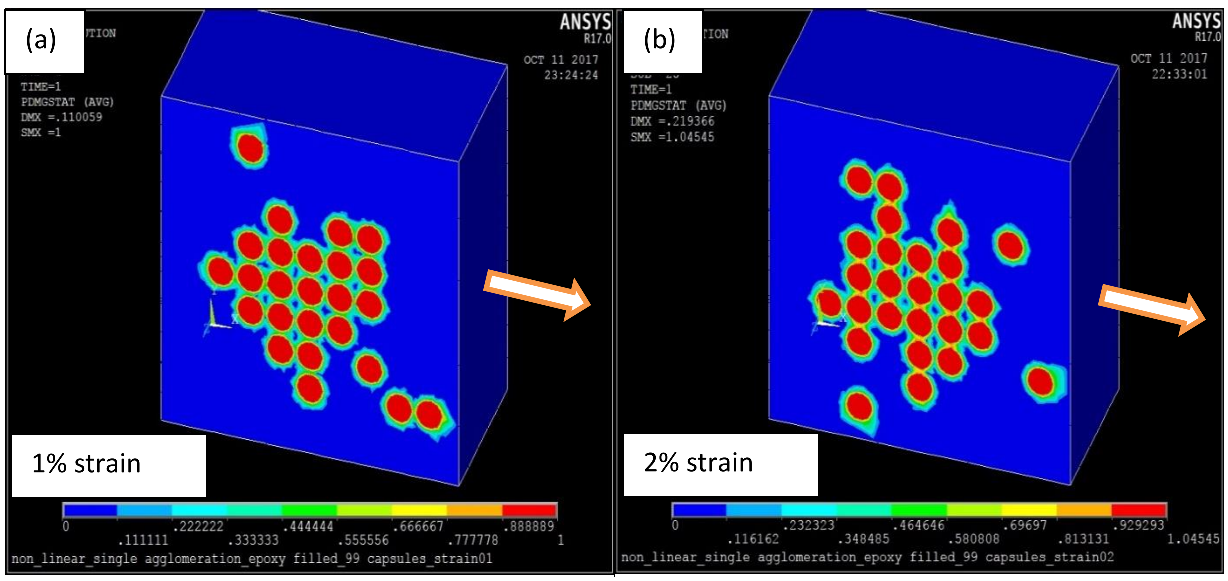

Figure 43. Comparison of damage between (a) 1% strain and (b) 2% strain for RVE containing 99 solid epoxy filled PUF capsules half of which are agglomerated at the centre of the RVE and half are dispersed in the remaining RVE.

In Figure 42(a) and 42(b), the blue areas represent undamaged elements while the red areas represent partially damaged elements. When the RVE is subject to 1% strain, the capsules are seen to get partially damaged with areas surrounding the capsule varying between undamaged and partially damaged. When the strain is increased to 2%, the damage spreads vertically through the matrix in between the capsules. When the capsules are in close vertical proximity, the partially damaged areas bridge vertically through the matrix.

4.2.3 Epoxy filled capsules, multiple agglomerations + dispersion: 1% strain to 2% strain

This section presents the damage progression for the RVE containing 99 solid epoxy filled PUF capsules where there are 3 agglomerations and the remaining capsules are dispersed in the rest of the matrix (Figure 44). These cross sections have been obtained by inserting a cutting plane parallel to the x-y plane in the centre of the RVE.

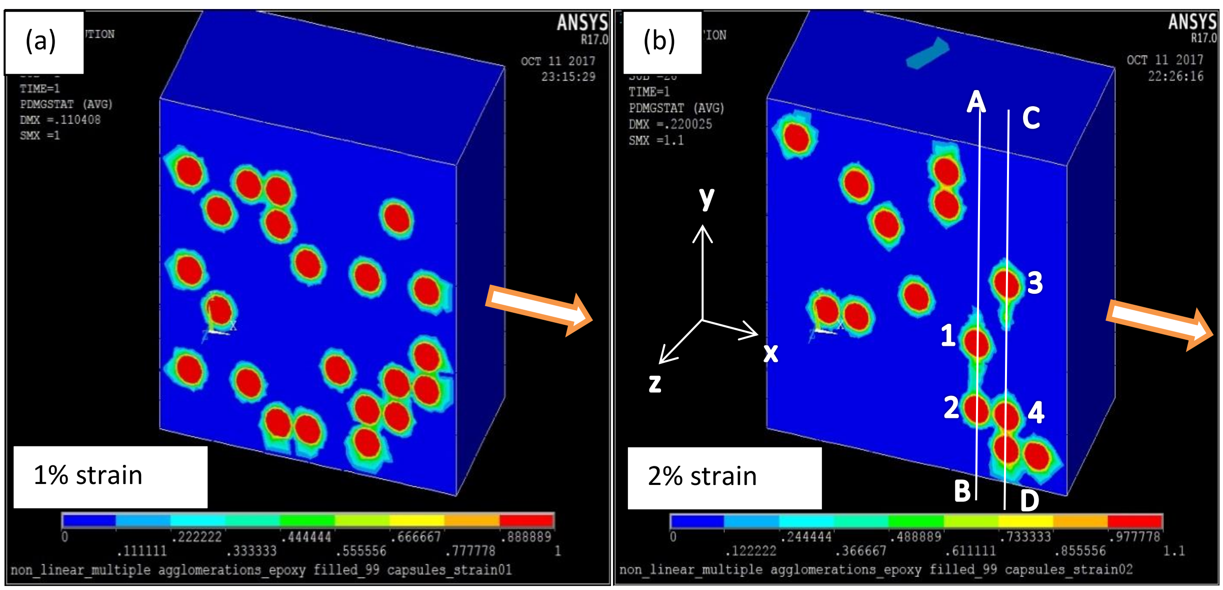

Figure 44. Comparison of damage between (a) 1% strain and (b) 2% strain for RVE containing 99 solid epoxy filled PUF capsules with 3 agglomerations and the rest dispersed in the remaining RVE.

In Figure 43(a) and 43(b), the blue areas represent undamaged elements while the red areas represent partially damaged elements. When the RVE is subject to 1% strain, the capsules are seen to get partially damaged with areas surrounding the capsule varying between undamaged and partially damaged. When the strain is increased to 2%, the damage spreads vertically through the matrix in between the capsules. There are instances where the damage spreads for a longer distance and bridges a wider vertical gap between capsules. To further investigate the damage patterns, two cutting planes parallel to plane y-z were introduced at A-B and C-D. The capsules 1,2 and 3,4 were labelled so they can be easily situated in Figures 45(a) and 45(b).

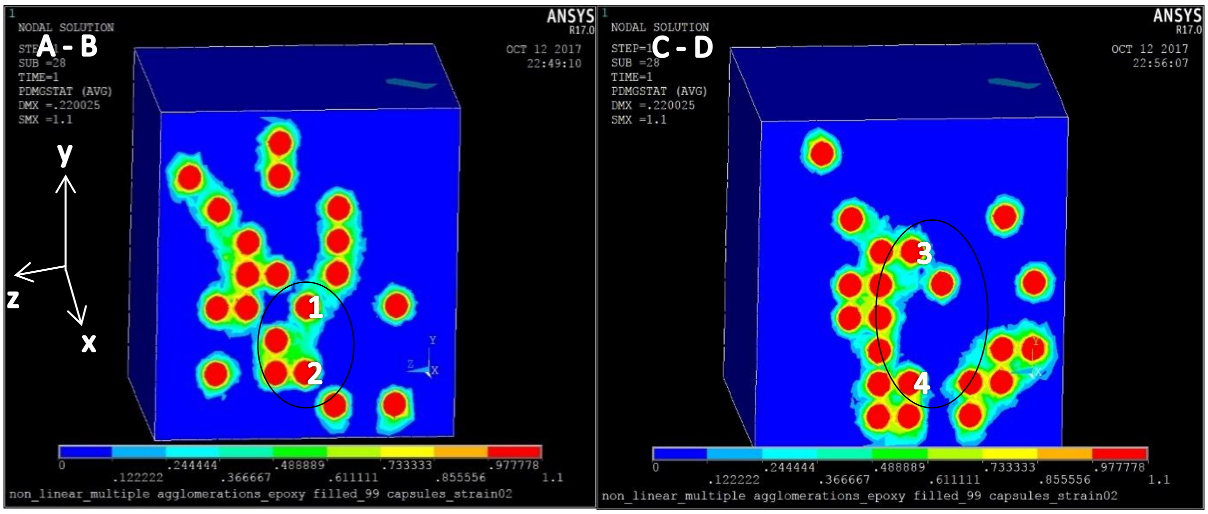

Figure 45. Cutting planes (a) A-B and (b) C-D parallel to plane y-z.

In both cases, the damage bridge can be attributed to the presence of adjacent capsules in the x-y plane.

4.2.4 Epoxy filled capsules, pure dispersion: 1% strain to 2% strain

This section presents the damage progression for the RVE containing 99 solid epoxy filled PUF capsules where the capsules are dispersed in the matrix and follow a random uniform distribution (Figure 46). These cross sections have been obtained by inserting a cutting plane parallel to the x-y plane in the centre of the RVE.

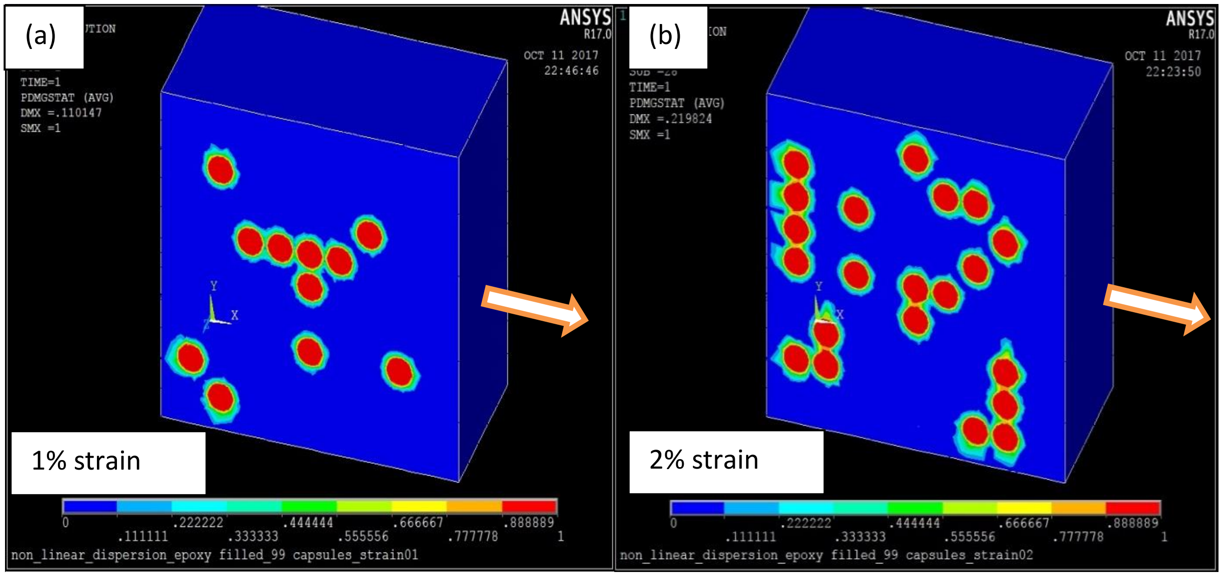

Figure 46. Comparison of damage between (a) 1% strain and (b) 2% strain for RVE containing 99 epoxy filled PUF capsules dispersed in the RVE.

In Figure 46(a) and 46(b), the blue areas represent undamaged elements while the red areas represent partially damaged elements. When the RVE is subject to 1% strain, the capsules are seen to get partially damaged with areas surrounding the capsule varying between undamaged and partially damaged. When the strain is increased to 2%, the damage spreads vertically through the matrix in between the capsules.

4.2.5 Solid PUF particles, pure agglomeration: 1% strain to 2% strain

This section presents the damage progression for the RVE containing 99 solid PUF particles which are agglomerated at the centre of the RVE (Figure 47). These cross sections have been obtained by inserting a cutting plane parallel to the x-y plane in the centre of the RVE.

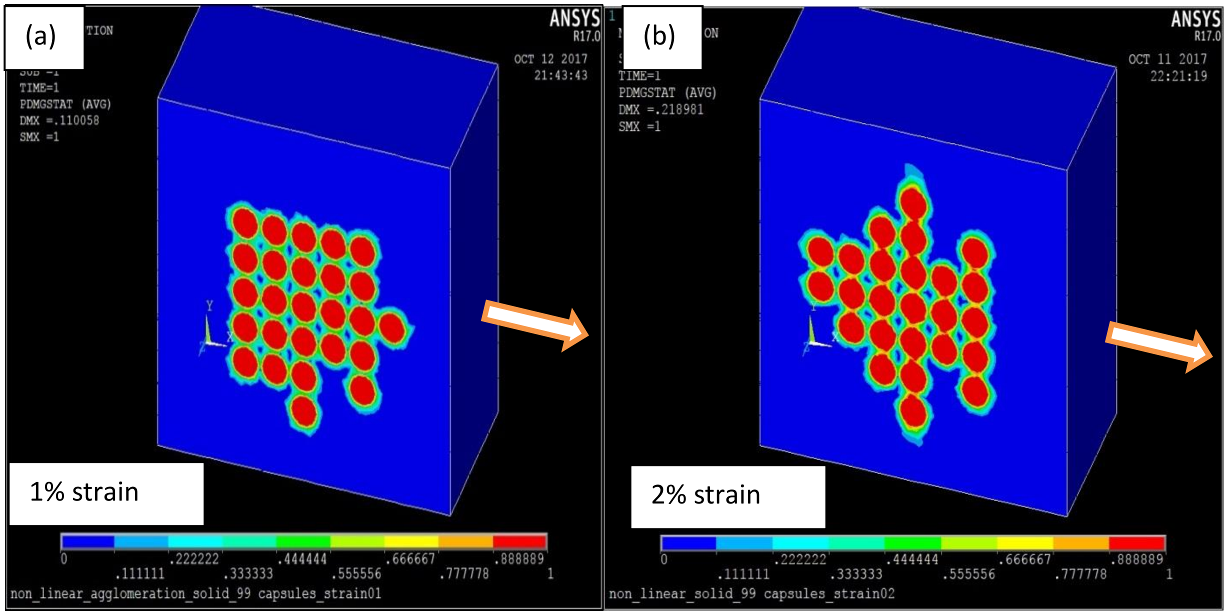

Figure 47. Comparison of damage between (a) 1% strain and (b) 2% strain for RVE containing 99 solid PUF particles which are agglomerated at the centre of the RVE.

In Figures 47(a) and 47(b), the blue areas represent undamaged elements while the red areas represent partially damaged elements. When the RVE is subject to 1% strain, the capsules are seen to get partially damaged with areas surrounding the capsule varying between undamaged and partially damaged. When the strain is increased to 2%, the partial damage is seen to spread vertically in between the particles.

4.2.6 Solid PUF particles, single agglomeration + dispersion: 1% strain to 2% strain

This section presents the damage progression for the RVE containing 99 solid PUF particles where 50% of the capsules are agglomerated at the centre of the RVE and the remaining capsules are dispersed in the rest of the matrix (Figure 48). These cross sections have been obtained by inserting a cutting plane parallel to the x-y plane in the centre of the RVE.

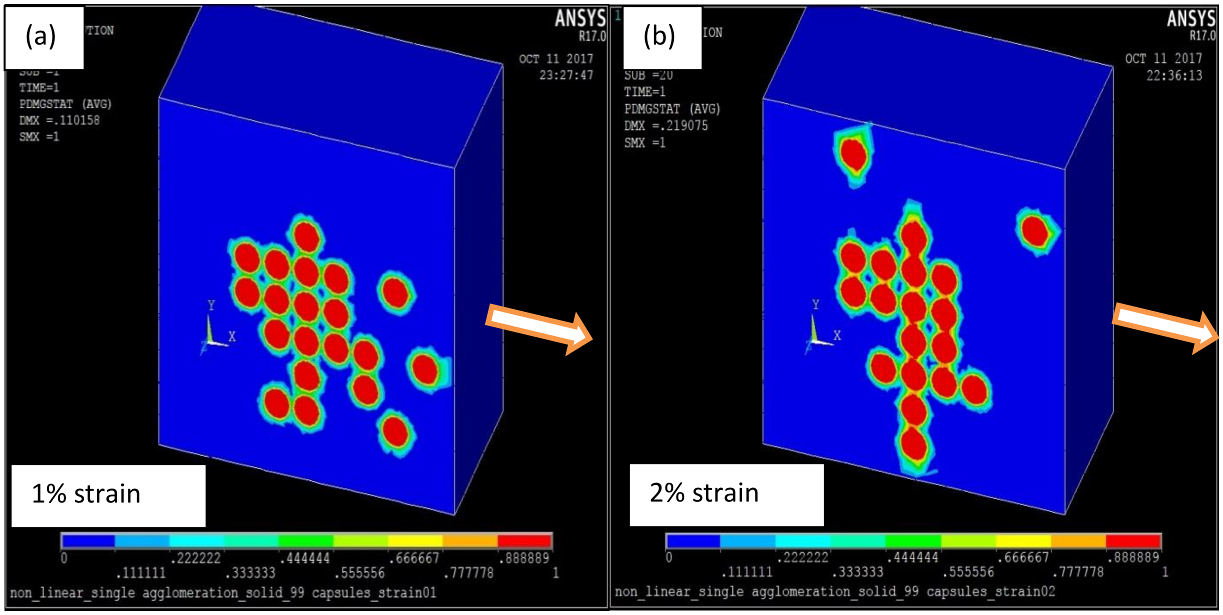

Figure 48. Comparison of damage between (a) 1% strain and (b) 2% strain for RVE containing 99 solid PUF particles half of which are agglomerated at the centre of the RVE and half are dispersed in the remaining RVE.

In Figures 48(a) and 48(b), the blue areas represent undamaged elements while the red areas represent partially damaged elements. When the RVE is subject to 1% strain, the capsules are seen to get partially damaged with areas surrounding the capsule varying between undamaged and partially damaged. When the strain is increased to 2%, the partial damage is seen to spread vertically in between the particles. For the 2% strain case, the damage areas are seen to grow larger. When capsules are in close vertical proximity, the partially damaged areas can sometimes form a bridge between the capsules.

4.2.7 Solid PUF particles, multiple agglomerations + dispersion: 1% strain to 2% strain

This section presents the damage progression for the RVE containing 99 solid PUF particles where there are 3 agglomerations and the remaining capsules are dispersed in the rest of the matrix (Figure 49). These cross sections have been obtained by inserting a cutting plane parallel to the x-y plane in the centre of the RVE.

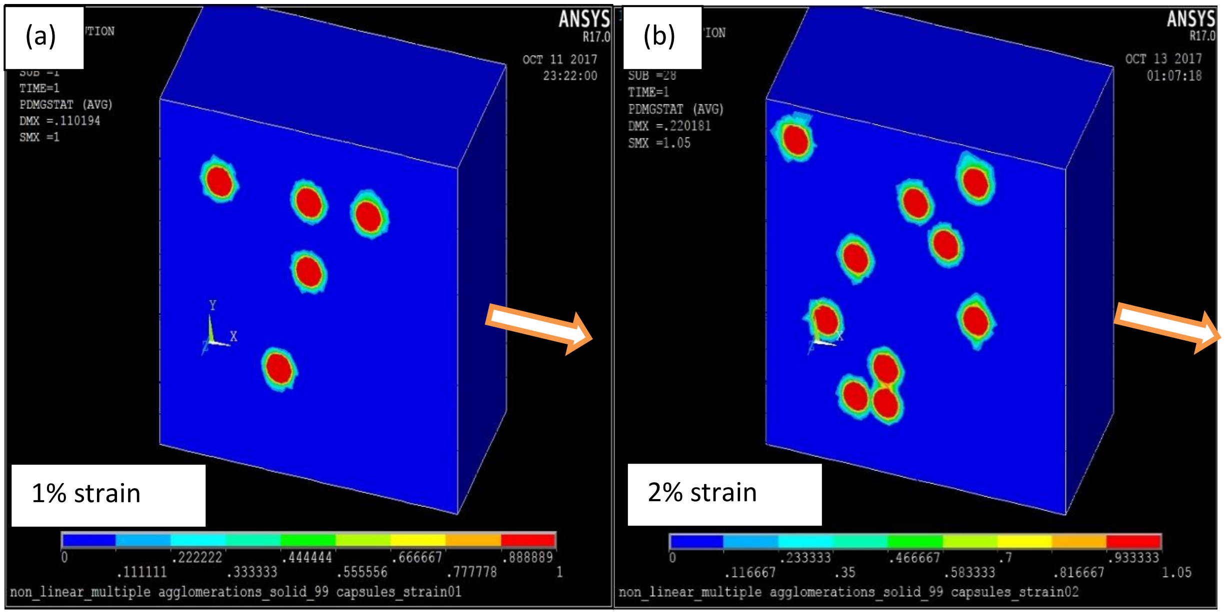

Figure 49. Comparison of damage between (a) 1% strain and (b) 2% strain for RVE containing 99 solid PUF particles with 3 agglomerations and the rest dispersed in the remaining RVE.

In Figures 49(a) and 49(b), the blue areas represent undamaged elements while the red areas represent partially damaged elements. When the RVE is subject to 1% strain, the particles are shown to be partially damaged with areas surrounding the capsule varying between undamaged and partially damaged. When the strain is increased to 2%, the partial damage is seen to spread vertically in between the particles. There are instances where the damage spreads for a longer distance and bridges a wider vertical gap between capsules. There are instances where the damage spreads even in the absence of particles which are in close vertical proximity.

4.2.8 Solid PUF particles, pure dispersion: 1% strain to 2% strain

This section presents the damage progression for the RVE containing 99 solid PUF particles where the capsules are dispersed in the matrix and follow a random uniform distribution (Figure 50). These cross sections have been obtained by inserting a cutting plane parallel to the x-y plane in the centre of the RVE.

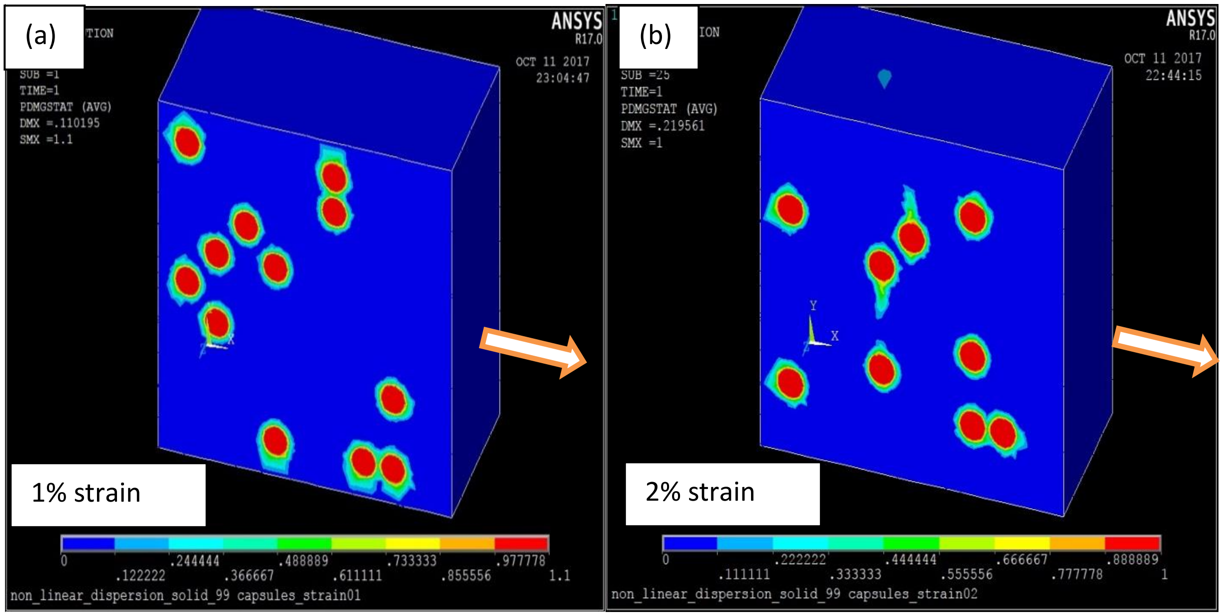

Figure 50. Comparison of damage between (a) 1% strain and (b) 2% strain for RVE containing 99 solid PUF particles dispersed in the RVE.

In Figure 50(a) and (b), the blue areas represent undamaged elements while the green areas represent partially damaged elements. When the RVE is subject to 1% strain, the capsules are seen to get partially damaged with areas surrounding the capsule varying between undamaged and partially damaged. When the strain is increased to 2%, the partial damage is seen to spread vertically in between the particles. The damage does not spread horizontally, and the matrix is still seen to be intact in between the particles in a direction parallel to the strain applied. There are instances where the damage spreads for a longer distance into the matrix in the absence of particle in close vertical proximity.

4.2.9 Hollow capsules, pure agglomeration: 1% strain to 2% strain

This section presents the damage progression for the RVE containing 99 hollow PUF capsules which are agglomerated at the centre of the RVE (Figure 51). These cross sections have been obtained by inserting a cutting plane parallel to the x-y plane in the centre of the RVE.

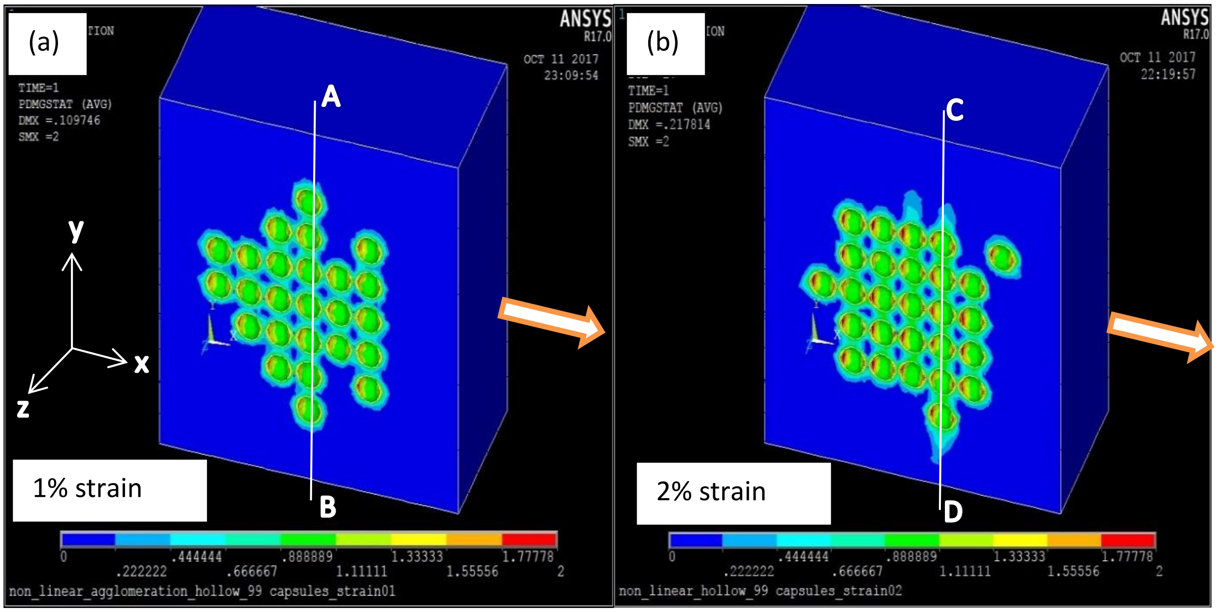

Figure 51. Comparison of damage between (a) 1% strain and (b) 2% strain for RVE containing 99 hollow PUF capsules which are agglomerated at the centre of the RVE.

In Figures 51(a) and 51(b), the blue areas represent undamaged elements, the green areas represent partially damaged elements and the red areas represent completely damaged elements. When the RVE is subject to 1% strain (the strain direction is indicated by the arrow), the damage starts at the hollow capsules. Most of the body of the hollow capsule gets partially damaged (green). The areas around the capsules range between intact (blue) to partially damaged (green). The damage variation inside the capsule ranges from partially damaged (green) to completely damage (red). When the strain is increased to 2%, the areas of partial damage can be seen to widen through the matrix. There are instances where the partial damage reaches further out vertically. This can be attributed to the presence of other capsules in the z-direction. When cutting planes, A – B and C – D, parallel to the y-z plane are inserted in the centre of the RVEs, the following images can be observed (Figure 52).

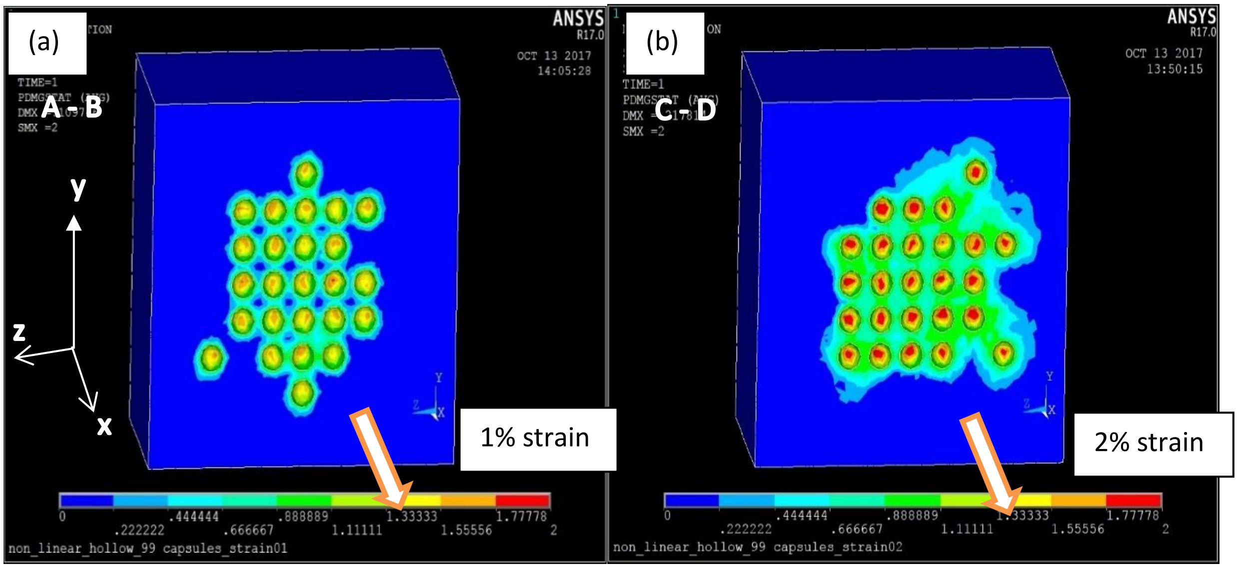

Figure 52. Cross sectional view of RVEs when the cutting plane is parallel to the y-z plane for the case of (a) 1% strain and (b) 2% strain.

When Figures 52(a) and 52(b) are compared, when the strain is increased, the damage areas tend to spread in a direction that is perpendicular to the direction of the strain applied. Therefore, when a strain is applied to the RVE, the damage will start at the capsule and will spread in a direction perpendicular to the strain direction. The presence of nearby capsules in the same vertical plane will help to bridge the damage areas. If healing agents are present inside the capsules, this may help in the release of more healing agents into the cracks as the cracks will adopt trajectories that go through nearby capsules.

4.2.10 Hollow capsules, single agglomeration + dispersion: 1% strain to 2% strain

This section presents the damage progression for the RVE containing 99 hollow PUF capsules where 50% of the capsules are agglomerated at the centre of the RVE and the remaining capsules are dispersed in the rest of the matrix (Figure 53). These cross sections have been obtained by inserting a cutting plane parallel to the x-y plane in the centre of the RVE.

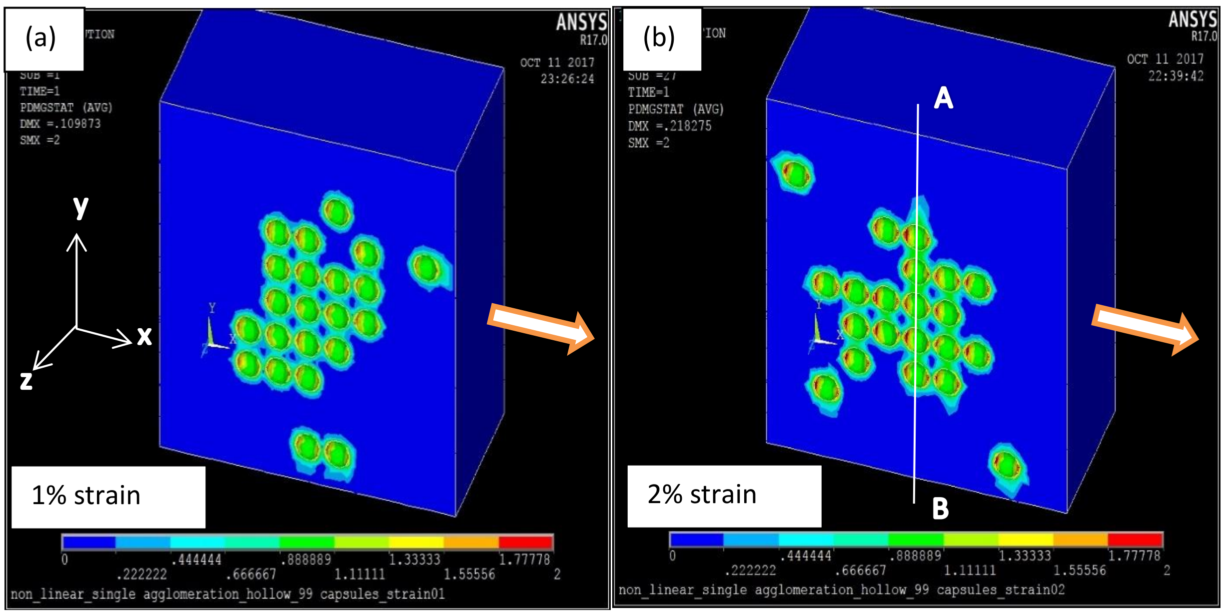

Figure 53. Comparison of damage between (a) 1% strain and (b) 2% strain for RVE containing 99 hollow PUF capsules half of which are agglomerated at the centre of the RVE and half are dispersed in the remaining RVE.

In Figures 53(a) and 53(b), the blue areas represent undamaged elements, the green areas represent partially damaged elements and the red areas represent completely damaged elements. When the RVE is subjected to 1% strain, the capsule walls get partially damaged with red spots in a straight-line parallel to the strain direction. When the strain increases to 2%, the partial damage spreads vertically in the matrix between vertically adjacent capsules. This damage spread can also be observed to a lesser extent around the capsules which are dispersed in the matrix. The red areas (complete damage) become wider; however, they do not spread into the matrix. If a cutting plane A-B is inserted parallel to plane y-z, it can be observed what causes the spike in partial damage (light blue & green areas) vertically upwards from the topmost capsule.

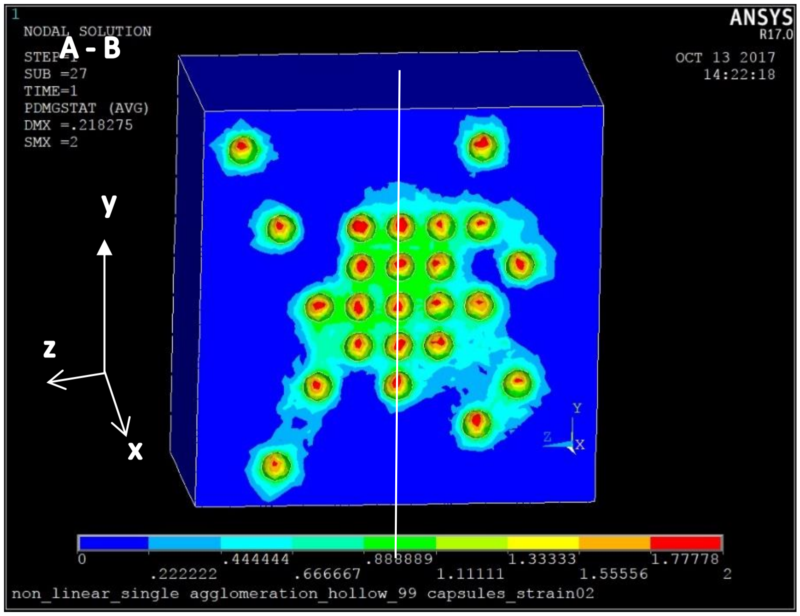

Figure 54. Cross sectional view of RVEs when the cutting plane is parallel to the y-z plane for the case of 2% strain.

The damage spike is due to the presence of adjacent capsules. This further reinforces the idea that the presence of nearby hollow capsules helps to propagate the damage by offering a path of low damage resistance. If the capsules are filled with healing agents, this pattern of damage propagation may help in the release of healing agents into the cracks.

4.2.11 Hollow capsules, multiple agglomerations + dispersion: 1% strain to 2% strain

This section presents the damage progression for the RVE containing 99 hollow PUF capsules where there are 3 agglomerations and the remaining capsules are dispersed in the rest of the matrix (Figure 55).

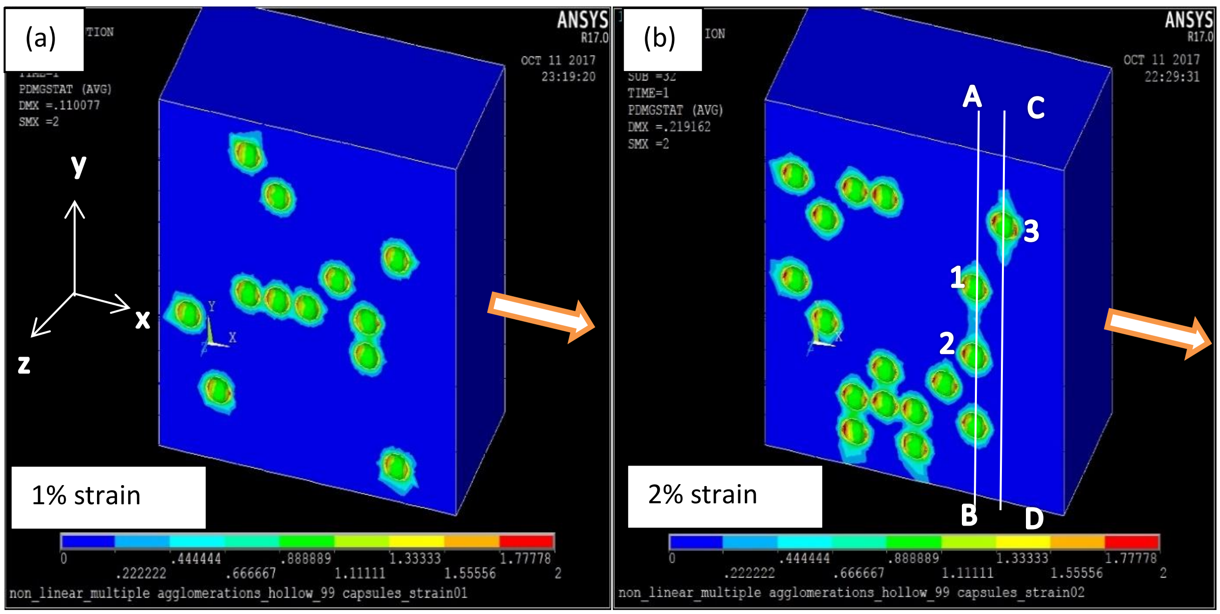

Figure 55. Comparison of damage between (a) 1% strain and (b) 2% strain for RVE containing 99 hollow PUF capsules with 3 agglomerations and the rest dispersed in the remaining RVE.

In Figures 55(a) and 55(b), the blue areas represent undamaged elements, the green areas represent partially damaged elements and the red areas represent completely damaged elements. When the RVE is subjected to 1% strain, the capsule walls get partially damaged with red spots in a straight-line parallel to the strain direction. When some capsules are in close vertical proximity, the partial damage tends to bridge between the capsules. When the strain increases to 2%, the partial damage spreads vertically in the matrix. There are instances where the damage spreads for a longer distance and bridges a wider vertical gap between capsules. This damage spread can also be observed to a lesser extent around the capsules which are dispersed in the matrix. The red areas (complete damage) become wider; however, they do not spread into the matrix. The damage spikes around capsules 1,2 and 3 were investigated by inserting 2 cutting planes, A – B and C – D parallel to plane y-z (Figure 56).

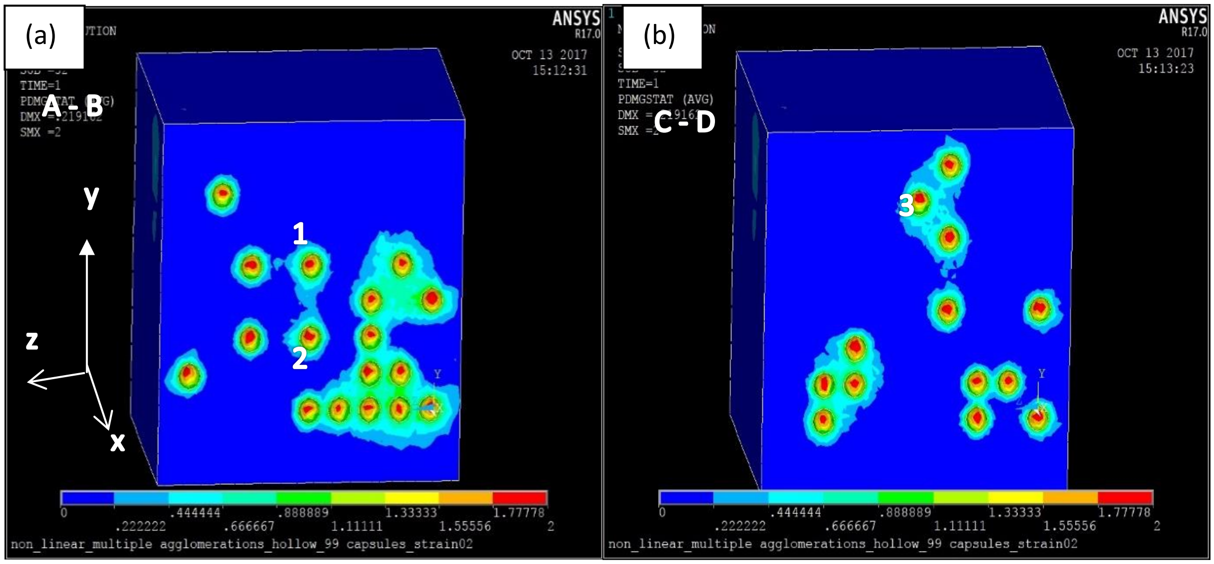

Figure 56. Cross sectional view of RVEs when the cutting plane is parallel to the y-z plane for the cutting planes (a) A – B and (b) C – D.

Between capsules 1 and 2, it looks like the damage is bridging between the capsules in the absence of adjacent capsules. For the case of capsule 3, the damage spikes were caused by the proximity of 2 other capsules.

4.2.12 Hollow capsules, pure dispersion: 1% strain to 2% strain

This section presents the damage progression for the RVE containing 99 hollow PUF capsules where the capsules are dispersed in the matrix and follow a random uniform distribution (Figure 57).

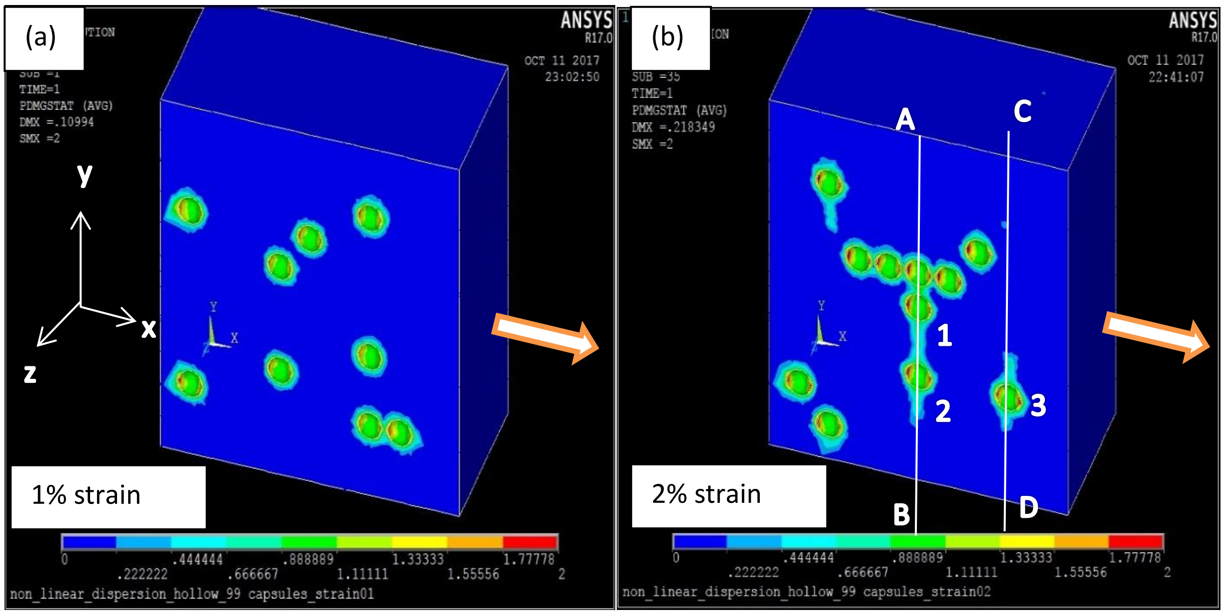

Figure 57. Comparison of damage between (a) 1% strain and (b) 2% strain for RVE containing 99 hollow PUF capsules dispersed in the RVE.

In Figures 57(a) and 57(b), the blue areas represent undamaged elements, the green areas represent partially damaged elements and the red areas represent completely damaged elements. When the RVE is subjected to 1% strain, the capsule walls get partially damaged with red spots in a straight-line parallel to the strain direction. When some capsules are in close vertical proximity, the partial damage tends to bridge between the capsules. When the strain increases to 2%, the partial damage spreads vertically in the matrix. There are instances where the damage spreads for a longer distance and bridges a wider vertical gap between capsules. This damage spread can also be observed around the capsules which are dispersed in the matrix. The red areas (complete damage) become wider, however, they do not spread into the matrix. To further investigate the damage spikes between capsules 1 and 2 and around capsule 3, two cutting planes, A – B and C – D, parallel to plane y-z were inserted.

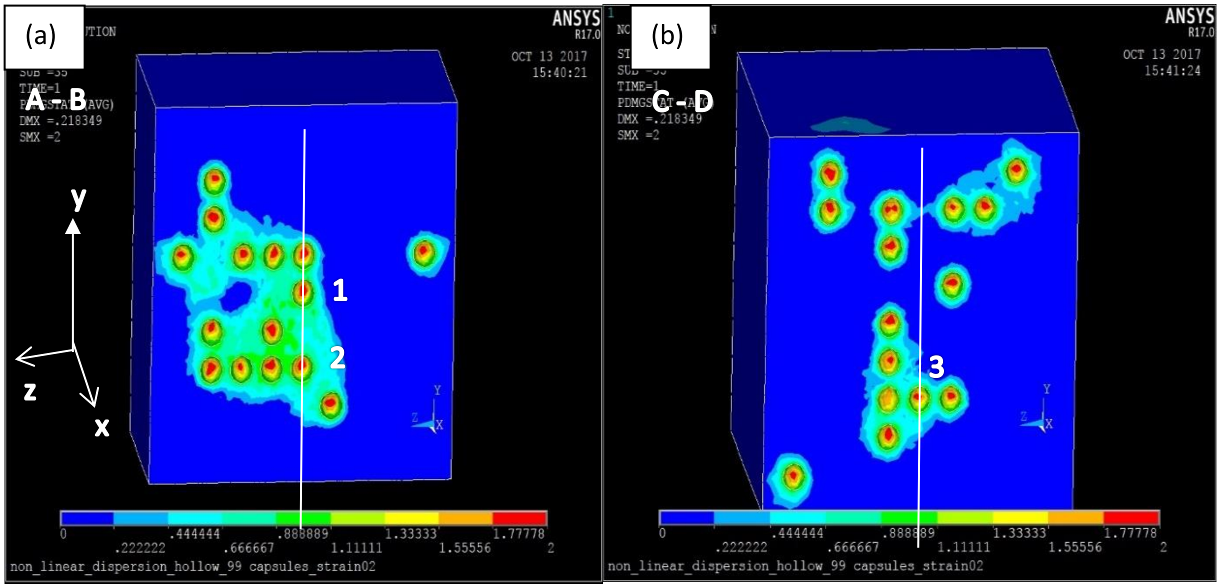

Figure 58. Cross sectional view of RVEs when the cutting plane is parallel to the y-z plane for the cutting planes (a) A – B and (b) C – D.

In Figure 58(a), there are several hollow capsules close to capsules 1 and 2. The same can be observed in Figure 58(b) where there are several capsules adjacent to capsule 3. This shows that when particles clump together, they tend to act as a bridge for damage propagation.

In several cross-sectional models, it can be observed that when the capsules are placed close to the boundaries of the RVE, the damage contours tend to point towards the RVE boundary. This phenomenon can be seen in all models where the capsules are formed closest to the RVE boundaries. Some prominent examples of this phenomenon are illustrated in Figure 59 (a) – (d). A possible explanation for this behaviour would be the modelling process. Since there is no material beyond the RVE boundary, for the capsules that are formed at the boundaries, the capsule will consider the boundary as the path of least damage resistance.

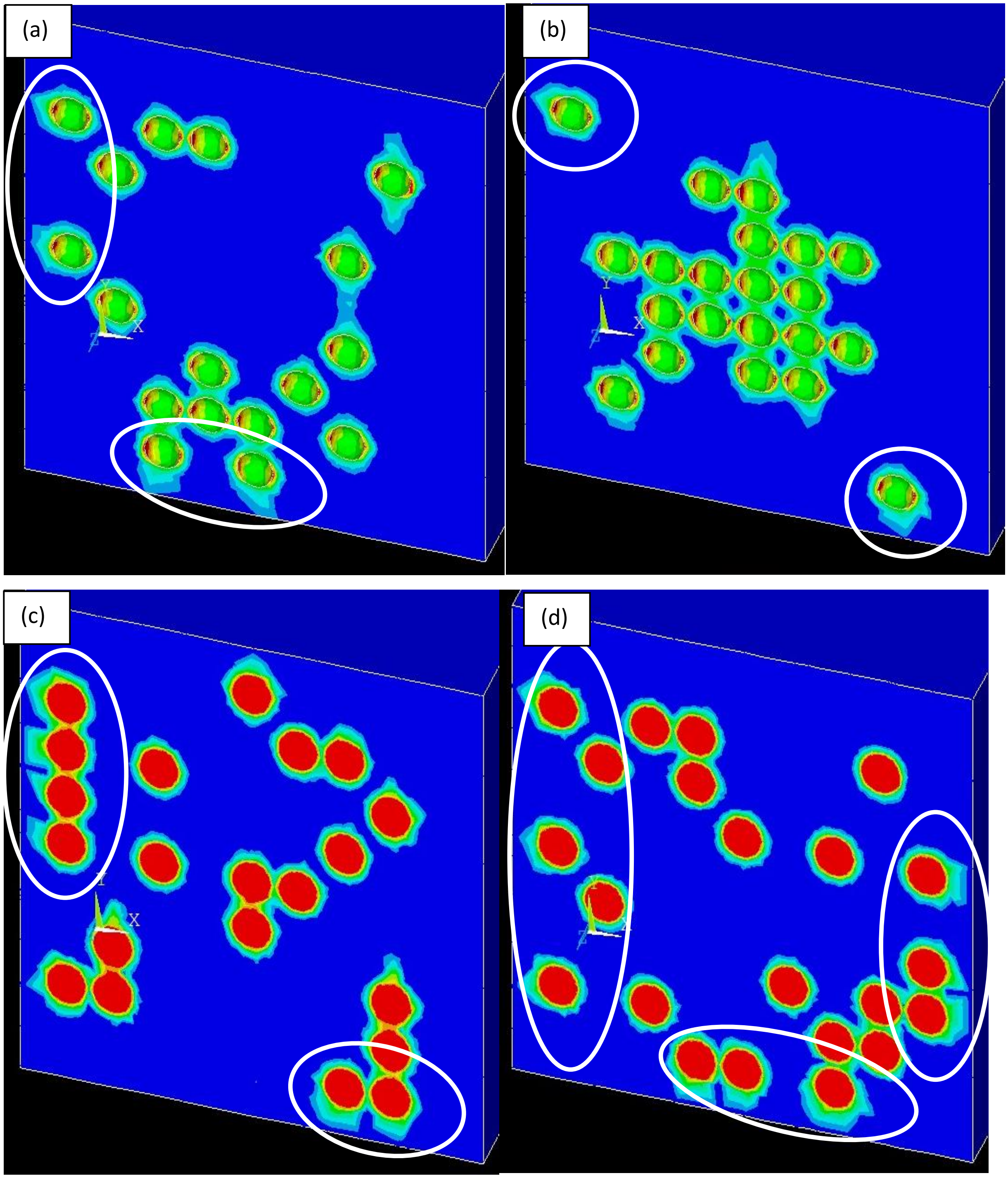

Figure 59. Illustration of the damage spike around capsules which are close to the RVE boundaries. These images are magnified versions of (a) Figure 54b, (b) Figure 52b, (c) Figure 45b, (d) Figure 43a.

5. Conclusions

The internal stress contours and the internal damage progressions of capsule-polymer composites were studied by running finite element simulations. Parameters such as material configurations, number of capsules and capsule distribution were varied to observe their effects on the RVE behaviour. Several findings were made:

- The capsule distribution influences the elastic modulus of the RVE. For the cases of capsules with solid fillings (solid epoxy and solid PUF), it is observed that the elastic modulus increases more when the capsules are distributed through the RVE. The increase in elastic modulus is less significant when the capsules are agglomerated at the centre of the RVE. This effect is reversed for the hollow capsule case. The elastic modulus suffers a significant drop when the hollow capsules are uniformly distributed through the RVE. This drop in elastic modulus is less significant when the hollow capsules are agglomerated at the centre of the RVE.
- The number of capsules influences the volume fraction of components and therefore affects the elastic modulus of the RVE. For the cases of capsules with solid fillings (solid epoxy and solid PUF), it is observed that the elastic modulus increases as the number of capsules increases. For the case of hollow capsules, it is observed that the elastic modulus decreases as the number of hollow capsules increases.
- In our case, for the specified material properties, it was observed that hollow capsules tend to decrease the elastic modulus of the composite. A possible cause for this phenomenon is that hollow capsules can be considered as voids and will therefore weaken the overall structure of the RVE.
- The damage models can be used to observe the how the damage progresses internally throughout the RVE and how capsule agglomeration and dispersion can influence the damage path. The damage follows a mode 1 type failure whereby the damage progresses in a direction perpendicular to the direction of the applied strain. It has also been observed that when capsules are close to each other, they provide a path of least resistance to the damage propagation.

- Capsules that agglomerate tend to facilitate the damage propagation in the matrix. If the capsules contain healing agents, this will cause the release of said healing agents into the crack.
- When designing capsule based self-healing composites, the material parameters must be carefully considered so that the composite can self-heal without being too prone to internal crack formation and catastrophic failure.

6. Future work

Due to time and resource limitations, certain objectives had to be abandoned. With appropriate funding, this work can be further enhanced in the following ways:

- Experimental works can be conducted to validate the computational model.
- With more time and software resources, models with higher capsule packing can be created. In other words, a model with higher number of capsules per unit volume can be created by fitting more capsules into the interstitial spaces between the existing capsules.
- With more powerful hardware and software support, models with higher capsule numbers and finer meshes can be created. This will increase the accuracy of the results.
- Powerful hardware and software can enable fracture simulation using extended finite element method (XFEM).
- With more powerful hardware and software expertise, fluid elements can be inserted into the hollow capsule model to simulate flow of healing agents out of the capsules.
- For the damage model, the application of higher strains requires a larger number of sub-steps to achieve the solution. This increase in sub-steps is very demanding in terms of CPU and memory usage. More powerful hardware will enable the application of higher strains.

References

Al-Madani, R. A., Jarnaz, M., Alkharmaji, K., & Essuri, M. (2013). *Finite Element Modeling of Composites System in Aerospace Application.* Paper presented at the Applied Mechanics and Materials.

Baghani, M., Naghdabadi, R., Arghavani, J., & Sohrabpour, S. (2012). A thermodynamically-consistent 3D constitutive model for shape memory polymers. *International Journal of Plasticity, 35*, 13-30.

Brown, E. N., White, S. R., & Sottos, N. R. (2004). Microcapsule induced toughening in a self-healing polymer composite. *Journal of Materials Science, 39*(5), 1703-1710.

Chawla, N., Sidhu, R., & Ganesh, V. (2006). Three-dimensional visualization and microstructure-based modeling of deformation in particle-reinforced composites. *Acta materialia, 54*(6), 1541-1548.

Chen, C., Ji, H., & Wang, H. (2013). Damage properties simulations of self-healing composites. *Journal of nanoscience and nanotechnology, 13*(10), 6679-6686.

Dementsov, A., & Privman, V. (2008). Three-dimensional percolation modeling of self-healing composites. *Physical Review E, 78*(2), 021104.

Grande, A., Coppia, S., Di Landroa, L., Salaa, G., Giacomuzzob, C., Francesconib, A., & Rahmanc, M. (2012). *An experimental study of the self-healing behavior of ionomeric systems under ballistic impact tests.* Paper presented at the Proc. of SPIE Vol.

Grujicic, M., Bell, W., Arakere, G., He, T., Xie, X., & Cheeseman, B. (2010). Development of a meso-scale material model for ballistic fabric and its use in flexible-armor protection systems. *Journal of materials engineering and performance, 19*(1), 22-39.

Guo, X., Ji, R., Weng, G., Zhu, L., & Lu, J. (2014). Micromechanical simulation of fracture behavior of bimodal nanostructured metals. *Materials Science and Engineering: A, 618*, 479-489.

Guo, X., Yang, G., & Weng, G. (2016). The saturation state of strength and ductility of bimodal nanostructured metals. *Materials Letters, 175*, 131-134.

Rockey, K. C., Evans, H. R., Griffiths, D. W., & Nethercot, D. A. (1983). The finite element method: a basic introduction. *New York, Halsted Press, 1983, 248 p*.

Hall, J., Qamar, I., Rendall, T., & Trask, R. (2015). A computational model for the flow of resin in self-healing composites. *Smart Materials and Structures, 24*(3), 037002.

Hia, I. L., Pasbakhsh, P., Chan, E.-S., & Chai, S.-P. (2016). Electrosprayed Multi-Core Alginate Microcapsules as Novel Self-Healing Containers. *Scientific reports, 6*.

Keller, M., & Sottos, N. (2006). Mechanical properties of microcapsules used in a self-healing polymer. *Experimental Mechanics, 46*(6), 725-733.

Kim, H. S. (2000). On the rule of mixtures for the hardness of particle reinforced composites. *Materials Science and Engineering: A, 289*(1-2), 30-33.

Koumpias, A., Tserpes, K., & Pantelakis, S. (2014). Progressive damage modelling of 3D fully interlaced woven composite materials. *Fatigue & Fracture of Engineering Materials & Structures, 37*(7), 696-706.

Lanzara, G., Yoon, Y., Liu, H., Peng, S., & Lee, W. (2009). Carbon nanotube reservoirs for self-healing materials. *Nanotechnology, 20*(33), 335704.

Laurenzi, S., Pastore, R., Giannini, G., & Marchetti, M. (2013). Experimental study of impact resistance in multi-walled carbon nanotube reinforced epoxy. *Composite Structures, 99*, 62-68.

Lee, J. Y., Buxton, G. A., & Balazs, A. C. (2004). Using nanoparticles to create self-healing composites. *The Journal of chemical physics, 121*(11), 5531-5540.
Lim, C., Shim, V., & Ng, Y. (2003). Finite-element modeling of the ballistic impact of fabric armor. *International Journal of Impact Engineering, 28*(1), 13-31.
Ouyang, Q., Guo, X., & Feng, X. (2016). 3D microstructure-based simulations of strength and ductility of bimodal nanostructured metals. *Materials Science and Engineering: A, 677*, 76-88.
Roach, D. P., Delong, W. A., White, S., Yepez, E., Rackow, K. A., & Reedy Jr, E. D. (2007). *Use of composite materials, health monitoring and self-healing concepts to refurbish our civil and military infrastructure*. Retrieved from
Sanada, K., Mizuno, Y., & Shindo, Y. (2015). Damage progression and notched strength recovery of fiber-reinforced polymers encompassing self-healing of interfacial debonding. *Journal of Composite Materials, 49*(14), 1765-1776.
Shojaei, A. (2015). Modeling of self-healing smart composite materials. *Recent Advances in Smart Self-healing Polymers and Composites, Woodhead Publishing*, 21-52.
Shojaei, A., Sharafi, S., & Li, G. (2015). A multiscale theory of self-crack-healing with solid healing agent assisted by shape memory effect. *Mechanics of Materials, 81*, 25-40.
Shokrieh, M. M., & Rafiee, R. (2010). Stochastic multi-scale modeling of CNT/polymer composites. *Computational Materials Science, 50*(2), 437-446.
Singh, I., Shedbale, A., & Mishra, B. (2016). Material property evaluation of particle reinforced composites using finite element approach. *Journal of Composite Materials, 50*(20), 2757-2771.
Sun, C., Shen, R., Song, M., & Du, Y. (2012). *Mechanical Behaviors of Sic Particle Reinforced Al Matrix Composites: A Study Based on Finite Element Method.* Paper presented at the Advanced Materials Research.
Thakur, V. K., & Kessler, M. R. (2015). Self-healing polymer nanocomposite materials: A review. *Polymer, 69*, 369-383.
Tsangouri, E., Aggelis, D., & Van Hemelrijck, D. (2015). Quantifying thermoset polymers healing efficiency: a systematic review of mechanical testing. *Progress in Polymer Science, 49*, 154-174.
Urban, M. W. (2009). Stratification, stimuli-responsiveness, self-healing, and signaling in polymer networks. *Progress in Polymer Science, 34*(8), 679-687.
Valavala, P., & Odegard, G. (2005). Modeling techniques for determination of mechanical properties of polymer nanocomposites. *Rev. Adv. Mater. Sci, 9*, 34-44.
Wang, H. W., Ji, H. W., Shao, W. Q., & Miao, H. (2011). *3D Finite Element Modeling for Particle-Reinforced Polymer Composites for Wind Energy Application.* Paper presented at the Advanced Materials Research.
White, S. R., Sottos, N., Geubelle, P., Moore, J., Kessler, M. R., Sriram, S., . . . Viswanathan, S. (2001). Autonomic healing of polymer composites. *Nature, 409*(6822), 794-797.
Williams, G., Bond, I., & Trask, R. (2009). Compression after impact assessment of self-healing CFRP. *Composites Part A: Applied Science and Manufacturing, 40*(9), 1399-1406.
Wool, R. P. (2008). Self-healing materials: a review. *Soft Matter, 4*(3), 400-418.
Wu, D. Y., Meure, S., & Solomon, D. (2008). Self-healing polymeric materials: a review of recent developments. *Progress in Polymer Science, 33*(5), 479-522.
Zhang, M. Q., & Rong, M. Z. (2012). Theoretical consideration and modeling of self-healing polymers. *Journal of Polymer Science Part B: Polymer Physics, 50*(4), 229-241.

Zhong, N., & Post, W. (2015). Self-repair of structural and functional composites with intrinsically self-healing polymer matrices: A review. *Composites Part A: Applied Science and Manufacturing*, *69*, 226-239.